Transient Dynamics and Stability Boundaries in Electric Power System with DC Transmission

Yoshihiko Susuki

November 2004

Transient Dynamics and Stability Boundaries in Electric Power System with DC Transmission

Yoshihiko Susuki

A Dissertation
Presented to the Faculty
of Kyoto University
in Candidacy for the Degree
of Doctor of Philosophy

November 2004

Abstract

Direct Current (DC) transmission systems have been recently applied to conventional electric power systems. For example, The Kii Channel High Voltage DC Link in Japan is well-known as one of the largest dc systems in the world. The dc systems have some advantages of power delivery: they can connect different alternative current (ac) power systems under desynchronized operation and control electric power in ac transmission systems rapidly and arbitrary. These abilities have been utilized for various situation of power system operation and control. In addition, the dc systems have a great potential for operation and control of future complex power networks.

This dissertation is concerned with transient stability of electric power systems with dc transmission. The understanding of the transient stability is of paramount importance to adopt the dc transmission into conventional ac power systems. In this dissertation, transient dynamics and stability boundaries are addressed for the ac/dc power systems. Transient dynamics is closely related to synchronization phenomena in ac power systems, which have not been revealed in the field of nonlinear dynamics, and essentially determines the transient stability. Stability boundaries are basin boundaries of attraction of equilibrium points or periodic solutions, which imply acceptable operating conditions of the systems, in corresponding mathematical models. Unfortunately, the transient dynamics and stability boundaries have not been fully understood, although they are essential for the transient stability estimation.

In this dissertation, the transient dynamics and stability boundaries are discussed for a practical ac/dc power system. The discussion is based on two different dynamical systems; they are described by a differential equation, which is called by swing equation, and a differential-algebraic equation (DAE). These dynamical systems are derived for the prac-

tical system. In this dissertation, some dynamical features of the systems are investigated numerically and theoretically. Analytical and effective criteria are also proposed for the stability boundary analysis.

In the former part of this dissertation, transient dynamics and stability boundaries are analyzed which are affected by constant electric power which flows into the dc link. The analysis is based on the non-autonomous swing equation system. The swing equation has a unidirectional external force which corresponds to both the dc power and a periodic power swing. The former part considers some dynamical characteristics of the swing equation system and shows that the fractal structure grows in a stability boundary caused by the dc external forcing. The fractal boundary implies a new dynamical feature of the ac/dc power system under periodic power disturbance. Furthermore, analytical criteria are derived for stability boundaries of the swing equation system. The criteria are established based on the Melnikov's perturbation methods and make it possible to evaluate the stability boundaries analytically.

The latter part discusses transient dynamics and stability boundaries with considering dc system's operation and electric power balance in the ac/dc systems. The discussion is expanded through the DAE system. The DAE system keeps the structural characteristics of power conversion and control setup in the dc link, and explicitly describes the power relation between the ac and dc systems. This part examines some dynamical features of the DAE system numerically and clarifies a stability boundary through several basin portraits. Moreover, complete characterization of stability boundaries in the DAE system is theoretically derived using an energy function for an associated singularly perturbed system. The theoretical result is also confirmed via several numerical results on a stability boundary. Furthermore, discontinuous solutions of the DAE system are discussed which are due to some practical fault conditions. The obtained results in this part delineate how the dc system affects the dynamical characteristics of the transient dynamics and stability boundaries.

Acknowledgments

I would like to begin by thanking my adviser and mentor, Professor Takashi Hikihara. He has shown great patience and generosity while guiding me into several research areas of engineering science. He always left his door open to all students and faculty to create an open atmosphere, in which I was challenged to achieve my potential. In addition, the care and respect he has for his students make it a pleasure to work with him. I am honored to be his student.

I would also like to thank Professor Yoshisuke Ueda of Future University – Hakodate for his insightful suggestions and encouragement. He introduced me to differential equations and nonlinear dynamics as a pioneer of chaos and complex systems. His introduction as well as his sincere attitude towards nonlinear phenomena have become my research basis. I would also like to thank Professor Hsiao-Dong Chiang of Cornell University for his collaboration and fruitful advice. He provided me with opportunities to work on nonlinear system theory and to stay Ithaca as a visiting scholar. Since then I have shared his wealth of knowledge about nonlinear systems. I am very grateful to all of them.

I would also like to thank Professor Philip Holmes of Princeton University for his valuable comments and discussion. He provided me with opportunities to discuss about my research in Princeton and Kyoto. In particular, his questions about singular perturbation reminded me to correct several mistakes in Chapter 6.

I thank the numerous faculty and students in the Graduate School of Engineering of Kyoto University for expanding my knowledge base. Specially, I would like to thank Professor Kazuo Tsuchiya and Professor Yasuharu Ohsawa both for their valuable suggestions and for serving on my dissertation committee. I would also like to thank all the members of Professor Ueda's and Professor Hikihara's research groups, which include

Professor Tsuyoshi Funaki, Ms. Keiko Saito, Mr. Satoshi Kida in Matsushita Electric Industrial Co., Ltd., Mr. Kohei Yamasue, and Mr. Yasuhiro Takama, for providing me with an enriching research environment, valuable discussion and encouragement.

I am grateful for the support of the Japan Student Services Organization (JASSO); the Nakanishi Scholarship Foundation; the Japan Society for the Promotion of Science (JSPS), the 21st Century COE Program (Grant No. 14213201); and the Circle for the Promotion of Science and Engineering, Research Grant, 2003.

In closing, I would like to thank my parents, Kunihiko and Fumie Susuki, for their constant support and warm encouragement.

Contents

Abstract **iii**

Acknowledgments **v**

Notations and acronyms **xi**

1 Introduction **1**

1.1 Transient dynamics and stability boundaries 4

1.2 System model 5

1.3 Purpose and overview 6

2 Transient dynamics and fractal stability boundary **15**

2.1 Swing equation system 16

2.1.1 Derivation 16

2.1.2 Dynamical properties 17

2.2 Bifurcation diagram 19

2.3 Fractal growth in stability boundary 20

2.3.1 Global bifurcation and self-similar structure 20

2.3.2 Doubly asymptotic points and fractal stability boundary 21

2.3.3 Physical interpretation 22

2.4 Summary and discussion 22

3 Stability boundary analysis via Melnikov's method **35**

3.1 Perturbed Hamiltonian system 36

3.2 Melnikov's perturbation method 37

3.3 An analytical criterion for stability boundaries 42
3.4 Application to swing equation system 43
3.4.1 Numerical simulations and analytical criteria 43
3.4.2 Physical interpretation and remaining problem 44
3.5 Summary 45

4 Subharmonic Melnikov functions and stability boundaries 51
4.1 Preliminaries 52
4.2 An analytical criterion for basin boundaries of resonant solutions 53
4.2.1 Action angle coordinates transformation 53
4.2.2 Perturbed Hamiltonian system for resonant solutions 54
4.2.3 An analytical criterion 56
4.3 Illustrative examples 58
4.3.1 Greenspan and Holmes system 58
4.3.2 Swing equation system 60
4.4 Summary 61

5 Differential-algebraic equation system and stability boundary 67
5.1 Differential-algebraic equation system 68
5.1.1 Derivation 68
5.1.2 Reduction to swing equation system 71
5.2 Fundamental concepts of differential-algebraic equation system 72
5.2.1 Summarized theory as dynamical system 72
5.2.2 Numerical methods 73
5.3 Equilibrium points 74
5.4 Global structure of stability boundary 75
5.4.1 Basin portraits around equilibrium points 75
5.4.2 Hyperbolic saddle point and stability boundary 75
5.4.3 Global configuration of basin portraits 76
5.5 Summary 77

6 Stability boundaries and discontinuous dynamics **95**

6.1 Preliminaries 96

6.2 Singular perturbation, energy function, and stability boundary 98

6.2.1 Singular perturbation technique 98

6.2.2 Energy function and stability boundary 100

6.3 Characterization of stability boundaries 102

6.3.1 Reduction of DAE system 103

6.3.2 AC power system 104

6.3.3 AC/DC power system 105

6.4 Concrete structure of stability boundary: Numerical results revisited . . . 107

6.4.1 Hyperbolic saddle point in differential-algebraic equation system . . 108

6.4.2 Periodic orbit in singularly perturbed system 108

6.4.3 Remarks and discussion 109

6.5 Discontinuous solutions and transient stability 110

6.5.1 Faults setting and external jump 111

6.5.2 Numerical simulations 111

6.5.3 Discontinuous solutions and boundary layer systems 112

6.5.4 Discussion 113

6.6 Summary 114

7 Conclusion **125**

Bibliography **129**

Published papers **141**

Notations and acronyms

Frequently used notations

Symbol	Meaning
$\mathbb{R}$	real numbers
$\mathbb{S}^1$	unit circle
$\mathbb{Z}$	integer numbers
$\mathscr{F}$	discrete dynamical system
$\mathscr{M}$	stable map
$\mathscr{P}$	Poincaré map
$\mathcal{H}$, $\mathcal{K}$	Hamiltonian functions
$\bar{\mathcal{M}}^{m/n}$	subharmonic Melnikov function
$\mathcal{U}$	potential function
$\mathcal{W}$	energy function
A	stability region
b	critical value of one generator-infinite bus system
C^r	r times differentiable
D	damping coefficient in generator
d^{s}	signed distance between points on homoclinic orbit and stable manifold

e_d	d-axis terminal voltage of generator
e_q	q-axis terminal voltage of generator
G_α	gain constant of rectifier controller
H	inertia constant
h	step size of numerical integration; one-to-one correspondence
	; variable
I	action variable
I_{dc}	dc current
$I_{\mathrm{dc(ref)}}$	reference dc current
K_V, K_I	coupling coefficients between ac and dc systems
L	constraint set
L_d	d-axis synchronous reactance
L'_d	d-axis transient reactance
L_{dc}	dc line reactance
L_q	q-axis synchronous reactance
L_∞	ac line reactance
$p_{\mathrm{e(dc)}}$	electric power flow into dc link
p_{g}	electrical output power of generator
p_{m}	mechanical input power of generator
R_{dc}	dc line resistance
S	singular surface
T	period of perturbation terms: $\Omega T = 2\pi$
T_I, T_θ, T_x, T_y	action angle variables transformation and its differentiable inverse
T'_d	d-axis transient short-circuit time constant

T'_{d0}	d-axis transient open-circuit time constant
t	normalized time
V_0	exciter voltage referred to armature circuit
$V_{\mathrm{dc(i)}}$	dc voltage input of inverter
$V_{\mathrm{dc(r)}}$	dc voltage output of rectifier
V_{i}	ac bus voltage at inverter side
V_∞	infinite bus voltage
v_{r}	terminal voltage of generator
W	invariant manifold
X_{c}	commutating reactance
$\boldsymbol{p}_{-1}$	center
$\boldsymbol{p}_0$	hyperbolic saddle point
$\boldsymbol{p}^{\varepsilon}_{-1}$	non-resonant sink
$\boldsymbol{p}^{\varepsilon}_{0}$	non-resonant saddle
$\boldsymbol{q}$	$(x, y)^{\mathrm{T}}$ where $x, y \in \mathbb{R}$
$\boldsymbol{q}^0$	point on homoclinic orbit
$\boldsymbol{q}^{\mathrm{s}}_{\varepsilon}$	intersection between homoclinic orbit and stable manifold
α	firing angle of rectifier
Γ_{s}	stable component
γ	margin angle of inverter
∂A	stability boundary
δ	rotor position with respect to synchronous reference axis
δ_{r}	related variable to terminal voltage of generator: $e_d = v_{\mathrm{r}} \sin \delta_{\mathrm{r}}$ and $e_q = v_{\mathrm{r}} \cos \delta_{\mathrm{r}}$

ε	positive perturbation parameter; ratio of amplitude of exciting power swing to critical value b
θ	angle variable; rotor angular displacement of generator
μ	positive perturbation parameter
σ	variable
ϕ	phase
φ_{r}	power factor angle of rectifier
Ω	angular frequency of perturbation terms and exciting power swing
ω	rotor speed deviation relative to system angular frequency ω_{b}
ω_{b}	system angular frequency
J	skew symmetric matrix
M	positive-definite diagonal matrix
S (D, resp.)	completely stable (directly unstable, resp.) fixed point for discrete dynamical system; stable focus (saddle point, resp.) for continuous dynamical system
${}^{j}\mathsf{S}^{k}_{(i)}$	i-th completely stable j-th kind k-periodic point so as D for discrete dynamical system; i-th stable focus ($j(=1)$-th kind) k-periodic point so as D for continuous dynamical system
$\mathrm{D}\mathcal{H}(\boldsymbol{q})$	gradient vector of $\mathcal{H}(\boldsymbol{q})$
$\mathrm{D}_x \boldsymbol{f}$, $\dfrac{\partial \mathcal{H}}{\partial x}$	partial derivative of $\boldsymbol{f}$ with respect to $\boldsymbol{x}$; $\mathcal{H}$ with respect to x
$\dfrac{\mathrm{d}\boldsymbol{q}}{\mathrm{d}t}$	time derivative of $\boldsymbol{q}$
T	transpose operation of vectors
$\|\ \ \|$	Euclidean norm

List of acronyms

Acronym	Meaning
AC, ac, a.c.	Alternative Current
AVR	Automatic Voltage Regulator
BDF	Backward Differential Formula
BL	Boundary Layer
DAE	Differential-Algebraic Equation
DC, dc, d.c.	Direct Current
EP	Equilibrium Point
FACTS	Flexible AC Transmission System
ICC	Invariant Closed Curve
IRK	Implicit Runge-Kutta
HV, hv	High Voltage
ODF	One-Degree-of-Freedom
PSS	Power System Stabilizer
QP	Quasi-Periodic
SP	Singularly Perturbed
STATCOM	STATic COMpensator
UEP	Unstable Equilibrium Point
UPFC	Unified Power Flow Controller

CIGRÉ	Conseil Intenational des Grands Réseaux Électriques (International Council on Large Electric Systems)
IEE	Institute of Electrical Engineers
IEEE	Institute of Electrical and Electronics Engineers
IEEJ	Institute of Electrical Engineers, Japan
IEICE	Institute of Electronics, Information and Computer Engineers (Japan)
ISCIE	Institute of Systems, Control and Information Engineers (Japan)
SIAM	Society for Industrial and Applied Mathematics

Chapter 1

Introduction

Synchronization is a subject of research on dynamics resulting from nonlinearity. Nonlinear dynamics has scored a great success in offering a comprehensive perspective on engineering and science [3,35,88,93,108]. Various interesting phenomena appear in nonlinear systems, which include regular and chaotic motions, coexisting attractors, smooth and fractal basin boundaries, local and global bifurcations. The synchronization is particularly centered around the field of nonlinear dynamics. Many researches attain positive results on synchronization phenomena of van der Pol oscillators in the beginning of nonlinear oscillation theory [3,43,100]. A phase-locked loop, which exploits the synchronization, is well-known as an important technique in communication engineering [104]. An electric power system has been also attracting a lot of interests as a typical complex network [4,29,81] in which the synchronization appears.

An alternative current (ac) power system is a fairly large network of interacting dynamical systems: they are synchronous machines, distributed power sources, and special types of loads. All synchronous generators in the ac system usually run at the same frequency and supply electric power to loads via transmission lines, transformers, and so on. If some of the generators fall out of step, in other words, lose synchronism due to event disturbances which include generator outages, short-circuits caused by lightning, sudden large load changes, and so on, then the power supply becomes indeterminate and may break down in the worst case. This prejudices human activities in modern society: such large blackouts actually occurred in the United States and Canada [99], Great Britain, Denmark

and Sweden, and Italy in 2003. Thus, the synchronization is an essential phenomenon involving the power supply and should be comprehended in terms of nonlinear dynamics and power system engineering.

The synchronization in the ac power system is physically different from that in electronic circuits. Unfortunately, the difference has not been recognized by both nonlinear dynamics and power system researchers except a seminal lecture by Takagi [83] and some technical reports by Ueda *et al.* [95, 96]. To clarify the purpose of this dissertation, some of the different features are introduced below.

The synchronization is related to electric power transmission in the ac power system. As mentioned before, the synchronization in the electronic circuits is studied for the van der Pol oscillators and the phase-locked loops. They have various types of nonlinearity as *elements* which play a key role in the phenomenon: the van der Pol equation is modeled based on the vacuum-tube oscillator with the nonlinear characteristic [43, 100]; the phase-locked loops contain nonlinear phase comparators [104]. On the other hand, the synchronized operation of the generators is essentially not related to various nonlinear elements in the ac system such as circuit breakers and loads. Here, in the context of power system engineering [51,60], the *swing equation* has been utilized to consider the synchronized operation:

$$\frac{\mathrm{d}^2\delta}{\mathrm{d}t^2} + D\frac{\mathrm{d}\delta}{\mathrm{d}t} + b\sin\delta \;=\; p_{\mathrm{m}}. \tag{1.1}$$

The equation represents the synchronized operation of one generator connected to an infinite bus[1] via transmission lines and transformers. δ denotes the rotor position compared with the infinite bus, D the damping coefficient in the generator, b the critical value of power transmission, and p_{m} the mechanical power input of the generator. The swing equation (1.1) has the nonlinear restoring force $b\sin\delta$ which corresponds to electric power output of the generator. Namely, the nonlinearity originates from the *electric power balance* relation between the generator and the infinite bus.

The ac power system, in which the synchronization appears, is a complex network of interacting time-periodic dynamical systems. In the case of coupled van der Pol oscillators, each one is described by a self-oscillatory system, which has a stable limit cycle.

[1] An *infinite bus* is a source of voltage constant in phase, magnitude, and frequency, and is not affected by the amount of current withdrawn from it [51].

This description provides us with a universal mathematical model and insightful results on the synchronization phenomena in the electronic circuits, various physical and biological systems: see e.g. [43,55]. However, the methodology cannot be applied to the synchronization in the ac system, because the dynamics of each synchronous generator is described by a typical *periodic* system. Namely, the synchronized operation of the generators is regarded as the dynamics of coupled periodic systems through electric power transmission. The mechanism behind the synchronization remains to be elucidated in terms of nonlinear dynamics including modeling, analysis, and control.

Direct current (dc) transmission here offers a fruitful system model to attack the synchronization phenomenon. The synchronization imposes several limitations of power transmission on the ac transmission system; for example, we cannot regulate the power supply arbitrarily and rapidly, because its amount and direction are strongly governed by the synchronized operation of the generators. On the other hand, a dc link can be operated in principle under *desynchronized* state with ac power systems, and the operation is therefore worthy of attention to unravel the synchronization phenomenon. Moreover, an electric power system *with dc transmission* is definitely a non-trivial research object of nonlinear dynamics, in one part of which all generators run at the *same* frequency, while in another part all generators are operated with the *different* frequency via dc links. Furthermore, the dc links have an important ability to regulate their electric power independently on the ac system's operation. This ability makes it possible to investigate some dynamic and control aspects of the synchronization: what mathematical model is relevant to describing the dynamics of the generators with considering power balance relation between the ac and dc systems?; how is the dynamics affected by electric power which flows in the dc links?; and, as a control problem, consider a power balance-based control strategy of the dc links which regulates the overall dynamics. Hence, the ac/dc power system has a great potential to reveal and tame the synchronization phenomenon from the viewpoints of nonlinear dynamics and power system engineering.

1.1 Transient dynamics and stability boundaries

Transient stability is of important concern with both safe operation of power systems and the synchronization phenomenon. Many definitions of stability are proposed in engineering and science [82]. The transient stability is closely related to a power system's ability to reach an acceptable operating condition following an event disturbance [14,51,60]. After clearing a large disturbance which is added to a power system, a generator settles down an acceptable condition or loses synchronism depending on the system's dynamics and the kind of the disturbance. The physical process is roughly described as follows. If the mechanical power input of the generator greatly exceeds its electric power output as a result of the disturbance, then the excess power is stored as the kinetic energy in the generator, and its rotor speed increases. After the generator is again connected to the power system by clearing the disturbance, the rotor speed and the electric output power will converge to an acceptable steady state or reach unsafe states at which the power supply may break down. Thus, the stability problem is the study on whether the generator remains in synchronism or not; the corresponding nonlinear phenomenon is called *transient dynamics* [18].

The concept of *stability boundaries* is centered around nonlinear dynamical system approach to the analysis of the transient dynamics and stability. From the above discussion, the transient stability is concerned with the synchronization through electric power transmission. This naturally raises the requirement for the application of dynamical system theory to the transient analysis. Before now, many researches have reported the applications to various nonlinear phenomena in power systems: see e.g. [1,26,54,72,94,97,101,109]. In particular, the stability boundaries are of paramount importance for investigating the transient dynamics and stability. The stability boundaries imply basin boundaries of attraction of equilibrium points or periodic solutions, which coincide with desirably operating conditions of power systems, in corresponding dynamical systems. By using the concept, we can interpret the transient stability mathematically as follows. Starting from an initial state after clearing a disturbance, will the associated trajectory settle down to an attractor which denotes an acceptable steady state? In other words, the stability problem is to determine whether the initial point is located inside a stability boundary or not. The understanding of the stability boundary is hence inevitable for the stability estimation.

The main matter of concern to the field of nonlinear dynamics is the global structure of stability boundaries. The analysis is performed using theoretical and numerical methods. Topological and dynamical characterization of the stability boundaries is reported for a fairly large class of autonomous dynamical systems in [16, 110]. The theoretical result shows concrete structures of the stability boundaries based on global invariant manifolds of hyperbolic critical sets. The important characterization is generalized into a class of nonlinear dynamical systems described by differential-algebraic equations in [15, 102, 103]. On the other hand, complicated stability boundaries, which possibly become *fractal*, are phenomenologically discussed for various engineering and physical systems: see e.g. [28, 36, 61, 65, 79]. Such complicated boundaries are particularly reported for transient stability problems of ac power systems in [42, 94, 101]. The boundaries are of much importance for the stability estimation, because we cannot inherently predict the dynamics of the ac systems if their states are placed around the boundaries. Cell-to-cell mapping [47] is also well-known as an established numerical method for analyzing basin structures in nonlinear systems. These previous results motivate the research in this dissertation as explained in the following section.

1.2 System model

This dissertation addresses a practical electric power system with dc transmission in Japan to examine the transient dynamics and stability boundaries. High voltage (hv) dc transmission systems have been recently applied to conventional electric power systems [5, 40, 59, 71]; supplemental general facts of dc transmission are given at the end of this chapter. A hvdc link was particularly commissioned in 2000 which connects ac 500 kV networks of The Shikoku and The Kansai Electric Companies across Kii Channel [30, 41, 77]. The hvdc link is designed at the rating of $\pm$500 kV and 2800 MW for the future expansion; it is now being operated at $\pm$250 kV and 1400 MW. The hvdc link is well-known as one of the largest dc systems in the world. The research in this dissertation is motivated by the practical system: The Kii HVDC Link and The Tachibana-wan Coal Thermal Power Station [30, 77] shown in Fig. 1.1. In the figure, generator denotes The Tachibana-wan Power Station, dc transmission line, rectifier, and inverter The Kii Channel HVDC Link, and

ac transmission line the ac one which connects The Tachibana-wan Power Station and The Chugoku Electric Power Company/The Nakanishi Transmission Line. The Nakanishi Line connects two different networks of The Kansai and The Chugoku Electric Power Companies. The Tachibana-wan Power Station consists of three units which amount to 2.8 GW in the region of The Shikoku Electric Power Company. Half of the electric power generated by the station is delivered to the Kansai area via the hvdc link.

The Kii Channel HVDC Link has an important role in not only delivering the electric power but also stabilizing the ac power system. The hvdc link constitutes an ac-dc loop transmission in the middle of 60 Hz and 500 kV networks. The loop system is expected to improve the overall ac system performance by using several dc link's abilities [30, 77]. For example, dc power modulation is proposed in [30, 89] for damping power swings which possibly occur in the 60 Hz and 500 kV networks. Fig. 1.2 shows the practical measurement of the frequency and power swings at The Nakanishi Transmission Line [80]. The power swing is also expected to be damped by the dc power modulation. Thus, the hvdc link plays the primary role as a backbone transmission system, and it is therefore important to reveal the transient stability of the ac/dc power system.

1.3 Purpose and overview

This dissertation aims to clarify the transient dynamics and stability boundaries in the electric power system with dc transmission. The analysis is performed based on two mathematical models: *swing equation* and *differential-algebraic equation* (DAE) systems. Some dynamical features of these mathematical models are examined numerically and theoretically. Analytical and effective criteria are also proposed for stability boundaries of the swing equation system. The rest part in the section explains the contents of this dissertation.

Chapters 2–4 address transient dynamics and stability boundaries affected by constant electric power which flows into the dc link. As discussed before, the dc link in Fig. 1.1 can ideally regulate its electric power independently on the synchronized operation in the ac power system. This naturally proposes the following problem: how the constant electric power which flows in the dc link affects the transient dynamics of the ac/dc power system.

Although the understanding is inevitable for clarifying the transient stability, the dynamical behavior has not been fully clarified.

In Chapter 2, we derive and analyze the non-autonomous swing equation system to tackle the above problem. The swing equation has a unidirectional external force which corresponds to both the dc power and a periodic power swing. The power swing is based on the practical measurement in Fig. 1.2. Although the system has the common mathematical structure to various physical and engineering systems [25, 27, 28, 36, 37, 48, 66, 73], the dynamical behavior affected by the dc external force has not been sufficiently discussed. Chapter 2 analyzes some dynamical features of the swing equation system and shows that the *fractal* structure grows in a stability boundary caused by the dc external forcing. The fractal boundary implies a new dynamical feature of the ac/dc power system under the periodic power disturbance.

Chapter 3 proposes an analytical criterion for stability boundaries of the swing equation system. Since the swing equation system is *non-autonomous*, the classical Lyapunov's direct method [56,69] is not applicable to the non-autonomous system. Generally speaking, no analytical and effective approach has been reported to analyze stability boundaries in non-autonomous systems. In this chapter, we derive an analytical criterion for stability boundaries in one-degree-of-freedom (ODF) time-periodic perturbed Hamiltonian systems, which include the swing equation system. The criterion is derived based on the *Melnikov's perturbation method* [62] for locating homoclinic points in periodically perturbed differential equation systems. It can be *analytically* calculated with the information about the corresponding integrable Hamiltonian systems. In addition to the derivation, this chapter applies the proposed criterion to the analysis of the stability boundaries in the swing equation system and shows the effectiveness of the criterion.

Chapter 4 discusses basin boundaries of resonant solutions in the swing equation system. The proposed criterion in Chapter 3 addresses the basin boundaries of *non-resonant* solutions and is not effective if the genesis of *resonant* solutions happens in the non-autonomous systems. To overcome the disadvantage, we consider the basin boundaries of the resonant solutions in ODF time-periodic perturbed Hamiltonian systems based on the *subharmonic Melnikov functions* [62] and related theories [32, 33, 35, 108]. An analytical criterion is then derived for the basin boundaries of the resonant solutions. The derived criterion is

established with the corresponding integrable Hamiltonian systems and therefore makes it possible to clarify stability boundaries related to the resonant solutions analytically. This chapter also applies the present criterion to the stability boundary analysis of the swing equation system.

Chapters 5 and 6 analyze transient dynamics and stability boundaries with considering dc system's operation and electric power balance relation between the ac and dc systems. Chapters 2–4 examine the transient stability based on the swing equation system. It is then assumed that the dc link is ideally operated, and its electric power is constant. This assumption is, however, insufficient for considering transient stability involving dynamical characteristics of the dc system. For example, the dc power modulation is considered in [21, 23, 30, 89, 98] for damping power swings in ac transmission systems. The control strategy exploits an effective characteristic in the rapid regulation of the electric power according to event disturbances. Obviously, such ac/dc systems cannot be analyzed under the previous assumption. Thus it is necessary to consider the transient dynamics and stability boundaries related to the dc operation and the power balance relation.

In Chapter 5, we derive a DAE system for the transient stability analysis involving dynamical characteristics of the dc system. The DAE system keeps the structural characteristics of power conversion and control setup, and explicitly describes the electric power relation between the ac and dc systems. It is noted that similar DAE systems are derived for general ac/dc power systems in [11, 67, 68]. This chapter numerically investigates some dynamical features of the DAE system and clarifies a stability boundary through several basin portraits. The obtained result shows a new insight on the dynamical features of the stability boundary.

Chapter 6 performs two theoretical studies related to the stability boundaries in the DAE system. The first study is to characterize the stability boundaries using the *singular perturbation technique*. The singular perturbation plays an important role in studying multi-time scale dynamical and control systems: see e.g. [34, 49, 53]. In this chapter, we derive complete characterization of the stability boundaries via an energy function for the associated singularly perturbed (SP) system. The derivation strongly relies on some fundamental results reported in [15]. The obtained characterization shows entire global structures of the stability boundaries in the solution space of the DAE system. In addition,

the characterization is examined via several numerical results on a stability boundary in Chapter 5. On the other hand, the second work is to analyze discontinuous solutions which are due to structural change of the network configuration. To apply the analytical results in Chapters 5 and 6 to the practical stability estimation, it is necessary to consider particular discontinuous solutions in the DAE system with respect to practical faults conditions. The existence of the discontinuous solutions has been already reported for network-preserving power system models in [14,15,18,74,111]. In this chapter, we numerically and analytically examine several discontinuous solutions of the DAE system and clarify a fault condition under which the DAE system is not valid for the transient stability analysis. The obtained results in this chapter delineate how the dc operation affects the transient dynamics and stability boundaries.

Chapter 7 concludes this dissertation with brief summary and collects future research directions.

In summary, this dissertation is concerned with the transient stability of the electric power system with dc transmission. One future goal of this research is to clarify the mechanism behind the synchronization through electric power transmission. To find a clue as to the mechanism, the transient dynamics and stability boundaries are here addressed for the ac/dc power system. Obviously, the dynamical features show one aspect of the synchronization; however, the obtained results will shed a ray of light on the open problem. In addition, another goal is to establish comprehensive methodologies for operation and control of future power supply networks involving various dc-based power apparatuses; they are hvdc links, HVDC Light, UPFC [20], and distributed power sources. Although the obtained results here are restricted to the particular ac/dc system, they can be applied without essential modification to other practical systems. The author believes that this dissertation contains significant contributions towards the future goals.

Supplemental general facts of dc transmission

One of the important objectives of electric power systems is to deliver electric power from generating facilities to customers. An electric power system consists of three individual sections: generation, transmission, and distribution. Generation of electric power

is basically undertaken by synchronous machines: recently distributed power sources have been increased such as photovoltaic and wind power generations. In the transmission and distribution sections, two different schemes are basically available for the delivery of electric power: ac and dc transmission. They have both advantages and disadvantages of the power delivery and are therefore utilized as appropriate according to their conditions. Without their adequate adoption, safe planning and operation could not be achieved for present and future power systems.

AC transmission is usually adopted in hv power transmission systems. An ac transmission system connects two different ac power systems under the synchronized operation. Transformers can be here used to connect parts of ac systems which are operated at different voltage levels. In fact, this promoted the adoption of the hvac link in the early days of power systems. However, the ac transmission has several disadvantages for system operation and planning. The ac interconnected power system possesses an inherent limitation of the power delivery caused by ac line characteristics. It appears as a serious problem in long distance or cable transmission. Furthermore, it is hard to control electric power rapidly and arbitrarily, because the ac link is tightly formed under the synchronized operation of all the generators. This especially makes it impossible to connect power systems with different frequencies via the ac link.

DC transmission, on the other hand, has recently appeared in conventional ac power systems. A dc link mainly consists of converter stations and dc lines [5, 40, 59, 71]. The stations convert ac voltages into dc ones and vice versa using rectification of power devices, and dc lines connect these stations via smoothing reactors and filters. The dc link can be in principle operated under desynchronized state with ac power systems, although the rectification need to be controlled in synchronization with ac voltages. This has stimulated the adoption of the dc link to connect ac power systems with different frequencies. In addition, the ac/dc interconnected system does not basically possess any limitation of the power delivery except heat capacity of the dc lines. On the other hand, the dc transmission has some disadvantages: inability to use the transformers to change voltage levels and high cost of conversion equipment, and so on [67].

Modern dc transmission begun in 1954 when a 100 kV and 20 MW dc link was established between the Swedish mainland and the island of Gotland [52, 59, 67]. The converter

stations used mercury arc valves for rectification. In the 1970s, the innovation of hv power semiconductor devices made it possible to use thyristors for power conversion. Since then the application of the dc transmission has increased until there are now schemes in every continent over 70 installations with excess of 60 GW; individual links range from 20 MW to 6300 MW in capacity [40]. In Japan, since a 125 kV and 300 MW dc link started to be operated in 1965 to connect ac 50 Hz and 60 Hz networks at Sakuma, 6 dc links have been in service with combined capacity in 4.9 GW [59]. A hvdc link was particularly commissioned in 2000 which connected ac 500 kV networks of The Shikoku and The Kansai Electric Companies across Kii Channel at the rating of $\pm$500 kV and 2800 MW [30,41,77]. The hvdc link is well-known as one of the largest dc systems in the world. The rationale behind such adoptions is identified by technical abilities and non-technical issues related to the dc transmission.

The dc transmission has been traditionally utilized in areas where there is a clear financial advantage or where it is technically the only solution. From the above discussion and [5,40,59,71], the application areas of the dc transmission are as follows:

1. *Long distance transmission*: for long distance, dc links involve lower costs than ac transmission systems because the dc lines can be designed in a simpler way than ac ones. The dc links can also overcome inherent limitation of the power delivery caused by long ac links.

2. *Submarine cable transmission*: similar economical advance of dc links is also valid for submarine cable power delivery. There is also no limit to distance in the dc cable connection since the dc links do not need any continuous charging current.

3. *Asynchronous connection*: dc links make it possible to connect different ac power systems under the desynchronized operation. The connection can also be used to improve reliability/performance of the ac power systems.

Many dc links are in redundant application areas: for example, The Kii Channel HVDC Link is mainly categorized into the areas 2 and 3. In addition to these applications, another necessity of the dc transmission has recently appeared in response to global trends in power industry.

The dc technology plays a key role in future power transmission under competitive power markets [40]. Nowadays, regulatory reforms of power markets have a substantial impact on conventional power systems. As a result, competitive power markets will be introduced into the conventional systems. The introduction imposes it on system engineers to develop a comprehensive strategy for delivering electric power in safe, reliable, and economic manner. Then, the dc transmission has a potential to offer an essential solution for the requirement. For example, the long distance dc link is possibly used for delivering cheap electric power which is generated off the map. In addition, dc-based power apparatuses, many of which are categorized into FACTS (Flexible AC Transmission System) [20] devices such as STATCOM and UPFC, are considered as other schemes for operation of deregulated power systems. Hence, the importance of the dc technology has been increasing in electric power systems and has proposed the necessity of fundamental research of stability problem of electric power systems with dc transmission.

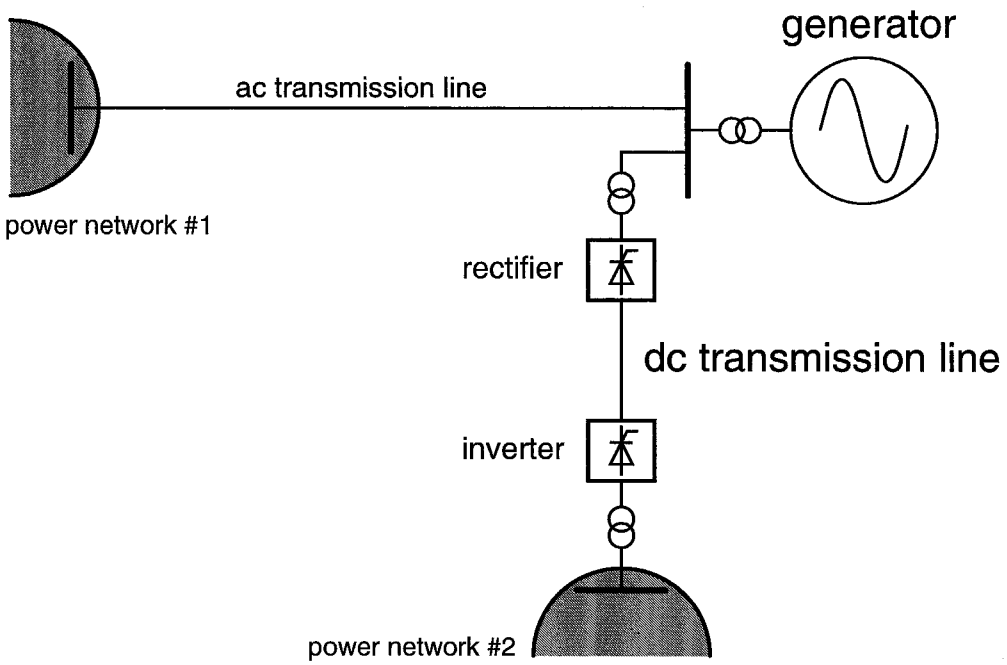

Figure 1.1 Conceptual diagram of electric power system with dc transmission. A generator runs on two power networks via an ac transmission line and a dc link. The objective of this dissertation is to study the transient dynamics of the power system affected by the dc link.

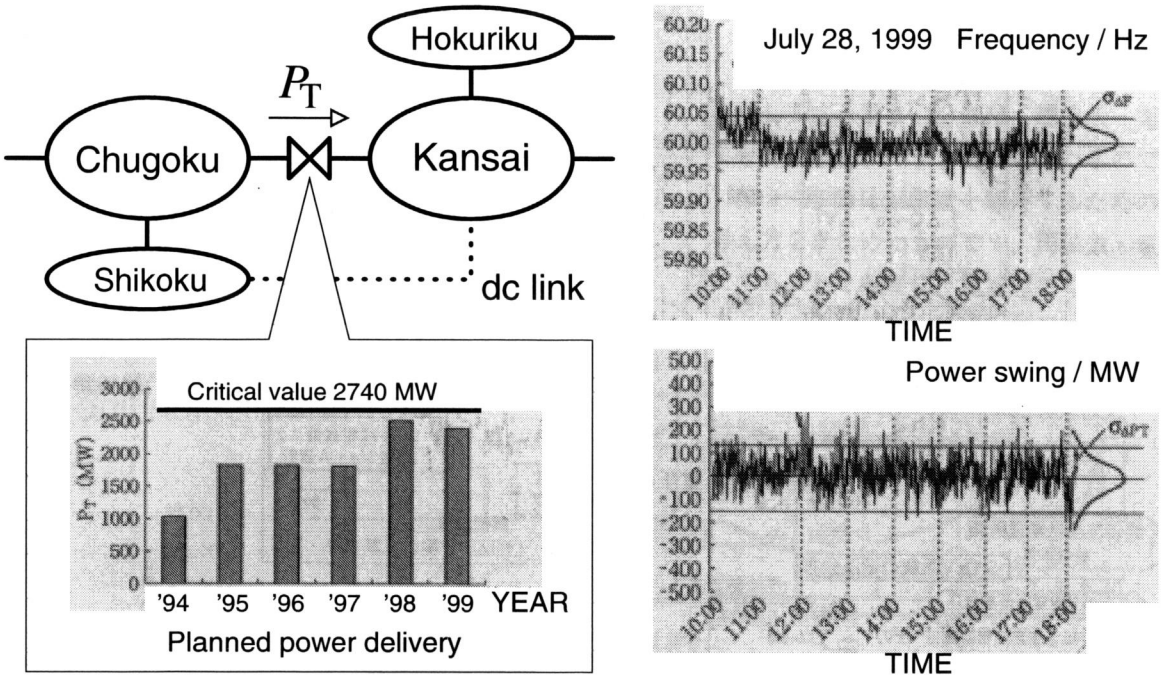

Figure 1.2 Practical measurement of frequency and power swings at The Nakanishi Transmission Line in Japan [80]. The measured power swing denotes the difference between actual and planned conveying volume. The transmission line connects the two large networks: the Kansai and Chugoku areas. The power swing is expected to be damped by the dc power modulation.

Chapter 2

Transient dynamics and fractal stability boundary

The second chapter analyzes transient dynamics affected by electric power which flows in the dc link. This analysis is performed based on an unsymmetrical swing equation system. The unsymmetry implies a unidirectional component of an external forcing which corresponds to both the dc power and a periodic power swing. The swing equation system has the common mathematical structure to various physical and engineering systems: forced pendulums [25, 36], Josephson junction circuits [37, 48, 73], phase-locked loops [27, 28, 66], and so on. However, the dynamical behavior affected by the dc external force has been unsolved for these systems, although some studies on Duffing equation with unsymmetrical force are reported in [43, 91]. The dynamical behavior remains unclear in the fields of not only power system dynamics but also nonlinear oscillation theory.

As an important aspect of the dynamical behavior we consider a stability boundary and its qualitative change in the swing equation system. This chapter shows that the fractal structure grows in the stability boundary caused by the dc external forcing. The fractal growth indicates from the viewpoint of power system stability that we cannot inherently predict the transient dynamics of the ac/dc system if its post-fault state is placed around the boundary. The fractal structure is numerically and analytically discussed through dynamical system theory.

2.1 Swing equation system

2.1.1 Derivation

A swing equation system is derived to represent the dynamics of the ac/dc power system shown in Fig. 2.1. The ac/dc system consists of one generator-infinite bus system and a dc link. An *infinite bus* in the figure is a source of voltage constant in phase, magnitude, and frequency, and not affected by the amount of current withdrawn from it [51]. A large power network is usually regarded as an infinite bus. A sinusoidal power swing in Fig. 2.1 is also assumed which exists in the ac transmission line and flows into the generator bus. The power swing is observed in the practical system as shown in Fig. 1.2; it is expected to be damped by the dc power modulation. In Fig. 2.1 the dc link is assumed to be ideally operated. The main reason is that this chapter aims to clarify the rotor dynamics of the generator affected by the constant dc power. It does not loose the generality of discussion. In the figure, $p_{\mathrm{e(ac)}}$ denotes the electric power which flows into the infinite bus, and can be approximately given by

$$p_{\mathrm{e(ac)}} = b\sin\delta - \varepsilon b\cos\Omega t, \tag{2.1}$$

where the physical meanings of variables and parameters are shown in Tab. 2.1. $p_{\mathrm{e(dc)}}$ denotes the constant dc power. The rotor dynamics of the generator is then represented as the following swing equation system with unsymmetrical force:

$$\begin{cases} \dfrac{\mathrm{d}\delta}{\mathrm{d}t} = \omega \\ \dfrac{\mathrm{d}\omega}{\mathrm{d}t} = -D\omega + p_{\mathrm{m}} - \left(p_{\mathrm{e(ac)}} + p_{\mathrm{e(dc)}}\right). \end{cases} \tag{2.2}$$

In the system, the external force $(p_{\mathrm{m}} - p_{\mathrm{e(dc)}}) + \varepsilon b\cos\Omega t$ is unidirectional; it is called unsymmetrical forcing. All variables and parameters of the system (2.2) are in per unit except angle which is in radian. The detailed derivation is given in the appendix at the end of this chapter.

The swing equation system (2.2) is relevant to analyzing the transient dynamics of the ac/dc power system under the assumption that the dc link is ideally operated. The transient dynamics and stability of ac power systems are essentially governed by electric

power balance in the networks of interacting generators and loads [51, 60]. From this physical point of view, the system (2.2) describes the power balance relation with the generator, infinite bus, and dc link. Furthermore, transient stability in multi-machine ac/dc systems is discussed in [70] via the similar swing equation system including control setup of rectifiers; swing dynamics in one generator-infinite bus system with UPFC is considered in [60] based on the same mathematical model. Hence, the transient dynamics of the ac/dc system can be discussed based on the system (2.2).

2.1.2 Dynamical properties

This subsection provides us with some dynamical properties of the swing equation system (2.2), which are often used in the following sections.

A. Two kinds of periodic solutions

The system (2.2) has two kinds of periodic solutions $(\delta(t), \omega(t))$ because of the periodicity of 2π for $\delta(t)$. In [63] one is called *first kind* periodic solution which has the following property:

$$\delta\left(t+\frac{2\pi}{\Omega}\right) \equiv \delta(t), \quad \omega\left(t+\frac{2\pi}{\Omega}\right) \equiv \omega(t) \quad \text{for } t \in \mathbb{R}, \tag{2.3}$$

and the other is a *second kind* periodic solution if there exists an integer number $m \in \mathbb{Z}\backslash\{0\}$ such that

$$\delta\left(t+\frac{2\pi}{\Omega}\right) \equiv \delta\left(t\right)+2m\pi, \quad \omega\left(t+\frac{2\pi}{\Omega}\right) \equiv \omega\left(t\right) \quad \text{for } t \in \mathbb{R}, \tag{2.4}$$

where each solution keeps the period $2\pi/\Omega$ constant.

B. Discrete dynamical system and stability

A *discrete dynamical system* on the cylindrical phase plane $\mathbb{S}^1 \times \mathbb{R}$ is introduced through the stroboscopic sampling of solutions in the system (2.2) at $t = 2n\pi/\Omega$ $(n \in \mathbb{Z})$:

$$\mathscr{F}_\lambda : \quad \mathbb{S}^1 \times \mathbb{R} \to \mathbb{S}^1 \times \mathbb{R}, \tag{2.5}$$

where λ denotes the set of parameters in the system (2.2). By utilizing the discrete system $\mathscr{F}_\lambda$, we can investigate the original non-autonomous system (2.2) indirectly through the

autonomous discrete system on $\mathbb{S}^1 \times \mathbb{R}$. The discrete system transforms the above periodic solutions to the fixed points at which associated linearized maps decide the kind of their stability. Tab. 2.2 shows the classification of stability in a fixed point if any eigenvalue of the linearized map differs from unity, that is, is of *general type* [57].

C. Doubly asymptotic points [9]

Directly or inversely unstable fixed points have the two types of invariant manifolds: *stable* and *unstable manifolds.* If stable and unstable manifolds intersect each other, the points of intersection are called *doubly asymptotic points.* A doubly asymptotic point is particularly called *homoclinic* if stable and unstable manifolds issue from the same fixed point or from two points which belong to the same periodic group. For convenience, let us say that homoclinic points of the former type are *simple.* On the other hand, a doubly asymptotic point is called *heteroclinic* if stable and unstable manifolds issue from the different points. A doubly asymptotic point is also said to be of *general case* if the two manifolds actually cross at the point, i.e., intersect *transversally.* In the contrary case, that is, if the two manifolds do not intersect transversely, the point is of *special case.* When a discrete dynamical system has no doubly asymptotic point of special type and no fixed or periodic point of not general type, the system is said to belong to the *general analytic case.* In the general analytic case on phase plane $\mathbb{R} \times \mathbb{R}$, homoclinic points have the following remarkable properties pertinent to the existence of chaotic attractors and fractal basin boundaries:

Theorem 2.1 [9] *In the general analytic case on phase plane,*

- *an arbitrary small neighborhood of a homoclinic point contains infinitely many periodic points;*
- *an arbitrary small neighborhood of a homoclinic point contains homoclinic points of simple type.*

D. Melnikov's perturbation method

An existence condition of doubly asymptotic points is given for invariant manifolds in the swing equation system (2.2). The system is one of ODF periodically perturbed

Hamiltonian systems. The Melnikov's method [62] therefore has a potential to clarify the global dynamics of the system (2.2): see e.g. [27, 35, 73, 108]. The Hamiltonian system, which $D = 0$, $p_{\mathrm{m}} - p_{\mathrm{e(dc)}} = 0$, and $\varepsilon = 0$, has the following homoclinic orbit:

$$(\delta_0^{\pm}(t), \omega_0^{\pm}(t)) = \left(\pm 2 \arcsin\left(\tanh(\sqrt{b}t)\right), \pm 2\sqrt{b}\,\mathrm{sech}(\sqrt{b}t)\right). \tag{2.6}$$

Under sufficiently small perturbation $(D, p_{\mathrm{m}} - p_{\mathrm{e(dc)}}, \varepsilon)$, we obtain the existence condition of doubly asymptotic points in the region $\omega > 0$ as follows:

$$\varepsilon b \geq \left| \frac{4D\sqrt{b}}{\pi} - \left(p_{\mathrm{m}} - p_{\mathrm{e(dc)}}\right) \right| \cdot \cosh\left(\frac{\Omega\pi}{2\sqrt{b}}\right). \tag{2.7}$$

The existence of doubly asymptotic points in the region $\omega < 0$ is also conditioned by

$$\varepsilon b \geq \left| \frac{4D\sqrt{b}}{\pi} + \left(p_{\mathrm{m}} - p_{\mathrm{e(dc)}}\right) \right| \cdot \cosh\left(\frac{\Omega\pi}{2\sqrt{b}}\right). \tag{2.8}$$

We should note that the obtained conditions correspond to the existence of *heteroclinic* points if the discrete system (2.5) is defined on phase plane $\mathbb{R} \times \mathbb{R}$ [92]. The derivation of the conditions is confirmed in [27].

2.2 Bifurcation diagram

Figure 2.2 shows the bifurcation diagrams in the control plane $(p_{\mathrm{m}} - p_{\mathrm{e(dc)}}, \varepsilon, \Omega)$ of the discrete dynamical system (2.5) at the following parameters:

$$D = 0.05, \quad b = 0.7. \tag{2.9}$$

The value of Ω in Fig. 2.2(a), i.e, $\Omega = 0.5$ corresponds to $2\pi/(0.86\ \mathrm{s})$ in the practical time. The angular frequency is included in the time range for the occurrence of *nonlinear resonance* [88,97], which is actually observed in Figs. 2.2(b) and (c), and sub-synchronous resonance [60]. All values of parameters are based on the practical system [30, 77, 80, 87]: see Fig. 1.2 and Tab. 2.3. In Fig. 2.2, the curves Melnikov Criteria present the boundaries in which doubly asymptotic points appear; the points qualitatively have the identical properties to those of heteroclinic points on the phase plane. The criteria are induced from the conditions (2.7) and (2.8). The curves Fold (Sync.) are the boundaries which correspond

to the occurrence of synchronization into second kind limit cycles which the system (2.2) under $\varepsilon = 0$ has depending on $p_{\rm m} - p_{\rm e(dc)}$. From the practical points of view, the synchronized state represents an unacceptable state of the ac/dc system shown in Fig. 2.3(c). In addition, the curves Period-Doubling (Sync.) correspond to the threshold sets of the period-doubling bifurcation of second kind sinks. The bifurcation sets Fold B show the generation of first kind *resonant* fixed points through the fold bifurcation. The resonant solutions usually have larger amplitude of oscillation than that of *non-resonant* solutions as shown in Figs. 2.3(a) and (b). Furthermore, the curves Period-Doubling C exhibit the period-doubling bifurcation sets with respect to the resonant sinks. The bifurcation sets Fold A in Figs. 2.2(b) and (c) represent the disappearance of non-resonant sinks and the resonant saddles by the fold bifurcation. Fig. 2.3(d) also shows an aperiodic steady state which corresponds to a second kind invariant closed curve in the discrete system (2.5); it coincides with another undesirable condition of the ac/dc system.

2.3 Fractal growth in stability boundary

This section discusses a global bifurcation and associated fractal stability boundary by the change of the dc external force $p_{\rm m} - p_{\rm e(dc)}$ under the parameters setting:

$$D = 0.05, \quad b = 0.7, \quad \Omega = 0.5. \tag{2.10}$$

2.3.1 Global bifurcation and self-similar structure

A global bifurcation scenario is investigated according to the change of $p_{\rm m} - p_{\rm e(dc)}$. Fig. 2.4 shows the phase and basin portraits of the discrete dynamical system (2.5) under $(p_{\rm m} - p_{\rm e(dc)}, \varepsilon) = (0.06, 0.1)$ and $(0.07, 0.1)$. In each phase portrait, the symbol ${}^{j}\mathsf{D}^{k}_{(i)}$ denotes the i-th directly unstable j-th kind k-periodic directly unstable point. The *solid* line in the figures represents the unstable manifold of the resonant fixed point ${}^{1}\mathsf{D}^{1}_{(2)}$ and the *broken* line its stable manifold. In the basin portraits, 401×401 cells are used as initial conditions for numerical integration, and the initial conditions are classified as follows: the *white* region is the basin of the non-resonant point ${}^{1}\mathsf{S}^{1}_{(1)}$ and the *black* the basin of the resonant one ${}^{1}\mathsf{S}^{1}_{(2)}$. In addition, the *gray* region shows the basin of the second kind sink ${}^{2}\mathsf{S}^{1}_{(2)}$ under

$p_{\mathrm{m}} - p_{\mathrm{e(dc)}} = 0.06$ and the invariant closed curve, denoted by ICC in Fig. 2.4(b), under $p_{\mathrm{m}} - p_{\mathrm{e(dc)}} = 0.07$. Here, Fig. 2.4 describes the qualitative change of the phase portraits by the global bifurcation scenario. Fig. 2.5 shows the global bifurcation scenario by the increase of $p_{\mathrm{m}} - p_{\mathrm{e(dc)}}$. In Fig. 2.5(a), the unstable manifold of ${}^1\mathsf{D}^1_{(2)}$ converges to ${}^1\mathsf{S}^1_{(2)}$ and does not intersect the stable manifold of ${}^1\mathsf{D}^1_{(2)}$. The small increase of $p_{\mathrm{m}} - p_{\mathrm{e(dc)}}$ raises the intersection of the stable and unstable manifolds of ${}^1\mathsf{D}^1_{(2)}$ as shown in Fig. 2.5(b). These points are doubly asymptotic points, and the qualitative change is a global bifurcation.

The basin boundary of ${}^1\mathsf{S}^1_{(2)}$ then shows the self-similar structure caused by the global bifurcation. Fig. 2.6 shows the magnifications of basin portraits in the neighborhood of ${}^1\mathsf{D}^1_{(2)}$. In Figs. 2.5(a) and 2.6(a), the basin boundary of ${}^1\mathsf{S}^1_{(2)}$ consists of the stable manifold of ${}^1\mathsf{D}^1_{(2)}$, and the basin boundary is smooth. When $p_{\mathrm{m}} - p_{\mathrm{e(dc)}}$ increases, the basin boundary in Fig. 2.6(b) appears to be complicated. Fig. 2.6(b) also shows that the boundary has the self-similarity for the magnification of the small rectangles.

2.3.2 Doubly asymptotic points and fractal stability boundary

The self-similar basin boundary does not necessarily become fractal on the cylindrical phase plane. Generally speaking, complicated basin boundaries possibly appear when doubly asymptotic points exist in the phase plane. In particular, if such boundaries exist in the phase plane and transversal homoclinic points appear, then the boundaries become fractal [65]. However, the criterion cannot be applied to the discrete system (2.5) because the system is defined on the cylindrical phase plane [92]. Thus it is necessary to reconsider the basin boundary structure through dynamical system theory.

The basin boundary in Fig. 2.6(b) has the infinite self-similar structure which is qualitatively identical to fractal structure caused by transversal homoclinic points on the phase plane. In Fig. 2.5(b), all doubly asymptotic points are based on the invariant manifolds of the *first kind* saddle ${}^1\mathsf{D}^1_{(2)}$. The first kind saddle is qualitatively identical to hyperbolic saddles of discrete dynamical systems on the phase plane. Fig. 2.5(b) also shows that the points consist of the intersection between the invariant manifolds which can be described in the rectangle region of this figure. Fig. 2.7 schematically shows the global bifurcation scenario and doubly asymptotic structures of the discrete system (2.5). These evidences imply

that the doubly asymptotic points in Fig. 2.5(b) qualitatively coincide with the transversal homoclinic points on the phase plane. Hence, we conclude that the self-similar boundary of ${}^{1}\mathsf{S}^{1}_{(2)}$ becomes fractal.

2.3.3 Physical interpretation

The fractal stability boundary indicates that the system behavior becomes unpredictable depending on the operation of the dc link. In Fig. 2.4, the stable manifold of ${}^{1}\mathsf{D}^{1}_{(2)}$ becomes a part of the basin boundary of the non-resonant point ${}^{1}\mathsf{S}^{1}_{(1)}$. In addition, ${}^{1}\mathsf{S}^{1}_{(2)}$ corresponds to an undesirable operation because of its large amplitude of oscillation as shown in Fig. 2.3. Namely, the fractal structure grows in the stability boundary of the acceptable operating condition in the ac/dc power system. This implies that we cannot precisely predict the transient dynamics of the ac/dc system when its state is placed around the boundary by some event disturbances.

We should note that the fractal boundary is a native dynamical feature of the ac/dc power system under external power disturbance. The system (2.2) is derived under the assumption that the dc link is ideally operated. The mechanism behind the fractal growth therefore originates from not switching operation in converter stations but the electric power balance in the ac/dc system. As mentioned in Section 2.1, the power balance relation essentially governs the transient dynamics of the ac/dc power system. Thus it can be stated that the transient dynamics inherently becomes indeterminate although the dc link is safety operated.

2.4 Summary and discussion

An aspect of the transient dynamics was numerically and analytically discussed based on the swing equation system (2.2). The system has the fractal basin boundary depending on the dc external forcing. In [28,31,36] the existence of fractal basin boundaries has been already reported for the similar swing equation systems. The fractal basin boundaries were, however, considered based on numerical simulation or the Melnikov's method. As discussed in Section 2.1, the Melnikov's method reveals only the existence of doubly asymptotic points

which are identical to *heteroclinic* points in the phase plane, and does not therefore justify the existence of the fractal basin boundaries. On the other hand, in this chapter, we characterize the fractal basin boundary of the system (2.2) based on doubly asymptotic structure in the cylindrical phase plane. Furthermore, in [42, 101], complicated stability boundaries were reported for multi-degree-of-freedom swing equation systems which are derived to analyze transient stability of ac power systems. It was then concluded that the boundaries would not become fractal, which were called truncated-fractal [101]. The fractal boundary in the chapter therefore shows a new indeterminate factor in power system stability.

Appendix to Section 2.1: Detailed derivation of swing equation system

The rotor dynamics of a generator is represented in [51, 60] as follows:

$$J\frac{\mathrm{d}^2\theta}{\mathrm{d}t} = \tau_{\mathrm{m}} - \tau_{\mathrm{e}}, \tag{2.11}$$

where J denotes the rotor moment of inertia, τ_{m} the mechanical input torque, and τ_{e} the electro-magnetic output torque. θ is the rotor angular displacement given by

$$\theta \triangleq \omega_{\mathrm{b}} t + \delta, \tag{2.12}$$

where ω_{b} stands for the system angular frequency and δ the rotor position with respect to synchronous reference axis. The mechanical input power p_{m} and electric output power p_{e} are given by

$$p_{\mathrm{m}} = \frac{\mathrm{d}\theta}{\mathrm{d}t}\tau_{\mathrm{m}}, \quad p_{\mathrm{e}} = \frac{\mathrm{d}\theta}{\mathrm{d}t}\tau_{\mathrm{e}}, \tag{2.13}$$

respectively. Since $\mathrm{d}\delta/\mathrm{d}t$ is usually much smaller than ω_{b} [51, 60], the following equation is obtained:

$$J\frac{\mathrm{d}^2\delta}{\mathrm{d}t^2} \simeq \frac{1}{\omega_{\mathrm{b}}}\left(p_{\mathrm{m}} - p_{\mathrm{e}}\right). \tag{2.14}$$

The rotor moment J is here given by

$$J \triangleq \frac{2HP_{\mathrm{r}}}{\omega_{\mathrm{b}}^2}, \tag{2.15}$$

where H denotes the inertia constant and $P_{\rm r}$ the rating of the generator. Thus the non-dimensional swing equation is derived as follows:

$$\begin{cases} \dfrac{\mathrm{d}\delta}{\mathrm{d}t^*} &= \omega^*, \\ \dfrac{\mathrm{d}\omega^*}{\mathrm{d}t^*} &= p_{\rm m}^* - p_{\rm e}^* - D^*\omega^*, \end{cases} \tag{2.16}$$

where

$$\begin{cases} t^* \triangleq t\sqrt{\dfrac{\omega_{\rm b}}{2H}} & : \text{normalized time,} \\ \omega^* \triangleq \dfrac{\mathrm{d}\delta}{\mathrm{d}t}\sqrt{\dfrac{2H}{\omega_{\rm b}}} & : \text{normalized rotor speed deviation relative to system angular frequency,} \\ p_{\rm m}^* \triangleq \dfrac{p_{\rm m}}{P_{\rm r}} & : \text{normalized mechanical input power,} \\ p_{\rm e}^* \triangleq \dfrac{p_{\rm e}}{P_{\rm r}} & : \text{normalized electric output power,} \\ D^* & : \text{damping coefficient in generator.} \end{cases} \tag{2.17}$$

The electric output power $p_{\rm e}^*$ flows into both the ac and dc transmission systems as shown in Fig. 2.1. $p_{\rm e}^*$ is decomposed into

$$p_{\rm e}^* = p_{\rm e(ac)}^* + p_{\rm e(dc)}^*. \tag{2.18}$$

where $p_{\rm e(ac)}^*$ and $p_{\rm e(dc)}^*$ stand for the electric power which flows in the ac and dc links, respectively. In $p_{\rm e(ac)}^*$, the power term $p_{\rm e(ac,sync)}$ is related to the synchronized operation with the infinite bus. From [51, 60] the term is approximately given by

$$p_{\rm e(ac,sync)}^* = \frac{E_\infty^* E_q'^*}{X^*}\sin\delta, \tag{2.19}$$

where E_∞^* is the infinite bus voltage, $E_q'^*$ the voltage source behind transient reactance, and X^* the combined reactance of the transient reactance of the generator, the reactance of step-up transformer and ac transmission line. The critical value b^* is defined by

$$b^* \triangleq \frac{E_\infty^* E_q'^*}{X^*}. \tag{2.20}$$

By adding the exciting power term in Section 2.1, $p_{\rm e(ac)}^*$ is represented as follows:

$$p_{\rm e(ac)}^* = p_{\rm e(ac,sync)}^* - \varepsilon b^* \cos\Omega^* t^*, \tag{2.21}$$

where ε denotes the ratio of amplitude of an exciting power swing to the critical value b^* and Ω^* the angular frequency of the exciting power swing. Chapter 2 omits $*$ on the variables and parameters for simplicity.

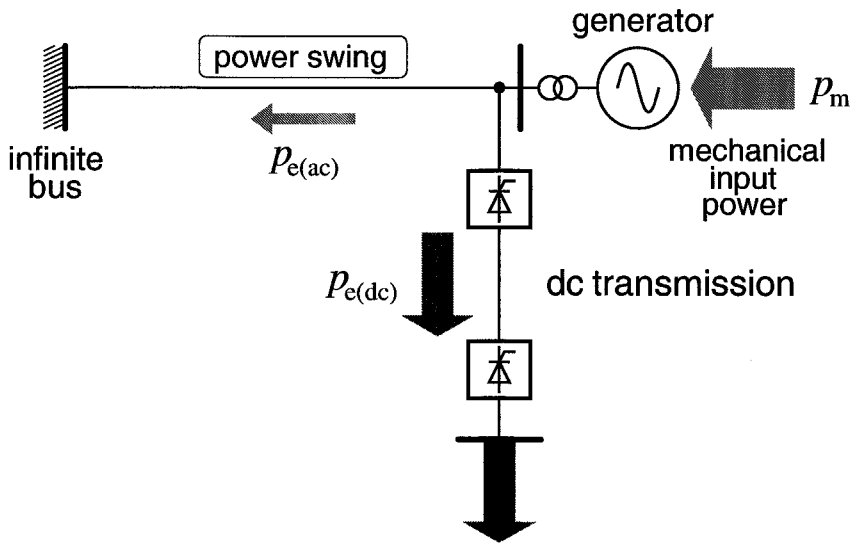

Figure 2.1 Configuration of ac/dc power system for swing equation system (2.2)

Table 2.1 Physical meanings of variables and parameters in swing equation system (2.2). All variables and parameters are in per unit except angle which is in radian.

δ	rotor position with respect to synchronous reference axis
ω	rotor speed deviation relative to system angular frequency
t	normalized time
D	damping coefficient in generator
b	critical value of one generator-infinite bus system
p_m	mechanical input power of generator
$p_{e(dc)}$	electric power which flows in dc link
ε	ratio of amplitude of exciting power swing to critical value
Ω	angular frequency of exciting power swing

Table 2.2 Classification of stability in fixed point of general type [57]

				symbol
sink	or	completely stable	$\|\rho_1\|,\ \|\rho_2\| < 1$	S
source	or	completely unstable	$\|\rho_1\|,\ \|\rho_2\| > 1$	U
saddle	or	directly unstable	$0 < \rho_1 < 1 < \rho_2$	D
saddle	or	inversely unstable	$-1 < \rho_1 < 0 < \rho_2$	I

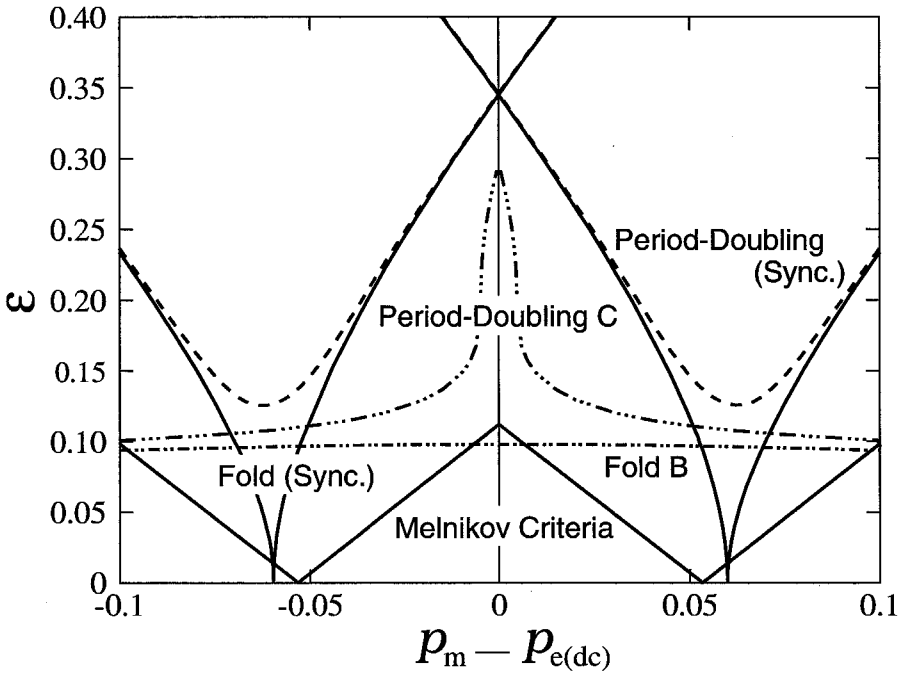

(a) $\Omega = 0.5$

Figure 2.2 Bifurcation diagrams of discrete dynamical system (2.5). The parameters setting is as follows: $D = 0.05$ and $b = 0.7$.

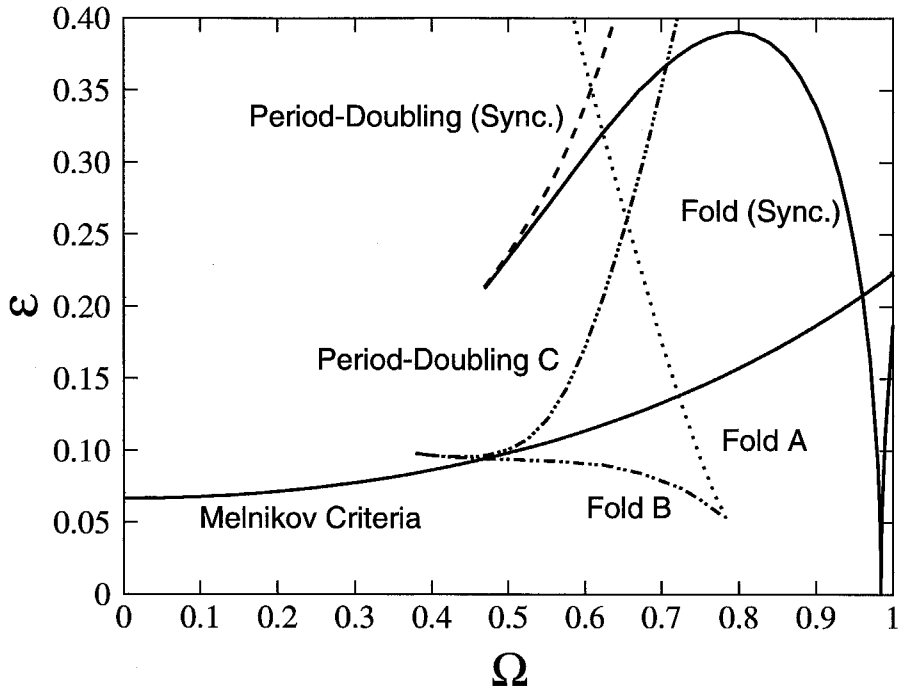

(b) $p_{\mathrm{m}} - p_{\mathrm{e(dc)}} = 0.1$

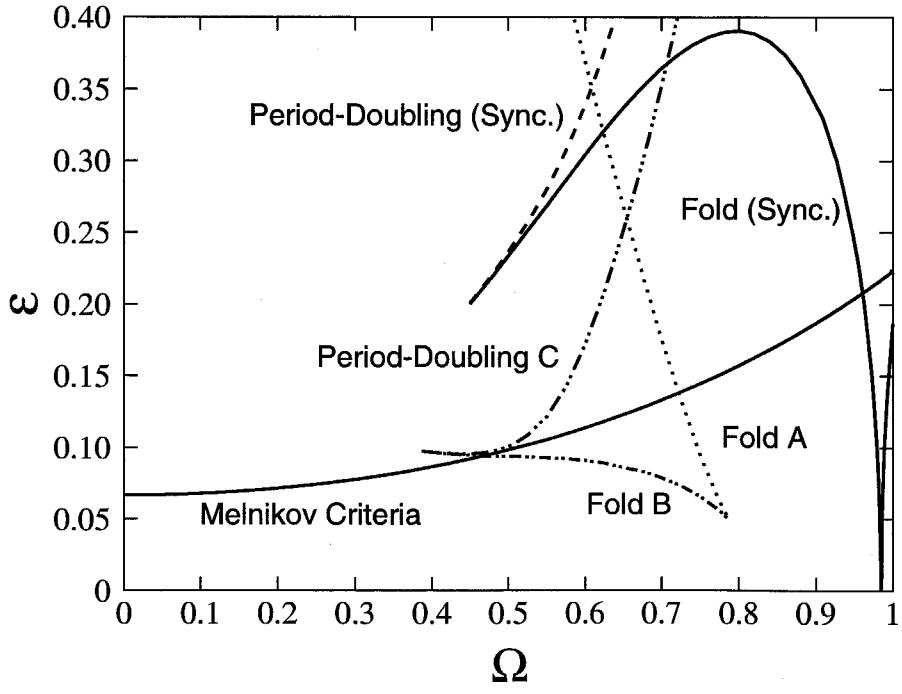

(c) $p_{\mathrm{m}} - p_{\mathrm{e(dc)}} = -0.1$

Figure 2.2 (*continued*)

Table 2.3 System parameters and base quantities for swing equation system (2.2)

(a) Network parameters

system frequency	60 Hz
ac line reactance	0.95 mH/km
ac line length	220 km
impedance of step-up transformer	0.16

(b) Parameters of generator

rating	2.80 GVA
inertia constant	0.89 s
d-axis transient reactance	0.34

(c) Base quantities

base quantities	generator side	infinite bus side
power	2.80 GVA	2.80 GVA
voltage	12.5 kV	500 kV
current	129.3 kA	3.233 kA
impedance	0.05581 Ω	89.29 Ω

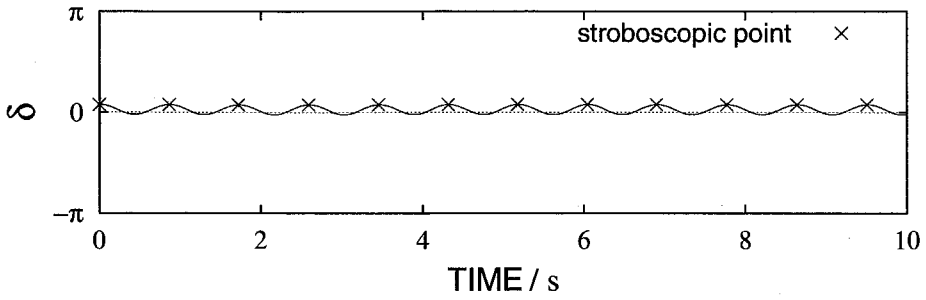

(a) First kind non-resonant solution at $(p_{\mathrm{m}} - p_{\mathrm{e(dc)}}, \varepsilon) = (0.06, 0.1)$

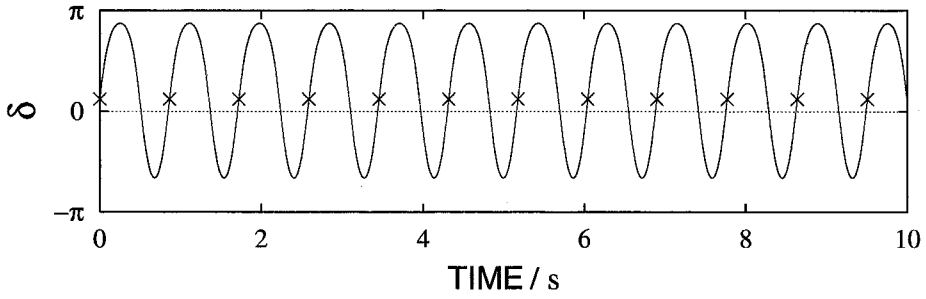

(b) First kind resonant solution at $(p_{\mathrm{m}} - p_{\mathrm{e(dc)}}, \varepsilon) = (0.06, 0.1)$

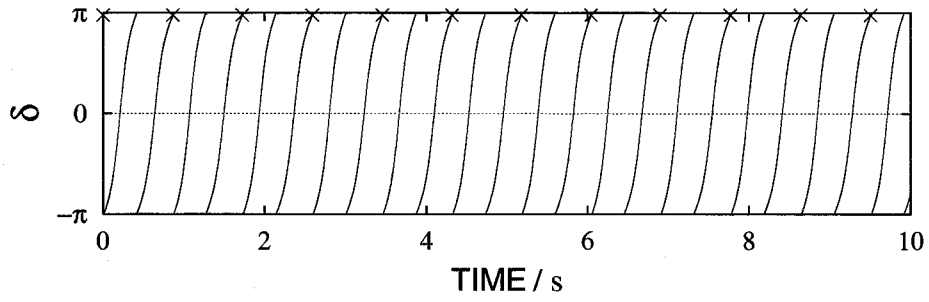

(c) Second kind solution at $(p_{\mathrm{m}} - p_{\mathrm{e(dc)}}, \varepsilon) = (0.06, 0.1)$

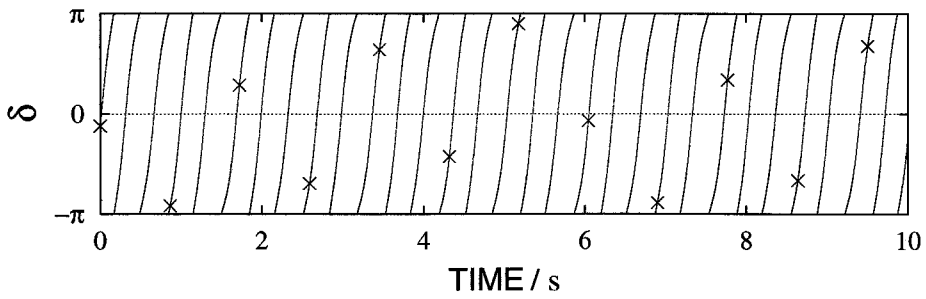

(d) Aperiodic solution which corresponds to second kind invariant closed curve at $(p_{\mathrm{m}} - p_{\mathrm{e(dc)}}, \varepsilon) = (0.07, 0.1)$

Figure 2.3 Waveforms of rotor position at steady states for swing equation system (2.2). The symbol × stands for the stroboscopic point through corresponding sampling $t = 2n\pi/\Omega$ $(n \in \mathbb{Z})$.

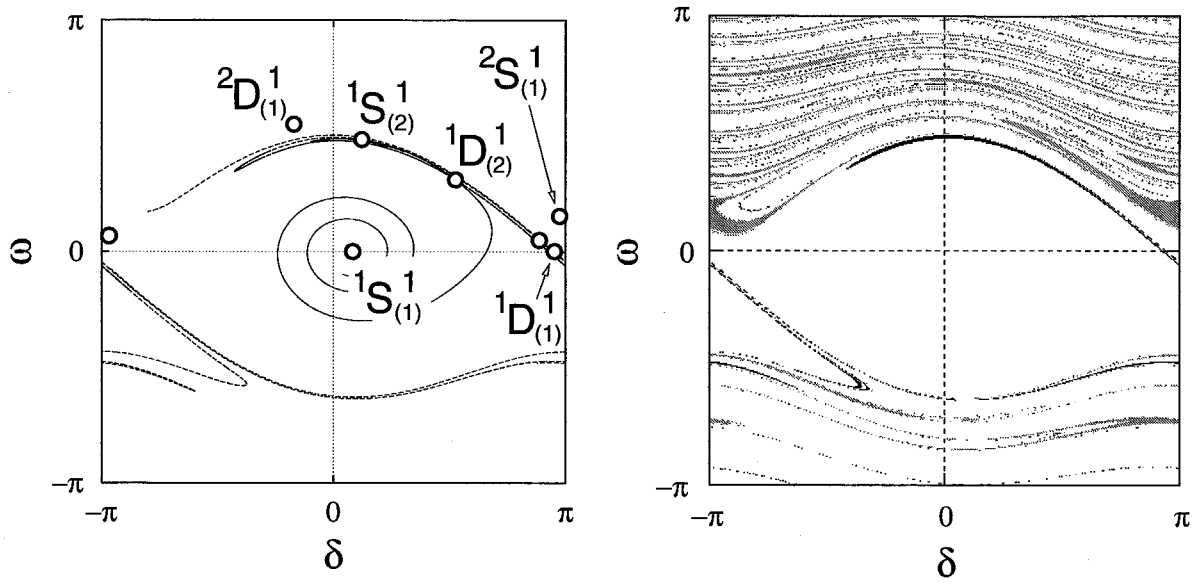

(a) $(p_{\mathrm{m}} - p_{\mathrm{e(dc)}}, \varepsilon) = (0.06, 0.1)$

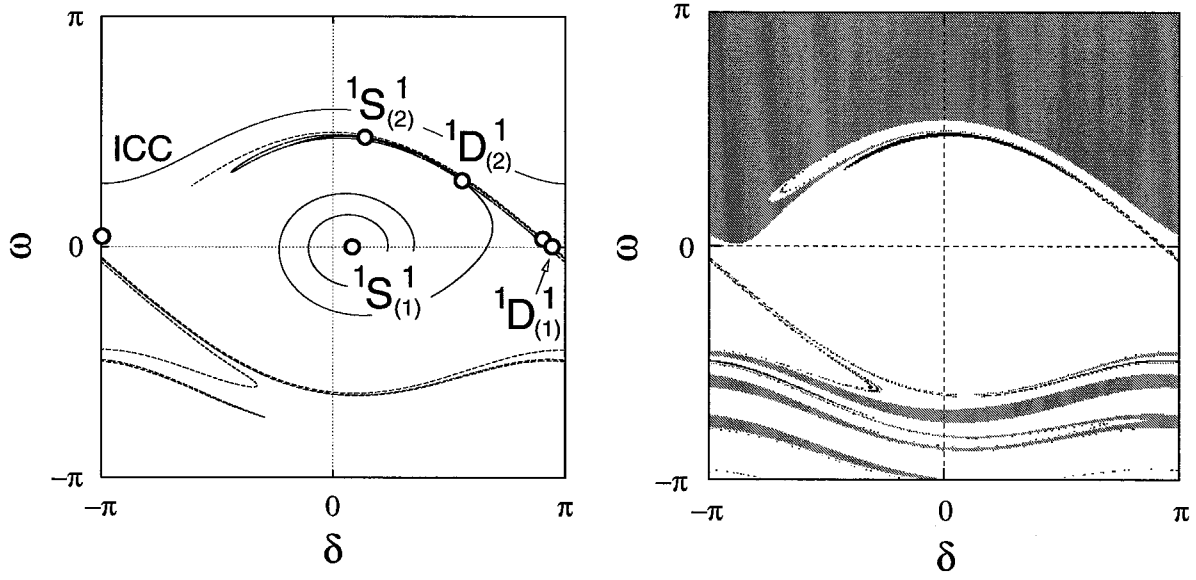

(b) $(p_{\mathrm{m}} - p_{\mathrm{e(dc)}}, \varepsilon) = (0.07, 0.1)$

Figure 2.4 Phase (left) and basin (right) portraits of discrete dynamical system (2.5) at $(p_{\mathrm{m}} - p_{\mathrm{e(dc)}}, \varepsilon) = (0.06, 0.1)$ and $(0.07, 0.1)$. The *solid* line in the phase portraits represents the unstable manifold of $^1\mathsf{D}^1_{(2)}$ and the *broken* line represents its stable manifold. In the basin portraits, the region is colored *white* for $^1\mathsf{S}^1_{(1)}$, *black* for $^1\mathsf{S}^1_{(2)}$, and *gray* for $^2\mathsf{S}^1_{(2)}$ under $p_{\mathrm{m}} - p_{\mathrm{e(dc)}} = 0.06$ and ICC under $p_{\mathrm{m}} - p_{\mathrm{e(dc)}} = 0.07$.

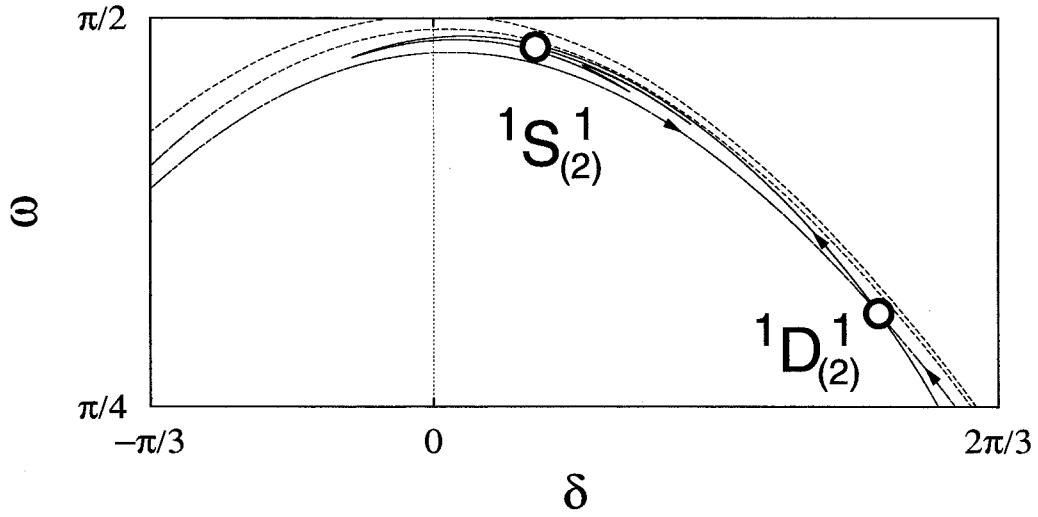

(a) $(p_{\mathrm{m}} - p_{\mathrm{e(dc)}}, \varepsilon) = (0.06, 0.1)$

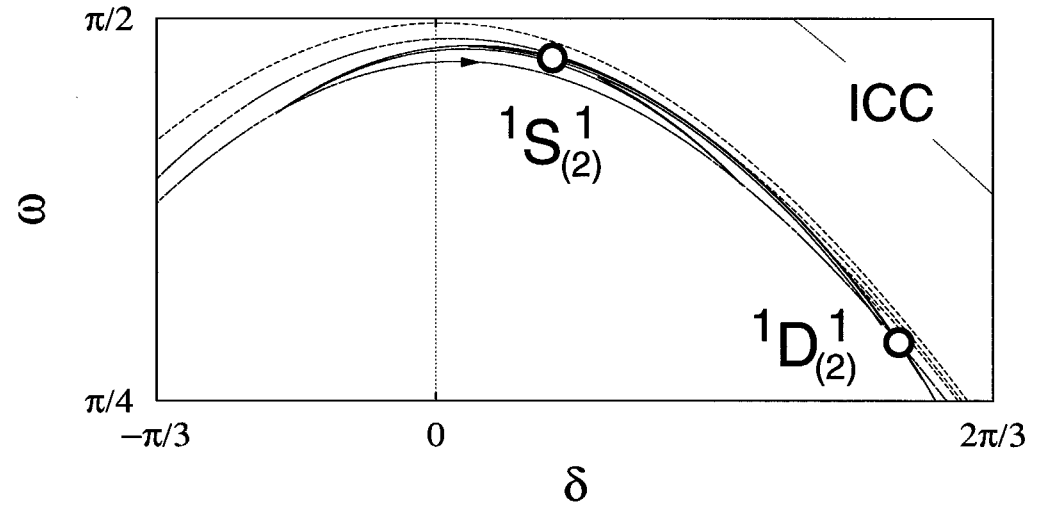

(b) $(p_{\mathrm{m}} - p_{\mathrm{e(dc)}}, \varepsilon) = (0.07, 0.1)$

Figure 2.5 Sequence of phase portraits of discrete dynamical system (2.5) at $(p_{\mathrm{m}} - p_{\mathrm{e(dc)}}, \varepsilon) = (0.06, 0.1)$ and $(0.07, 0.1)$. The *solid* and *broken* lines in the figures correspond to those in Fig. 2.4.

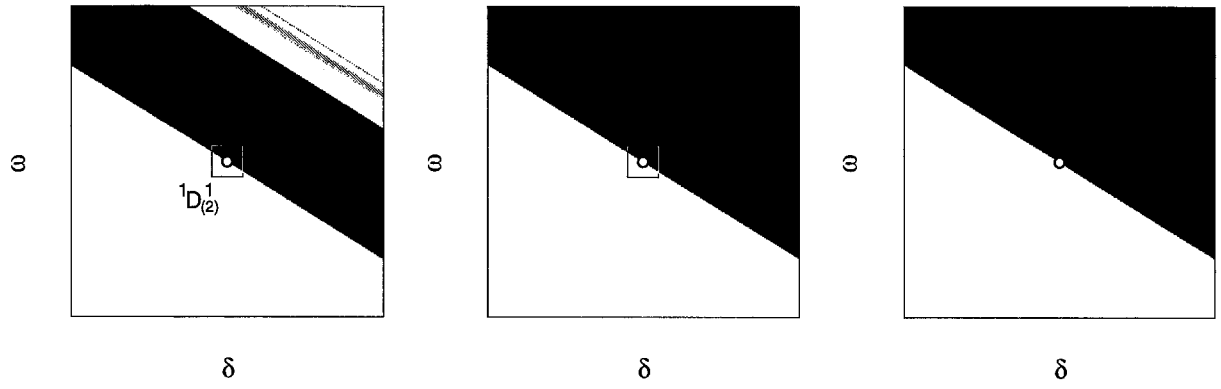

(a) $(p_{\mathrm{m}} - p_{\mathrm{e(dc)}}, \varepsilon) = (0.06, 0.1)$

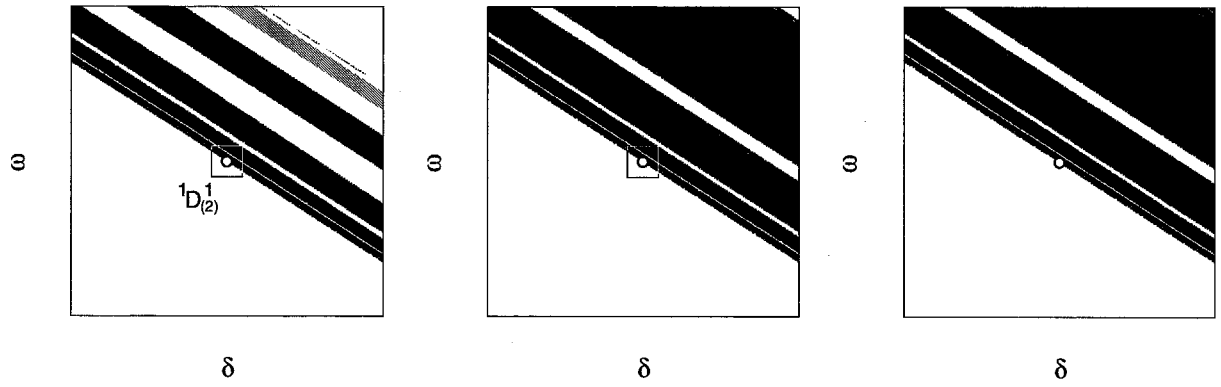

(b) $(p_{\mathrm{m}} - p_{\mathrm{e(dc)}}, \varepsilon) = (0.07, 0.1)$

Figure 2.6 Magnified sequences of basin portraits of neighboring domain of $^1\mathsf{D}^1_{(2)}$ in discrete dynamical system (2.5). The color in the portraits implies the same basin as Fig. 2.4. Each magnified basin portrait is obtained inside the small square in this figure.

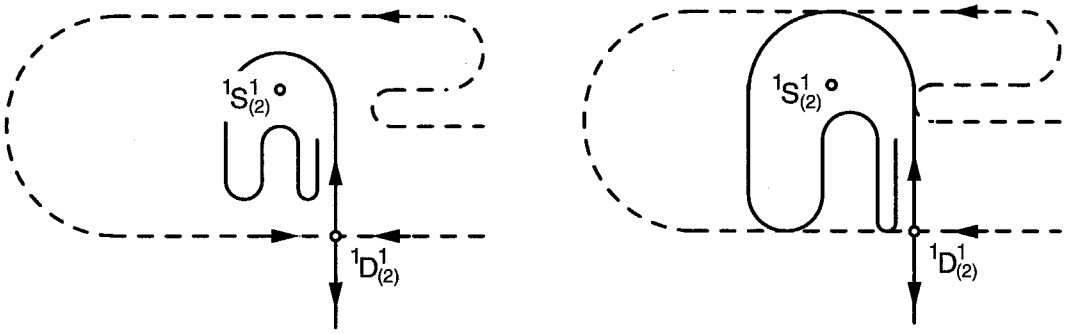

(a) $p_{\mathrm{m}} - p_{\mathrm{e(dc)}} = 0.06$

(b) $p_{\mathrm{m}} - p_{\mathrm{e(dc)}}$ is the critical value p^* satisfying $0.06 < p^* < 0.07$.

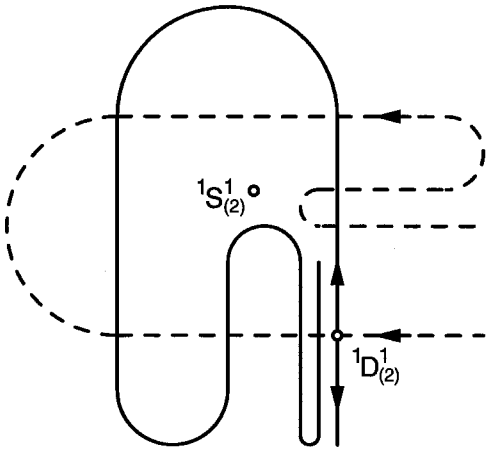

(c) $p_{\mathrm{m}} - p_{\mathrm{e(dc)}} = 0.07$

Figure 2.7 Sketch of global bifurcation by dc external forcing $p_{\mathrm{m}} - p_{\mathrm{e(dc)}}$. The *broken* and *solid* lines stand for the stable and unstable manifolds of $^1\mathrm{D}^1_{(2)}$ of the discrete dynamical system (2.5), respectively. The global bifurcation results in the fractal growth in the stability boundary.

Chapter 3

Stability boundary analysis via Melnikov's method

The present chapter addresses stability boundaries of the non-autonomous swing equation system. Chapter 2 discussed the non-autonomous swing equation system and the stability boundaries to clarify the transient dynamics of the ac/dc system. As is well-known, we cannot apply the Lyapunov's direct method [56, 69] to the stability boundary analysis of the non-autonomous system. Generally speaking, it is difficult to evaluate stability boundaries in non-autonomous systems analytically. For the present, the evaluation on the stability boundaries depends on the numerical calculation of each solution in initial value space: cell-to-cell mapping [47]. It is thus significant to establish an analytical criterion for the stability boundaries of the non-autonomous systems.

In this chapter, we propose an analytical criterion for stability boundaries in ODF time-periodic perturbed Hamiltonian systems. The criterion is derived via the Melnikov's perturbation method [62]. We here restrict our concerns to the stability boundaries that are analogous to homoclinic orbits in corresponding integrable Hamiltonian systems. The problem formulation is common to the original study by Melnikov. The Melnikov's method provides us with a signed distance between stable and unstable manifolds in the perturbed systems based on the homoclinic orbits. This suggests the possibility of measuring the distance between the homoclinic orbits and stable manifolds which correspond to the stability boundaries in the perturbed systems. In the following chapter, an analytical criterion for

the stability boundaries is proposed and applied to the stability boundary analysis of the swing equation system.

3.1 Perturbed Hamiltonian system

This chapter considers the following perturbed Hamiltonian system:

$$\begin{cases} \dfrac{\mathrm{d}x}{\mathrm{d}t} &= \dfrac{\partial}{\partial y}\mathcal{H}(x,y) &+ \varepsilon g_1(x,y,t), \\ \dfrac{\mathrm{d}y}{\mathrm{d}t} &= -\dfrac{\partial}{\partial x}\mathcal{H}(x,y) &+ \varepsilon g_2(x,y,t), \end{cases} \tag{3.1}$$

where $(x,y) \in \mathbb{R} \times \mathbb{R}$, and $\mathcal{H}(x,y)$ is the Hamiltonian, ε the small positive parameter, and $\varepsilon g_i(x,y,t)\,(i=1,2)$ the perturbation terms. The right-hand side of the system (3.1) is assumed to be tractable in the region we are interested. The perturbation terms are also assumed to have a periodicity on t with a period $T = 2\pi/\Omega$. The vector formulation of the system (3.1) is as follows:

$$\frac{\mathrm{d}\boldsymbol{q}}{\mathrm{d}t} = \mathsf{J}\mathrm{D}\mathcal{H}(\boldsymbol{q}) + \varepsilon \boldsymbol{g}(\boldsymbol{q},t), \tag{3.2}$$

where $\boldsymbol{q} \triangleq (x,y)^{\mathrm{T}}$ and $\boldsymbol{g}(\boldsymbol{q},t) \triangleq (g_1(x,y,t), g_2(x,y,t))^{\mathrm{T}}$. T represents the transpose operation of vectors. In addition,

$$\mathsf{J} \triangleq \begin{pmatrix} 0 & 1 \\ -1 & 0 \end{pmatrix}, \tag{3.3}$$

and

$$\mathrm{D}\mathcal{H}(\boldsymbol{q}) \triangleq \left(\frac{\partial}{\partial x}\mathcal{H}(x,y),\ \frac{\partial}{\partial y}\mathcal{H}(x,y)\right)^{\mathrm{T}}. \tag{3.4}$$

Setting $\varepsilon = 0$ in the system (3.1) induces the Hamiltonian system:

$$\begin{cases} \dfrac{\mathrm{d}x}{\mathrm{d}t} &= \dfrac{\partial}{\partial y}\mathcal{H}(x,y), \\ \dfrac{\mathrm{d}y}{\mathrm{d}t} &= -\dfrac{\partial}{\partial x}\mathcal{H}(x,y), \end{cases} \tag{3.5}$$

or

$$\frac{\mathrm{d}\boldsymbol{q}}{\mathrm{d}t} = \mathsf{J}\mathrm{D}\mathcal{H}(\boldsymbol{q}). \tag{3.6}$$

Since the Hamiltonian system (3.6) satisfies the integrability condition [6], all dynamics of the system (3.6) can be examined analytically. Additionally, the Hamiltonian system (3.6) holds the following assumptions:

Assumption 3.1 The Hamiltonian system (3.6) has a homoclinic orbit $\Gamma^0 \triangleq \{\boldsymbol{q}^0(t) \mid t \in \mathbb{R}\}$ to a saddle point $\boldsymbol{p}_0$.

Assumption 3.2 The interior of $\Gamma^0 \cap \{\boldsymbol{p}_0\}$ is filled with a continuous family of periodic orbits $\boldsymbol{q}^\alpha(t), \alpha \in (-1, 0)$ with period T_α. Letting $d(\boldsymbol{x}, \Gamma^0) \triangleq \inf_{\boldsymbol{q} \in \Gamma^0} ||\boldsymbol{x} - \boldsymbol{q}||$, we have $\lim_{\alpha \to 0} \sup_{t \in \mathbb{R}} d(\boldsymbol{q}^\alpha(t), \Gamma^0) = 0$ and $\lim_{\alpha \to 0} T_\alpha = +\infty$. $||\bullet||$ implies the Euclidean norm of vectors. The Hamiltonian system (3.6) also has a center $\boldsymbol{p}_{-1}$ enclosed by the continuous family of the periodic orbits.

Figure 3.1 shows the assumed phase structure of the Hamiltonian system (3.6). In the following, we restrict our analysis to a stability boundary which is analogous to the homoclinic orbit in the Hamiltonian system. This boundary possibly corresponds to the basin boundary of an *non-resonant* solution in the perturbed Hamiltonian system (3.2) as explained below. This chapter also uses a discrete dynamical system $\mathscr{F}$ under the stroboscopic sampling of the perturbed system (3.2) at a phase $\phi\ (= \Omega t) \in \mathbb{S}^1$.

3.2 Melnikov's perturbation method

The Melnikov's method provides us with a signed distance between the stable and unstable manifolds in the perturbed Hamiltonian system (3.2) based on the associated homoclinic orbit. This section outlines the Melnikov's method and analytically derives a signed distance between the homoclinic orbit and the stable manifold. This is possible by expanding the well-known derivation of Melnikov functions [35, 108].

First of all, if the perturbation ε is sufficiently small, the following lemmas provide us with the basic information about the discrete dynamical system $\mathscr{F}$.

Lemma 3.3 [35,108] *For sufficiently small ε, the perturbed Hamiltonian system* (3.2) *has a unique hyperbolic periodic solution of the saddle type $\boldsymbol{\gamma}_\varepsilon(t) = \boldsymbol{p}_0 + \boldsymbol{\mathcal{O}}(\varepsilon)$. Correspondingly,*

the stroboscopic observation at a phase ϕ_0 has a unique hyperbolic fixed point of the saddle type $\boldsymbol{p}_0^\varepsilon = \boldsymbol{p}_0 + \mathcal{O}(\varepsilon)$.

Lemma 3.4 [35, 108] *The local invariant manifolds of the fixed point on the stroboscopic phase ϕ_0 are C^r close to those of the equilibrium point $\boldsymbol{p}_0$. C^r here implies r times differentiable.*

The global stable and unstable manifolds of the fixed point $\boldsymbol{p}_0^\varepsilon$ can be obtained from their local stable and unstable manifolds by the time evolution of the discrete system $\mathscr{F}$. Furthermore, the discrete system holds the following assumption pertinent to the stability boundary analysis:

Assumption 3.5 A non-resonant fixed point $\boldsymbol{p}_{-1}^\varepsilon$, associated with $\boldsymbol{p}_{-1}$, of the discrete dynamical system $\mathscr{F}$ uniquely exists and is completely stable.

Assumption 3.5 is necessary for the evaluation of the basin boundary of the *non-resonant* fixed point $\boldsymbol{p}_{-1}^\varepsilon$. Here, non-resonance implies that the fixed point is associated with the assumed center or saddle point in the Hamiltonian system (3.6). Through the above lemmas and assumption, Fig. 3.2 describes the phase structure of the discrete system $\mathscr{F}$ under sufficiently small ε. In the figure, $\boldsymbol{q}^0(-t_0)$ denotes a point on the homoclinic orbit as a parameter $-t_0 \in \mathbb{R}$ and $\mathrm{D}\mathcal{H}(\boldsymbol{q}^0(-t_0))$ the normal vector at the point $\boldsymbol{q}^0(-t_0)$. In addition, $\boldsymbol{q}_\varepsilon^{\mathrm{s}}$ represents the intersection between the normal vector $\mathrm{D}\mathcal{H}(\boldsymbol{q}^0(-t_0))$ and the stable manifold of the saddle point $\boldsymbol{p}_0^\varepsilon$, and $\boldsymbol{q}_\varepsilon^{\mathrm{u}}$ the intersection between the normal vector $\mathrm{D}\mathcal{H}(\boldsymbol{q}^0(-t_0))$ and the unstable manifold of the saddle point $\boldsymbol{p}_0^\varepsilon$.

To estimate the stability boundary, we define the distance between the points $\boldsymbol{q}^0(-t_0)$ on the homoclinic orbit and $\boldsymbol{q}_\varepsilon^{\mathrm{s}}$ on the stable manifold. The Melnikov's method originally provides us with a signed distance between the points $\boldsymbol{q}_\varepsilon^{\mathrm{s}}$ and $\boldsymbol{q}_\varepsilon^{\mathrm{u}}$ under sufficiently small ε. The distance $d(\boldsymbol{q}^0(-t_0), \phi_0, \varepsilon)$ is defined between $\boldsymbol{q}_\varepsilon^{\mathrm{s}}$ and $\boldsymbol{q}_\varepsilon^{\mathrm{u}}$ along the normal vector $\mathrm{D}\mathcal{H}(\boldsymbol{q}^0(-t_0))$ by

$$d\left(\boldsymbol{q}^0(-t_0), \phi_0, \varepsilon\right) \triangleq \frac{\mathrm{D}\mathcal{H}(\boldsymbol{q}^0(-t_0)) \cdot (\boldsymbol{q}_\varepsilon^{\mathrm{s}} - \boldsymbol{q}_\varepsilon^{\mathrm{u}})}{||\mathrm{D}\mathcal{H}(\boldsymbol{q}^0(-t_0))||}. \tag{3.7}$$

The important distance $d^{\mathrm{s}}(\boldsymbol{q}^0(-t_0), \phi_0, \varepsilon)$ which should be evaluated is defined in the similar fashion by

$$d^{\mathrm{s}}\left(\boldsymbol{q}^0(-t_0), \phi_0, \varepsilon\right) \triangleq \frac{\mathrm{D}\mathcal{H}(\boldsymbol{q}^0(-t_0)) \cdot (\boldsymbol{q}_\varepsilon^{\mathrm{s}} - \boldsymbol{q}^0(-t_0))}{||\mathrm{D}\mathcal{H}(\boldsymbol{q}^0(-t_0))||}. \tag{3.8}$$

It is here noted that for $\varepsilon = 0$ the point $\boldsymbol{q}^0(-t_0)$ corresponds to the point $\boldsymbol{q}^{\mathrm{s}}_\varepsilon$, i.e.

$$d^{\mathrm{s}}\left(\boldsymbol{q}^0(-t_0), \phi_0, 0\right) \;=\; 0. \tag{3.9}$$

Taylor expansion of the formula (3.8) around $\varepsilon = 0$ here gives us

$$\begin{aligned} d^{\mathrm{s}}\left(\boldsymbol{q}^0(-t_0), \phi_0, \varepsilon\right) \;&=\; d^{\mathrm{s}}\left(\boldsymbol{q}^0(-t_0), \phi_0, 0\right) \\ &\quad + \left(\frac{\partial}{\partial\varepsilon} d^{\mathrm{s}}\left(\boldsymbol{q}^0(-t_0), \phi_0, \varepsilon\right)\right)\Big|_{\varepsilon=0} \varepsilon + \mathcal{O}(\varepsilon^2), \end{aligned} \tag{3.10}$$

where

$$\frac{\partial}{\partial\varepsilon} d^{\mathrm{s}}\left(\boldsymbol{q}^0(-t_0), \phi_0, \varepsilon\right) \;=\; \frac{1}{||\mathrm{D}\mathcal{H}(\boldsymbol{q}^0(-t_0))||}\, \mathrm{D}\mathcal{H}(\boldsymbol{q}^0(-t_0)) \cdot \frac{\partial \boldsymbol{q}^{\mathrm{s}}_\varepsilon}{\partial\varepsilon}. \tag{3.11}$$

The distance $d^{\mathrm{s}}(\boldsymbol{q}^0(-t_0), \phi_0, \varepsilon)$ can be therefore rewritten as follows:

$$d^{\mathrm{s}}\left(\boldsymbol{q}^0(-t_0), \phi_0, \varepsilon\right) \;=\; \varepsilon \frac{\Delta^{\mathrm{s}}\left(\boldsymbol{q}^0(-t_0), \phi_0\right)}{||\mathrm{D}H(\boldsymbol{q}^0(-t_0))\,||} + \mathcal{O}(\varepsilon^2), \tag{3.12}$$

where

$$\Delta^{\mathrm{s}}\left(\boldsymbol{q}^0(-t_0), \phi_0\right) \;\triangleq\; \mathrm{D}\mathcal{H}(\boldsymbol{q}^0(-t_0)) \cdot \frac{\partial \boldsymbol{q}^{\mathrm{s}}_\varepsilon}{\partial\varepsilon}\bigg|_{\varepsilon=0}. \tag{3.13}$$

On the standpoints of practical applications, it is desirable that the distance $d^{\mathrm{s}}(\boldsymbol{q}^0(-t_0), \phi_0, \varepsilon)$ can be calculated without the information of the stable manifold $\boldsymbol{q}^{\mathrm{s}}_\varepsilon$ in the perturbed system (3.2). This is achieved by using the Melnikov's original technique. The following time-dependent function $\tilde{\Delta}^{\mathrm{s}}\left(t;\, \boldsymbol{q}^0(-t_0), \phi_0\right)$ is first defined:

$$\tilde{\Delta}^{\mathrm{s}}\left(t;\, \boldsymbol{q}^0(-t_0), \phi_0\right) \;\triangleq\; \mathrm{D}\mathcal{H}(\boldsymbol{q}^0(t - t_0)) \cdot \boldsymbol{q}^{\mathrm{s}}_1(t), \tag{3.14}$$

where

$$\boldsymbol{q}^{\mathrm{s}}_1(t) \;\triangleq\; \frac{\partial}{\partial\varepsilon} \boldsymbol{q}^{\mathrm{s}}_\varepsilon(t)\bigg|_{\varepsilon=0}. \tag{3.15}$$

$\boldsymbol{q}^{\mathrm{s}}_\varepsilon(t)$ denotes the trajectory on the stable manifold and satisfies

$$\boldsymbol{q}^{\mathrm{s}}_\varepsilon(0) \;=\; \boldsymbol{q}^{\mathrm{s}}_\varepsilon, \tag{3.16}$$

and $\boldsymbol{q}^0(t - t_0)$ represents the solution on the homoclinic orbit. The formulas (3.13)–(3.16) obviously induce the distance $\Delta^{\mathrm{s}}(\boldsymbol{q}(-t_0), \phi_0)$:

$$\Delta^{\mathrm{s}}\left(\boldsymbol{q}^0(-t_0), \phi_0\right) \;\equiv\; \tilde{\Delta}^{\mathrm{s}}\left(0;\, \boldsymbol{q}^0(-t_0), \phi_0\right). \tag{3.17}$$

Differentiating the formula (3.14) with respect to t gives us the following formula:

$$\begin{aligned}\frac{\mathrm{d}}{\mathrm{d}t}\tilde{\Delta}^{\mathrm{s}}\left(t;\, \boldsymbol{q}^0(-t_0), \phi_0\right) &= \left(\frac{\mathrm{d}}{\mathrm{d}t}\mathrm{D}\mathcal{H}(\boldsymbol{q}^0(t-t_0))\right)\cdot \boldsymbol{q}_1^{\mathrm{s}}(t) \\ &\quad +\mathrm{D}\mathcal{H}(\boldsymbol{q}^0(t-t_0))\cdot\frac{\mathrm{d}}{\mathrm{d}t}\boldsymbol{q}_1^{\mathrm{s}}(t). \end{aligned} \tag{3.18}$$

The following lemma is now stated:

Lemma 3.6 *$\boldsymbol{q}_1^{\mathrm{s}}(t)$ satisfies the following formula:*

$$\frac{\mathrm{d}}{\mathrm{d}t}\boldsymbol{q}_1^{\mathrm{s}}(t) = \mathrm{J}\mathrm{D}^2\mathcal{H}(\boldsymbol{q}^0(t-t_0))\,\boldsymbol{q}_1^{\mathrm{s}}(t) + \boldsymbol{g}\left(\boldsymbol{q}^0(t-t_0), \Omega t+\phi_0\right). \tag{3.19}$$

(Proof) See the appendix at the end of this chapter.

Substituting the equation (3.19) into (3.18) results in the following formula:

$$\begin{aligned}\frac{\mathrm{d}}{\mathrm{d}t}\tilde{\Delta}^{\mathrm{s}}\left(t;\, \boldsymbol{q}^0(-t_0), \phi_0\right) &= \left(\frac{\mathrm{d}}{\mathrm{d}t}\mathrm{D}\mathcal{H}(\boldsymbol{q}^0(t-t_0))\right)\cdot \boldsymbol{q}_1^{\mathrm{s}}(t) \\ &\quad +\mathrm{D}\mathcal{H}(\boldsymbol{q}^0(t-t_0))\cdot\mathrm{J}\mathrm{D}^2\mathcal{H}(\boldsymbol{q}^0(t-t_0))\boldsymbol{q}_1^{\mathrm{s}}(t) \\ &\quad +\mathrm{D}\mathcal{H}(\boldsymbol{q}^0(t-t_0))\cdot\boldsymbol{g}\left(\boldsymbol{q}^0(t-t_0), \Omega t+\phi_0\right). \end{aligned} \tag{3.20}$$

In addition, the next lemma is obtained:

Lemma 3.7 [108] *The following relation is satisfied:*

$$\left(\frac{\mathrm{d}}{\mathrm{d}t}\mathrm{D}\mathcal{H}(\boldsymbol{q}^0(t-t_0))\right)\cdot\boldsymbol{q}_1^{\mathrm{s}}(t) + \mathrm{D}\mathcal{H}(\boldsymbol{q}^0(t-t_0))\cdot\mathrm{J}\mathrm{D}^2\mathcal{H}(\boldsymbol{q}^0(t-t_0))\,\boldsymbol{q}_1^{\mathrm{s}}(t) = 0. \tag{3.21}$$

By using Lemma 3.7, we can rewrite the equation (3.20) as

$$\frac{\mathrm{d}}{\mathrm{d}t}\tilde{\Delta}^{\mathrm{s}}\left(t;\, \boldsymbol{q}^0(-t_0), \phi_0\right) = \mathrm{D}\mathcal{H}(\boldsymbol{q}^0(t-t_0))\cdot\boldsymbol{g}\left(\boldsymbol{q}^0(t-t_0), \Omega t+\phi_0\right). \tag{3.22}$$

Integrating $\tilde{\Delta}^{\mathrm{s}}(t;\, \boldsymbol{q}^0(-t_0), \phi_0)$ from 0 to τ ($\tau > 0$) derives the following:

$$\begin{aligned}\tilde{\Delta}^{\mathrm{s}}\left(\tau;\, \boldsymbol{q}^0(-t_0), \phi_0\right) - \tilde{\Delta}^{\mathrm{s}}\left(0;\, \boldsymbol{q}^0(-t_0), \phi_0\right) &= \int_0^{\tau}\mathrm{D}\mathcal{H}(\boldsymbol{q}^0(t-t_0))\cdot \\ &\quad \cdot\boldsymbol{g}\left(\boldsymbol{q}^0(t-t_0), \Omega t+\phi_0\right)\mathrm{d}t. \end{aligned} \tag{3.23}$$

The following lemma is then naturally obtained:

Lemma 3.8 [108] *For the first term of the left-hand side of the equation* (3.23)*, the following limit is given:*

$$\lim_{\tau \to +\infty} \tilde{\Delta}^{\mathrm{s}} \left(\tau;\, \boldsymbol{q}^0(-t_0), \phi_0 \right) \;=\; 0. \tag{3.24}$$

According to the formula (3.17), we derive the function $\Delta^{\mathrm{s}}(\boldsymbol{q}^0(-t_0), \phi_0)$ as follows:

$$\Delta^{\mathrm{s}} \left(\boldsymbol{q}^0(-t_0), \phi_0 \right) \;=\; -\int_0^{+\infty} \mathrm{D}\mathcal{H}(\boldsymbol{q}^0(t-t_0)) \cdot \boldsymbol{g} \left(\boldsymbol{q}^0(t-t_0), \Omega t + \phi_0 \right) \mathrm{d}t, \tag{3.25}$$

by the transformation t to $t + t_0$,

$$\Delta^{\mathrm{s}} \left(\boldsymbol{q}^0(-t_0), \phi_0 \right) \;=\; -\int_{-t_0}^{+\infty} \mathrm{D}\mathcal{H}(\boldsymbol{q}^0(t)) \cdot \boldsymbol{g} \left(\boldsymbol{q}^0(t), \Omega(t+t_0) + \phi_0 \right) \mathrm{d}t. \tag{3.26}$$

The function $\Delta^{\mathrm{s}}(\boldsymbol{q}^0(-t_0), \phi_0)$ makes it possible to calculate the distance $d^{\mathrm{s}}(\boldsymbol{q}^0(-t_0), \phi_0)$ between the homoclinic orbit and the stable manifold. The calculation can be analytically performed because the original Hamiltonian system (3.6) is integrable. To derive an analytical criterion in the next section, the obtained properties about the Melnikov's method are now summarized:

Remark 3.9 The distance

$$d_1^{\mathrm{s}} \left(\boldsymbol{q}^0(-t_0), \phi_0 \right) \;\triangleq\; \varepsilon \frac{\Delta^{\mathrm{s}} \left(\boldsymbol{q}^0(-t_0), \phi_0 \right)}{||\mathrm{D}\mathcal{H}(\boldsymbol{q}^0(-t_0))||} \tag{3.27}$$

is a signed measure. The sign makes it possible to grasp the geometric relationship between the homoclinic orbit and the stable manifold.

Remark 3.10 The distance $d^{\mathrm{s}}(\boldsymbol{q}^0(-t_0), \phi_0)$ diverges to infinity as $t_0 \to \pm\infty$. This is because the norm of the normal vector $\mathrm{D}\mathcal{H}(\boldsymbol{q}^0(-t_0))$ converges to zero as $t_0 \to \pm\infty$. This implies that any point $\boldsymbol{q}^0(-t_0)$ in the neighborhood of the assumed saddle point $\boldsymbol{p}_0$ can not be modified by the distance $d^{\mathrm{s}}(\boldsymbol{q}^0(-t_0), \phi_0)$.

Remark 3.11 When the perturbation is independent on t, the distance between the homoclinic orbit and the stable manifold is also derived in the same fashion. This suggests that the proposed criterion in the next section can be applied to autonomous systems. The criterion drastically improves the conservative estimation of stability boundaries with other analytical methods such as the Lyapunov's direct method.

3.3 An analytical criterion for stability boundaries

We are now in a position to propose an analytical criterion for the stability boundaries in the non-autonomous systems. The above discussion naturally leads a method for modifying a point $\boldsymbol{q}^0(-t_0)$ on the homoclinic orbit Γ^0:

$$\boldsymbol{q}^{0\prime}(-t_0, \phi_0) \triangleq \boldsymbol{q}^0(-t_0) + \frac{d_1^s(\boldsymbol{q}^0(-t_0), \phi_0)}{||\mathrm{D}\mathcal{H}(\boldsymbol{q}^0(-t_0))||} \mathrm{D}\mathcal{H}(\boldsymbol{q}^0(-t_0)), \tag{3.28}$$

where $\boldsymbol{q}^{0\prime}(-t_0, \phi_0)$ denotes the modified point. The Melnikov's method states that under sufficiently small ε, $\boldsymbol{q}^{0\prime}(-t_0, \phi_0)$ is close to the stable manifold of the non-resonant fixed point $\boldsymbol{p}_{-1}^{\varepsilon}$, that is, the modified homoclinic orbit $\{\boldsymbol{q}^{0\prime}(-t_0, \phi_0)\}$ is a good estimation of the basin boundary of $\boldsymbol{p}_{-1}^{\varepsilon}$. Hence, we propose the modified orbit $\{\boldsymbol{q}^{0\prime}(-t_0, \phi_0)\}$ as an analytical criterion for the stability boundary of the perturbed Hamiltonian system (3.2).

Remark 3.12 The proposed criterion has the following advantages:

- The criterion can be calculated with the information about the Hamiltonian system (3.6), that is, the integrable system.
- Since the criterion is based on the stable manifold of the non-resonant point $\boldsymbol{p}_{-1}^{\varepsilon}$ which coincides with the target stability boundary, the criterion is not conservative such as the Lyapunov's direct method for the autonomous systems.

On the other hand, the disadvantages of the criterion can be indicated as follows:

- The criterion does not provide us with any *exact* sufficient condition for the basin boundary of the non-resonant solution; Remark 3.10 suggests the necessity of truncating the modified homoclinic orbit $\{\boldsymbol{q}^{0\prime}(-t_0, \phi_0)\}$ in a positive number $T_0 \in \mathbb{R}$ such that $|t_0| \leq T_0$ to obtain a good estimation of the stability boundary.
- The criterion is not necessarily applied to various stability boundaries which possibly appear in the perturbed system (3.2): for examples, (i) genesis of *resonant* solutions and associated basin boundaries; (ii) chaotic attractors and associated basin boundaries; and (iii) fractal growth in basin boundaries of non-resonant solutions.

To overcome the disadvantage (i), Chapter 4 shows an analytical approach to the basin boundaries of the resonant solutions.

Remark 3.13 If more than one saddle point with associated homoclinic orbit and family of periodic orbits exist in the Hamiltonian system (3.6), the proposed criterion can be applied to each homoclinic orbit separately.

3.4 Application to swing equation system

This section analyzes stability boundaries of the non-autonomous swing equation system based on the proposed criterion. The system is described by

$$\begin{cases} \mathcal{H}(\delta,\omega) &= \dfrac{1}{2}\omega^2 - b\cos\delta - \left(p_{\mathrm{m}} - p_{\mathrm{e(dc)}}\right)\delta, \\ g_1(\delta,\omega,t) &= 0, \\ g_2(\delta,\omega,t) &= -\tilde{D}\omega + a\cos\Omega t, \end{cases} \tag{3.29}$$

where the parameters are fixed as follows:

$$b = 0.7, \quad \varepsilon = 0.1, \quad \tilde{D} = 0.5, \quad \Omega = 0.05. \tag{3.30}$$

The setting is identical to that in Chapter 2 except Ω. The setting $\Omega = 0.05$, which is equal to $2\pi/(8.6\text{ s})$ in the practical time, is based on the practical measurement in Fig. 1.2. It should be noted that the non-autonomous system (3.29) possesses no resonant solution under the parameters setting.

3.4.1 Numerical simulations and analytical criteria

The proposed criterion is applied to the autonomous swing equation system (3.29) under $a = 0.0$. Fig. 3.3 shows the stability boundary, original homoclinic orbit, and analytical criterion in the swing equation system with $a = 0.0$. In the figure, the region is colored *light-gray* for a stable focus, i.e., an acceptable operating condition and *dark-gray* for a second kind limit cycle, i.e., an asynchronous state. Then the stability boundary corresponds to the boundary between the *light-gray* and *dark-gray* regions. In the figure, the *black* line describes the original homoclinic orbit and the *white* line the proposed criterion. In the autonomous case, since the derivative of the Hamiltonian $\mathcal{H}$ along a system trajectory is

non-positive, that is,

$$\frac{\mathrm{d}\mathcal{H}}{\mathrm{d}t} = -\varepsilon\tilde{D}\omega^2 \leq 0, \tag{3.31}$$

the Lyapunov's direct method [56,69] or the closest UEP method [17] gives us a sufficient condition for the stability boundary; the condition in the system (3.29) coincides with the homoclinic orbit which issues from the assumed saddle point. The proposed criterion in Fig. 3.3 obviously evaluates the correct stability boundary much better than the homoclinic orbit. This indicates that the criterion is effective for the analysis of the autonomous system.

Next we apply the proposed criterion to the non-autonomous swing equation system (3.29). Fig. 3.4 shows the stability boundaries, original homoclinic orbit, and analytical criteria in the discrete dynamical system $\mathscr{F}$ at the phase $\phi_0 = 0$ at $a = 0.7$. Fig. 3.5 also shows the stability boundaries, original homoclinic orbit, and analytical criteria at the phase $\phi_0 = k\pi/2$ $(k = 0, \ldots, 3)$ under $a = 0.7$ and $p_{\mathrm{m}} - p_{\mathrm{e(dc)}} = 0.2$. In the figures, the regions are colored *light-gray* for non-resonant sinks (acceptable operating conditions) and *dark-gray* for second kind invariant closed curves (asynchronous states). Figs. 3.4 and 3.5 imply that each criterion evaluates the stability boundary almost perfectly. These results make it clear that the analytical criterion is much effective for the stability boundary analysis of the swing equation system (3.29).

3.4.2 Physical interpretation and remaining problem

The numerical simulations in Figs. 3.3–3.5 suggest the possibility of dc link's ability to control the transient dynamics of the ac/dc system. The stability regions in Fig. 3.4 for which are colored *light-gray* become smaller as $|p_{\mathrm{m}} - p_{\mathrm{e(dc)}}|$ increases. This implies that we can change the size of the stability regions depending on the dc operation. The size of the stability regions is closely related to critical fault clearing time [60]; it is the longest fault duration for which the generator will remain in synchronism. That is, the obtained results imply that the dc link is possibly adopted to extend the critical clearing time. Then, the proposed criteria are much effective for guaranteeing both the effectiveness and application limit of the dc control, because they can evaluate the size of the stability region analytically.

On the other hand, the proposed criterion still has some problems related to resonant solutions. Chapter 2 considered the dynamical behavior affected by the resonant solution in the swing equation system (3.29). The complicated stability boundary was particularly shown related to the resonant solution in Figs. 2.4–2.7. As mentioned before, the proposed criterion hardly applies to non-autonomous systems with resonant solutions: for example, the criterion is not adequate for evaluating the basin boundary of ${}^{1}\mathsf{S}^{1}_{(1)}$ in Fig. 2.4, because of the existence of the resonant points ${}^{1}\mathsf{S}^{1}_{(2)}$ and ${}^{1}\mathsf{D}^{1}_{(2)}$. In addition to this, the fractal basin boundary in Fig. 2.5 cannot be clarified through the present approach. In order to tackle this problem, the next chapter shows a subharmonic Melnikov function approach to the stability boundaries related to the resonant solutions.

3.5 Summary

This chapter proposed an analytical criterion for the stability boundaries in the non-autonomous systems. The criterion was developed based on the Melnikov's perturbation method. In addition, the criterion was applied to the analysis of the stability boundaries in the swing equation system. Thereby, it was shown that that the proposed criterion was much effective to the stability boundary analysis. The criterion has some advantages in its easy and quick evaluation and many possibilities of expanding itself to various non-autonomous systems. Here we note that geometric relation between the homoclinic orbit and the stable manifold is here considered to derive the analytical criterion. This makes it possible to generalize the proposed criterion without special formulation if Melnikov's methods [107] for multi-degree-of-freedom perturbed Hamiltonian systems are considered.

Appendix to Section 3.2: Proof of Lemma 3.4

Applying the Gronwall's inequality [35, 108] to the basic systems (3.2) and (3.6), the following relationship is given:

$$||\boldsymbol{q}^{\mathrm{s}}_{\varepsilon}(t) - \boldsymbol{q}_0(t - t_0)|| \;=\; \mathcal{O}(\varepsilon) \;\text{ for }\; 0 \leq t < +\infty. \tag{3.32}$$

Using the system (3.2), $\boldsymbol{q}_\varepsilon^{\mathrm{s}}(t)$ satisfies

$$\frac{\mathrm{d}}{\mathrm{d}t}\boldsymbol{q}_\varepsilon^{\mathrm{s}}(t) \;=\; \mathrm{J}\mathrm{D}H(\boldsymbol{q}_\varepsilon^{\mathrm{s}}(t)) + \varepsilon \boldsymbol{g}\left(\boldsymbol{q}_\varepsilon^{\mathrm{s}}(t), \Omega t + \phi_0\right). \tag{3.33}$$

Since $\boldsymbol{q}_\varepsilon^{\mathrm{s}}(t)$ is of class C^r for ε and t, the system (3.33) can be differentiated with respect to ε. The interchange of the differential order by ε and t is obviously possible. By differentiating the system (3.33) with respect to ε and interchanging the differential order by ε and t, we thus obtain the following formula:

$$\frac{\mathrm{d}}{\mathrm{d}t}\left(\frac{\partial}{\partial\varepsilon}\boldsymbol{q}_\varepsilon^{\mathrm{s}}(t)\right) \;=\; \mathrm{J}\mathrm{D}^2H(\boldsymbol{q}_\varepsilon^{\mathrm{s}}(t))\frac{\partial}{\partial\varepsilon}\boldsymbol{q}_\varepsilon^{\mathrm{s}}(t) + \boldsymbol{g}\left(\boldsymbol{q}_\varepsilon^{\mathrm{s}}(t), \Omega t + \phi_0\right) + \boldsymbol{\mathcal{O}}(\varepsilon). \tag{3.34}$$

Using (3.32) for $\varepsilon = 0$ completes the proof of this lemma.

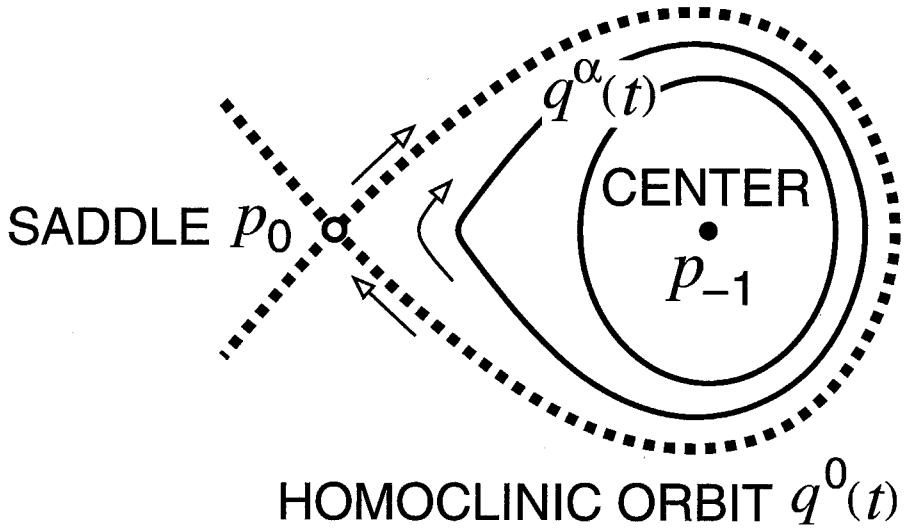

Figure 3.1 Assumed phase structure of the Hamiltonian system (3.6)

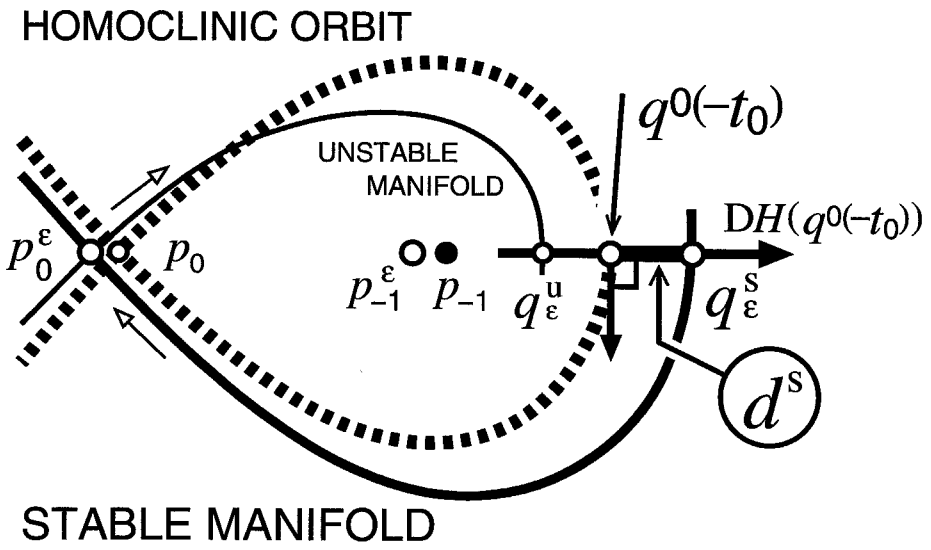

Figure 3.2 Schematic phase structure of discrete dynamical system $\mathscr{F}$ under sufficiently small ε. The stable manifold possibly corresponds to the basin boundary of the non-resonant fixed point $\boldsymbol{p}_{-1}^{\varepsilon}$.

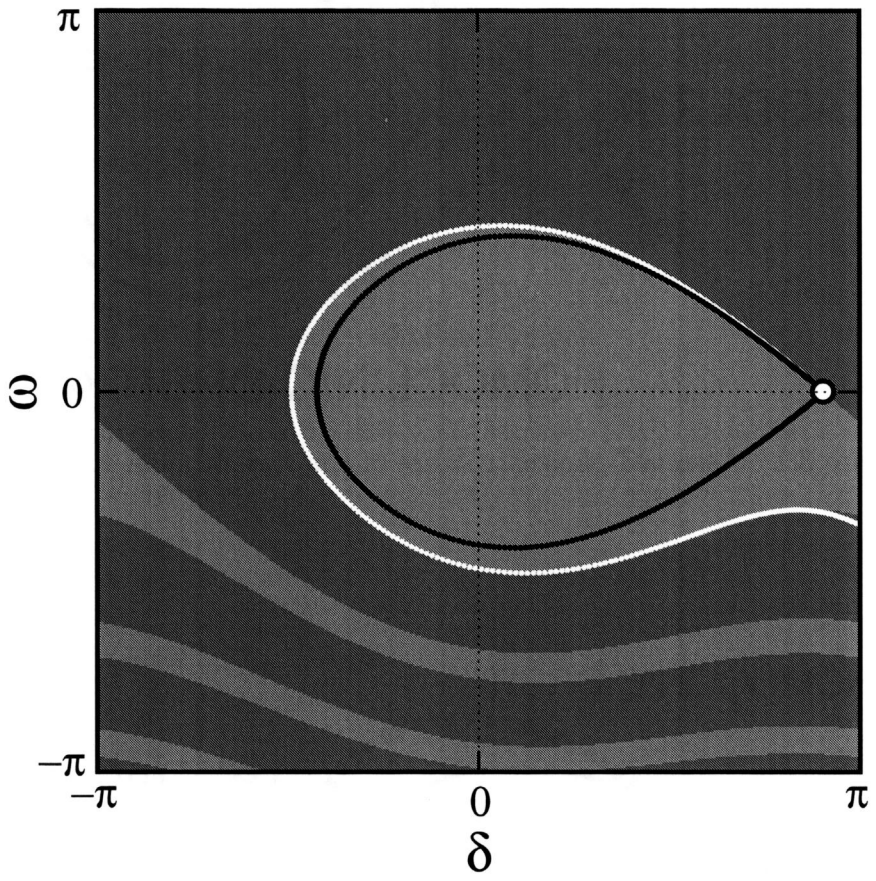

Figure 3.3 Stability boundary, original homoclinic orbit, and analytical criterion in autonomous swing equation (3.29) under $a = 0$ and $p_{\mathrm{m}} - p_{\mathrm{e(dc)}} = 0.2$. The region is colored *light-gray* for an acceptable operating condition and *dark-gray* for an asynchronous state, and the *black* line shows the original homoclinic orbit and the *white* line the proposed criterion. The symbol ◯ denotes the assumed saddle point.

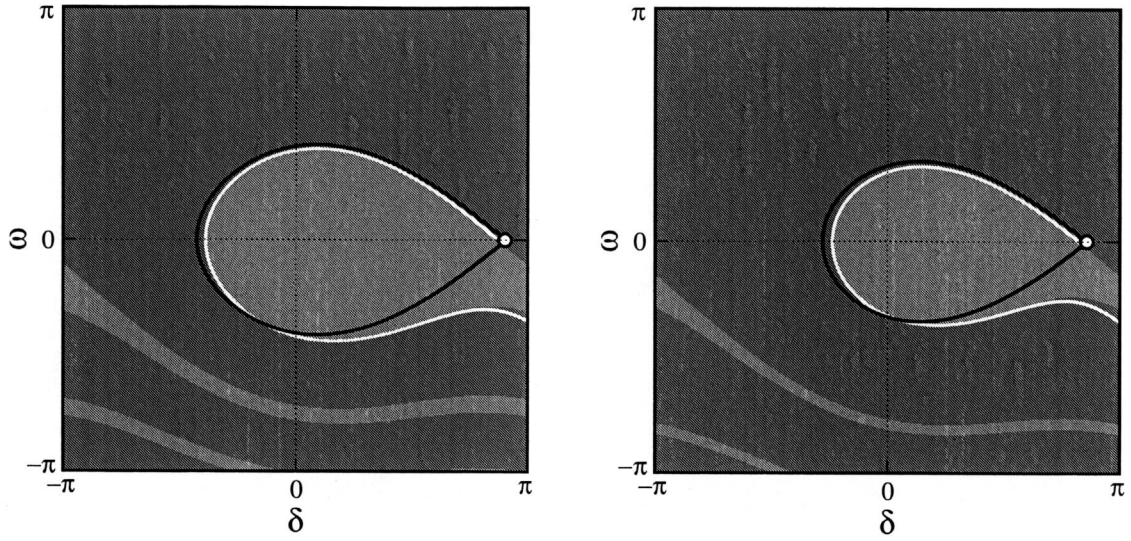

(a+) $p_{\mathrm{m}} - p_{\mathrm{e(dc)}} = 0.2$

(b+) $p_{\mathrm{m}} - p_{\mathrm{e(dc)}} = 0.3$

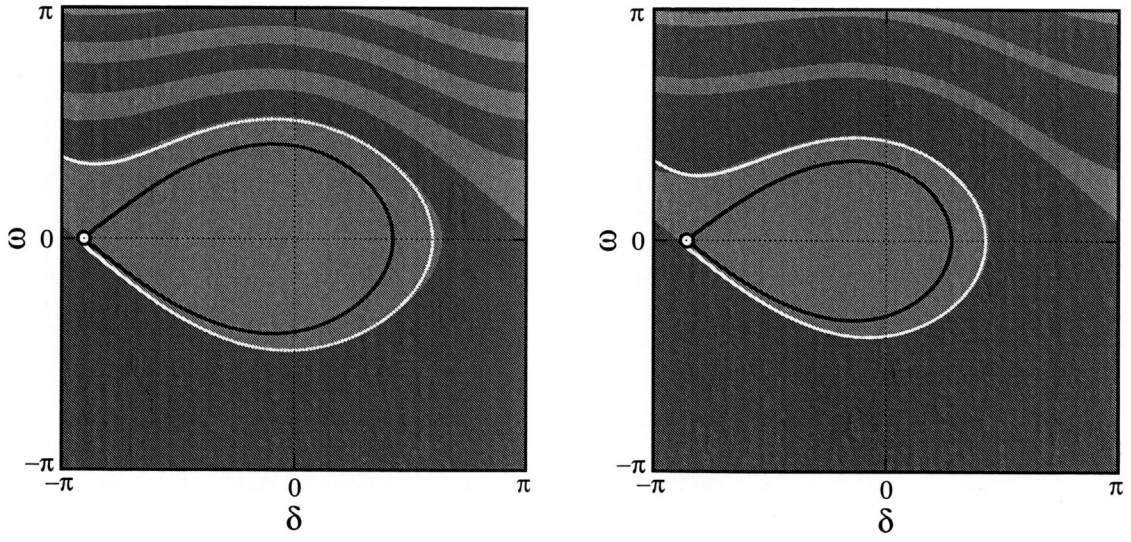

(a–) $p_{\mathrm{m}} - p_{\mathrm{e(dc)}} = -0.2$

(b–) $p_{\mathrm{m}} - p_{\mathrm{e(dc)}} = -0.3$

Figure 3.4 Stability boundaries, original homoclinic orbit, and analytical criteria in discrete dynamical system $\mathscr{F}$ at phase $\phi_0 = 0$ with $a = 0.7$. The region is colored *light-gray* for stable operating conditions and *dark-gray* for asynchronous states. Each symbol ◯ stands for the assumed saddle point.

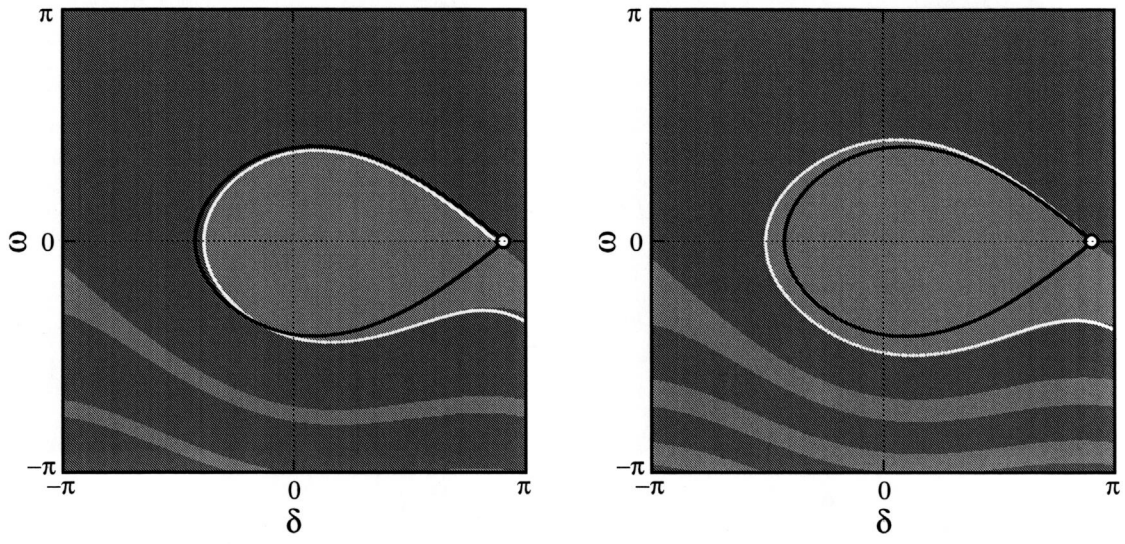

(a) $\phi_0 = 0$

(b) $\phi_0 = \pi/2$

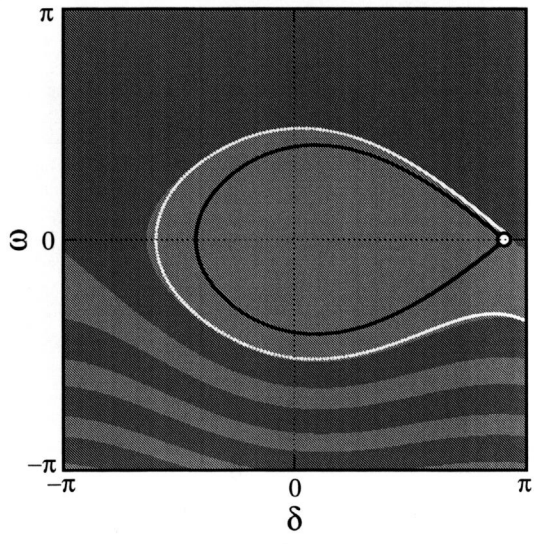

(c) $\phi_0 = \pi$

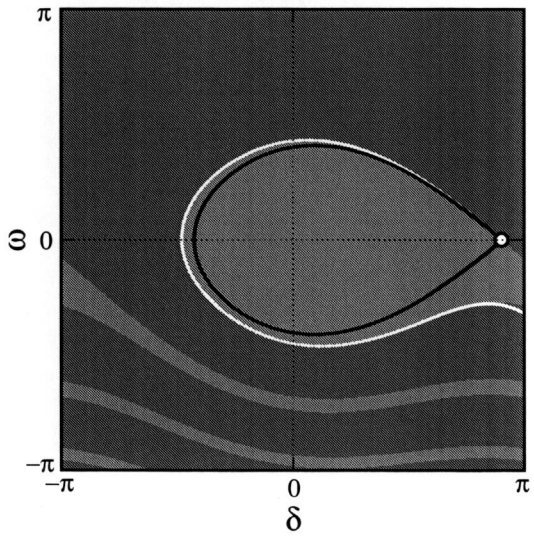

(d) $\phi_0 = 3\pi/2$

Figure 3.5 Stability boundaries, original homoclinic orbit, and analytical criteria in discrete dynamical system $\mathscr{F}$ at phase $\phi_0 = k\pi/2\,(k = 0, \ldots, 3)$ under $a = 0.7$ and $p_{\mathrm{m}} - p_{\mathrm{e(dc)}} = 0.2$

Chapter 4

Subharmonic Melnikov functions and stability boundaries

Chapter 3 proposed an analytical criterion for the stability boundaries in the ODF perturbed Hamiltonian systems. The analytical criterion addresses the basin boundaries of *non-resonant* solutions. It is not therefore effective if the genesis of the *resonant* solutions happens in the non-autonomous systems. Although the resonant solutions and associated basin structures are phenomenologically discussed in [43,79,97], no analytical and effective approach has been reported to the basin boundaries of the resonant solutions.

In this chapter, we discuss basin boundaries of the resonant solutions based on the subharmonic Melnikov functions [62] and related theories [32,33,35,108], thereby deriving an analytical criterion for the basin boundaries. At first, ODF time-independent perturbed Hamiltonian system for the resonant solutions is induced using coordinates transformations and averaging principle. By applying the previous method in Chapter 3 to the induced Hamiltonian system, an analytical criterion is derived for the basin boundaries of the resonant solutions. The derived criterion has a potential to clarify the stability boundaries related to the resonant solutions analytically, since it is established with corresponding integrable Hamiltonian system. This chapter also applies the derived criterion to the stability boundary analysis of the swing equation system.

4.1 Preliminaries

This chapter considers the perturbed Hamiltonian system (3.2) described by

$$\frac{\mathrm{d}\boldsymbol{q}}{\mathrm{d}t} = \mathrm{J}\mathrm{D}\mathcal{H}(\boldsymbol{q}) + \varepsilon \boldsymbol{g}(\boldsymbol{q}, t), \tag{4.1}$$

where again $\mathcal{H}$ is the Hamiltonian and ε the small positive parameter, and $\boldsymbol{q} = (x, y)^{\mathrm{T}} \in \mathbb{R} \times \mathbb{R}$, $\boldsymbol{g}(\boldsymbol{q}, t) = (g_1(x, y, t), g_2(x, y, t))^{\mathrm{T}}$,

$$\mathrm{J} = \begin{pmatrix} 0 & 1 \\ -1 & 0 \end{pmatrix}, \tag{4.2}$$

and

$$\mathrm{D}\mathcal{H}(\boldsymbol{q}) = \left(\frac{\partial}{\partial x}\mathcal{H}(x, y),\ \frac{\partial}{\partial y}\mathcal{H}(x, y) \right)^{\mathrm{T}}. \tag{4.3}$$

$\boldsymbol{g}(\boldsymbol{q}, t)$ has the periodicity of T $(= 2\pi/\Omega)$ for t. The system (4.1) under $\varepsilon = 0$ also holds the following assumptions; the assumed phase structure is schematically shown in Fig. 3.1.

Assumption 4.1 For $\varepsilon = 0$ the system (4.1) has a homoclinic orbit $\Gamma^0 \triangleq \{\boldsymbol{q}^0(t) \,|\, t \in \mathbb{R}\}$ to a saddle point $\boldsymbol{p}_0$.

Assumption 4.2 The interior of $\Gamma^0 \cap \{\boldsymbol{p}_0\}$ is filled with a continuous family of periodic orbits $\boldsymbol{q}^\alpha(t), \alpha \in (-1, 0)$ with period T_α. We have $\lim_{\alpha \to 0} \sup_{t \in \mathbb{R}} d(\boldsymbol{q}^\alpha(t), \Gamma^0) = 0$ and $\lim_{\alpha \to 0} T_\alpha = +\infty$. The system (4.1) under $\varepsilon = 0$ also has a center $\boldsymbol{p}_{-1}$ enclosed by the continuous family of the periodic orbits.

Assumption 4.3 T_α is a differentiable function of the Hamiltonian value $h_\alpha \triangleq \mathcal{H}(\boldsymbol{q}^\alpha(t))$ and $\mathrm{d}T_\alpha/\mathrm{d}h_\alpha > 0$ inside $\Gamma^0 \cap \{\boldsymbol{p}_0\}$.

A discrete dynamical system is also introduced for the transformed system as follows:

$$\begin{cases} \dfrac{\mathrm{d}\boldsymbol{q}}{\mathrm{d}t} = \mathrm{J}\mathrm{D}\mathcal{H}(\boldsymbol{q}) + \varepsilon \boldsymbol{g}(\boldsymbol{q}, \phi), \\ \dfrac{\mathrm{d}\phi}{\mathrm{d}t} = \Omega. \end{cases} \tag{4.4}$$

If we take a global section $\Sigma_{\phi_0} \triangleq \{(\boldsymbol{q}, \phi) \in \mathbb{R} \times \mathbb{R} \times \mathbb{S}^1 \,|\, \phi = \phi_0 \in \mathbb{S}^1\}$, for some fixed phase ϕ_0 the autonomous system (4.4) is transformed into a discrete dynamical system called by Poincaré map:

$$\mathscr{P}_{\phi_0}^{\varepsilon} : \Sigma_{\phi_0} \to \Sigma_{\phi_0}. \tag{4.5}$$

4.2 An analytical criterion for basin boundaries of resonant solutions

This section discusses the basin boundaries of resonant solutions based on the subharmonic Melnikov functions [62] and related theories [32, 33, 35, 108].

4.2.1 Action angle coordinates transformation

At first, in the interior of $\Gamma^0 \cap \{\boldsymbol{p}_0\}$ the system (4.1) can be transformed into another system via an action angle coordinates transformation [62, 108]. Fig. 4.1 shows the conceptual diagram of the action angle transformation in the system (4.1) under $\varepsilon = 0$. The transformation can be found as follows:

$$\begin{cases} I &= T_I(x,y) \triangleq \dfrac{1}{2\pi}\displaystyle\oint_{\mathcal{H}(x,y)=\mathcal{H}_c} y\mathrm{d}x, \\ \theta &= T_\theta(x,y) \triangleq \dfrac{2\pi}{T(\mathcal{H}_c)} s(x,y), \end{cases} \tag{4.6}$$

where $T(\mathcal{H}_c)$ denotes the period of the periodic orbit satisfying $\mathcal{H}(x,y) = \mathcal{H}_c = \text{const.}$. I plays the role of general parameter α in Assumptions 4.2 and 4.3, and each value I specifies a periodic orbit, that is, $\mathcal{H}_c$. $s(x,y)$ represents the time taken for the solution starting at $\boldsymbol{q}^0$ on the solid line L to reach $\boldsymbol{q}$ in Fig. 4.1. The transformation (4.6) is one of canonical transformations [6], and its differentiable inverse exists: $x = T_x(I,\theta)$ and $y = T_y(I,\theta)$. The perturbed system (4.1) is now represented as follows:

$$\begin{cases} \dfrac{\mathrm{d}I}{\mathrm{d}t} &= \varepsilon\left(\dfrac{\partial T_I}{\partial x}g_1 + \dfrac{\partial T_I}{\partial y}g_2\right) \triangleq \varepsilon F(I,\theta,t), \\ \dfrac{\mathrm{d}\theta}{\mathrm{d}t} &= \tilde{\Omega}(I) + \varepsilon\left(\dfrac{\partial T_\theta}{\partial x}g_1 + \dfrac{\partial T_\theta}{\partial y}g_2\right) \triangleq \tilde{\Omega}(I) + \varepsilon G(I,\theta,t), \end{cases} \tag{4.7}$$

where $\tilde{\Omega}(I)$ stands for the angular frequency of the periodic orbit satisfying $\mathcal{H}(I) = \mathcal{H}_c = \text{const.}$. The terms F and G apparently have the periodicity of T for t. A discrete system

$\tilde{\mathscr{P}}^{\varepsilon}_{\phi_0}$ can be defined by the transformed system:

$$\begin{cases} \dfrac{\mathrm{d}I}{\mathrm{d}t} &= & \varepsilon F(I,\theta,\phi), \\ \dfrac{\mathrm{d}\theta}{\mathrm{d}t} &= \tilde{\Omega}(I) &+ \varepsilon G(I,\theta,\phi), \\ \dfrac{\mathrm{d}\phi}{\mathrm{d}t} &= \Omega. \end{cases} \tag{4.8}$$

4.2.2 Perturbed Hamiltonian system for resonant solutions

The standard localized expansion is here used in the neighborhood of the following resonance relation:

$$m\tilde{\Omega}(I^{m/n}) \;=\; n\Omega \;=\; n\frac{2\pi}{T}, \tag{4.9}$$

where m and n are relatively prime integers and $I^{m/n}$ an action value satisfying the above relation; a region near $I = I^{m/n}$ in $\tilde{\mathscr{P}}^{\varepsilon}_{\phi_0}$ at $\phi_0 = 0$ (abbreviated as $\tilde{\mathscr{P}}^{\varepsilon}_{0}$) is called *resonance band*. A transformation for the localized expansion is as follows:

$$\begin{cases} I &= I^{m/n} + \sqrt{\varepsilon}h, \\ \theta &= \tilde{\Omega}(I^{m/n})t + \sigma. \end{cases} \tag{4.10}$$

It is regarded as a kind of van der Pol transformations [35, 39, 108]. A variational system is then obtained as follows:

$$\begin{cases} \dfrac{\mathrm{d}h}{\mathrm{d}t} &= \sqrt{\varepsilon}F(I^{m/n},\theta,t) &+ \varepsilon\dfrac{\partial F}{\partial I}(I^{m/n},\theta,t)h \\ &+ \mathcal{O}(\varepsilon^{3/2}), & \\ \dfrac{\mathrm{d}\sigma}{\mathrm{d}t} &= \sqrt{\varepsilon}\dfrac{\partial\tilde{\Omega}}{\partial I}(I^{m/n})h &+ \varepsilon\left\{\dfrac{1}{2}\dfrac{\partial^2\tilde{\Omega}}{\partial I^2}(I^{m/n})h^2 + G(I^{m/n},\theta,t)\right\} \\ &+ \mathcal{O}(\varepsilon^{3/2}), & \end{cases} \tag{4.11}$$

where $\theta = \tilde{\Omega}(I^{m/n})t + \sigma$.

ODF perturbed Hamiltonian system is now derived for the resonant solutions by applying the second order averaging [35, 39, 46, 108] to the variational system (4.11). The detailed process of averaging is shown in the appendix of this chapter. A second order

averaged system is obtained as follows:

$$\left\{\begin{array}{rcl} \dfrac{\mathrm{d}\overline{h}}{\mathrm{d}t} &=& \mu\dfrac{1}{2\pi n}\bar{\mathcal{M}}_1^{m/n}\left(\dfrac{\overline{\sigma}}{\tilde{\Omega}(I^{m/n})}\right) + \varepsilon\overline{\dfrac{\partial F}{\partial I}}(\overline{\sigma})\overline{h}, \\ \dfrac{\mathrm{d}\overline{\sigma}}{\mathrm{d}t} &=& \mu\dfrac{\partial\tilde{\Omega}}{\partial I}(I^{m/n})\overline{h} + \varepsilon\left\{\dfrac{1}{2}\dfrac{\partial^2\tilde{\Omega}}{\partial I^2}(I^{m/n})\overline{h}^2 + \overline{G}(\overline{\sigma})\right\}, \end{array}\right. \tag{4.12}$$

where $\mu \triangleq \sqrt{\varepsilon}$ is treated as an independent parameter, and

$$\left\{\begin{array}{rcl} \bar{\mathcal{M}}_1^{m/n}\left(\dfrac{\overline{\sigma}}{\tilde{\Omega}(I^{m/n})}\right) &\triangleq& \tilde{\Omega}(I^{m/n})\displaystyle\int_0^{mT} F(I^{m/n}, \tilde{\Omega}(I^{m/n})\tau + \overline{\sigma}, \tau)\mathrm{d}\tau, \\ \overline{\dfrac{\partial F}{\partial I}}(\overline{\sigma}) &\triangleq& \dfrac{1}{mT}\displaystyle\int_0^{mT}\dfrac{\partial F}{\partial I}(I^{m/n}, \tilde{\Omega}(I^{m/n})\tau + \overline{\sigma}, \tau)\mathrm{d}\tau. \\ \overline{G}(\overline{\sigma}) &\triangleq& \dfrac{1}{mT}\displaystyle\int_0^{mT} G(I^{m/n}, \tilde{\Omega}(I^{m/n})\tau + \overline{\sigma}, \tau)\mathrm{d}\tau, \end{array}\right. \tag{4.13}$$

$\bar{\mathcal{M}}_1^{m/n}(\overline{\sigma}/\tilde{\Omega}(I^{m/n}))$ is well-known as a *subharmonic Melnikov function* [32,33,35,108]. The averaged system (4.12) is ODF time-independent perturbed Hamiltonian system with a Hamiltonian $\mathcal{K}$:

$$\frac{\mathrm{d}\overline{\boldsymbol{q}}}{\mathrm{d}t} = \mathrm{J}\mathrm{D}\mathcal{K}(\overline{\boldsymbol{q}}) + \varepsilon\overline{\boldsymbol{g}}(\overline{\boldsymbol{q}}), \tag{4.14}$$

where $\overline{\boldsymbol{q}} \triangleq (\overline{\sigma}, \overline{h})^{\mathrm{T}}$ and

$$\left\{\begin{array}{rcl} \mathcal{K}(\overline{\boldsymbol{q}}) &\triangleq& \mu\left\{\dfrac{1}{2}\dfrac{\partial\tilde{\Omega}}{\partial I}(I^{m/n})\overline{h}^2 - \dfrac{1}{2\pi n}\displaystyle\int\bar{\mathcal{M}}_1^{m/n}\left(\dfrac{\overline{\sigma}}{\tilde{\Omega}(I^{m/n})}\right)\mathrm{d}\overline{\sigma}\right\}, \\ \mathrm{D}\mathcal{K}(\overline{\boldsymbol{q}}) &\triangleq& \left(\dfrac{\partial K}{\partial\overline{\sigma}}(\overline{\boldsymbol{q}}), \dfrac{\partial K}{\partial\overline{h}}(\overline{\boldsymbol{q}})\right)^{\mathrm{T}}, \\ \overline{\boldsymbol{g}}(\overline{\boldsymbol{q}}) &\triangleq& \left(\dfrac{1}{2}\dfrac{\partial^2\tilde{\Omega}}{\partial I^2}(I^{m/n})\overline{h}^2 + \overline{G}(\overline{\sigma}), \overline{\dfrac{\partial F}{\partial I}}(\overline{\sigma})\overline{h}\right)^{\mathrm{T}}. \end{array}\right. \tag{4.15}$$

Remark 4.4 The subharmonic Melnikov function $\bar{\mathcal{M}}_1^{m/n}(\overline{\sigma}/\tilde{\Omega}(I^{m/n}))$ provides us with the existence and stability conditions of the resonant fixed or periodic points in the discrete dynamical system $\tilde{\mathscr{P}}_0^{\varepsilon}$. In [108] $\bar{\mathcal{M}}_1^{m/n}(\overline{\sigma}/\tilde{\Omega}(I^{m/n}))$ is discussed in terms of $\tilde{\mathscr{P}}_{\phi_0}^{\varepsilon}$ and its first derivation, and is derived as the existence condition for m *resonant* periodic points of $\tilde{\mathscr{P}}_0^{\varepsilon}$. From [108], the condition of $\tilde{\mathscr{P}}_0^{\varepsilon}$ is identical to the existence condition for equilibrium points in the averaged system (4.14) under $\varepsilon = 0$, that is, $\bar{\mathcal{M}}_1^{m/n}(\overline{\sigma}/\tilde{\Omega}(I^{m/n})) = 0$ and

$\overline{h} = 0$. In addition, if $\bar{\mathcal{M}}_1^{m/n}(\overline{\sigma}/\tilde{\Omega}(I^{m/n}))$ has some zero points, then we have $2m$ zero points; associated m equilibrium points have the saddle-type stability. This property directly leads to the assumptions that the system (4.14) will hold in the next subsection.

Remark 4.5 The averaged system (4.14) possibly has the sufficient property to clarify the phase structure of the discrete dynamical system $\tilde{\mathscr{P}}_0^{\varepsilon}$ qualitatively. As noted in [32, 33, 35, 108], the second order averaging generally suffices to determine the stability for all equilibrium points, at least for $\partial\tilde{\Omega}(I^{m/n})/\partial I < +\infty$ and sufficiently small ε. In addition, through the phase structure of the system (4.14), we can grasp the phase structure in the resonance band (4.9) of $\tilde{\mathscr{P}}_0^{\varepsilon}$ qualitatively.

Remark 4.6 The phase structure of the averaged system (4.14) can be analytically examined based on the original system (4.1) under $\varepsilon = 0$. In addition, all phase structure of the averaged system (4.14) under $\varepsilon = 0$ can be understood analytically because of its integrable property.

4.2.3 An analytical criterion

This section states the main result in this chapter: an analytical criterion for the basin boundaries of the resonant solutions. The criterion is established based on the averaged system (4.14) and the previous method in Chapter 3. In order to apply the method to the averaged system, we make the following assumptions which are same to Assumptions 4.1 and 4.2:

Assumption 4.7 For $\varepsilon = 0$ the averaged system (4.14) has a homoclinic orbit $\overline{\Gamma}_{(i)}^0 \triangleq \{\overline{\boldsymbol{q}}_{(i)}^0(t) \,|\, t \in \mathbb{R}\}$ to each saddle point $\overline{\boldsymbol{p}}_{0(i)}$ for $i = 1, \cdots, m$.

Assumption 4.8 Each interior of $\overline{\Gamma}_{(i)}^0 \cap \{\overline{\boldsymbol{p}}_{0(i)}\}$ is filled with a continuous family of periodic orbits $\overline{\boldsymbol{q}}_{(i)}^{\alpha}(t), \alpha \in (-1, 0)$ with period $\overline{T}_{\alpha(i)}$. We have $\lim\limits_{\alpha\to 0} \sup\limits_{t\in\mathbb{R}} d(\overline{\boldsymbol{q}}_{(i)}^{\alpha}(t), \overline{\Gamma}_{(i)}^0) = 0$ and $\lim\limits_{\alpha\to 0} \overline{T}_{\alpha(i)} = +\infty$. The averaged system (4.14) under $\varepsilon = 0$ also has a center $\overline{\boldsymbol{p}}_{-1(i)}$ enclosed by each continuous family of the periodic orbits.

As mentioned in Chapter 3, for sufficiently small ε, each equilibrium point $\overline{\boldsymbol{p}}_{0(i)}^{\varepsilon}$ related to $\overline{\boldsymbol{p}}_{0(i)}$ in the averaged system (4.14) uniquely exists and becomes a saddle point. In addition, the averaged system holds the following assumption:

Assumption 4.9 Each equilibrium point $\overline{\boldsymbol{p}}^{\varepsilon}_{-1(i)}$ associated with $\overline{\boldsymbol{p}}_{-1(i)}$ for $i = 1, \cdots, m$ in the averaged system (4.14) uniquely exists and is an asymptotically stable point in the sense of Lyapunov.

Thus, for sufficiently small ε, the averaged system (4.14) has the same phase structure as that shown in Fig. 3.2 qualitatively.

We now derive an analytical criterion for the basin boundaries of the resonant solutions as same as the process in Chapter 3. The Melnikov's method naturally leads to a method for modifying a point $\overline{\boldsymbol{q}}^{0}_{(i)}(-\bar{t}_0)$ on each homoclinic orbit $\overline{\Gamma}_{(i)}$ for $i = 1, \cdots, m$:

$$\overline{\boldsymbol{q}}^{0\prime}_{(i)}(-\bar{t}_0) \triangleq \overline{\boldsymbol{q}}^{0}_{(i)}(-\bar{t}_0) + \frac{\overline{d}^{\mathrm{s}}_{1(i)}(\overline{\boldsymbol{q}}^{0}_{(i)}(-\bar{t}_0))}{||\mathrm{D}\mathcal{K}(\overline{\boldsymbol{q}}^{0}_{(i)}(-\bar{t}_0))||}\mathrm{D}\mathcal{K}(\overline{\boldsymbol{q}}^{0}_{(i)}(-\bar{t}_0)), \tag{4.16}$$

where

$$\overline{d}^{\mathrm{s}}_{1(i)}(\overline{\boldsymbol{q}}^{0}_{(i)}(-\bar{t}_0)) \triangleq \varepsilon\frac{1}{||\mathrm{D}\mathcal{K}(\overline{\boldsymbol{q}}^{0}_{(i)}(-\bar{t}_0))||}\left(-\int_{-\bar{t}_0}^{+\infty}\mathrm{D}\mathcal{K}(\overline{\boldsymbol{q}}^{0}_{(i)}(t))\cdot\overline{\boldsymbol{g}}(\overline{\boldsymbol{q}}^{0}_{(i)}(t))\mathrm{d}t\right). \tag{4.17}$$

As shown in Chapter 3, $\overline{\boldsymbol{q}}^{0\prime}_{(i)}(-\bar{t}_0)$ is close to the stable manifold of the the saddle point $\overline{\boldsymbol{p}}^{\varepsilon}_{0(i)}$, that is, each modified homoclinic orbit $\{\overline{\boldsymbol{q}}^{0\prime}_{(i)}(-\bar{t}_0)\}$ is expected to be a good estimation of the basin boundary of $\overline{\boldsymbol{p}}^{\varepsilon}_{-1(i)}$. Hence, each modified homoclinic orbit $\{\overline{\boldsymbol{q}}^{0\prime}_{(i)}(-\bar{t}_0)\}$ is derived as an analytical criterion for the basin boundaries of the resonant solutions.

Remark 4.10 The criterion can be directly derived with the integrable Hamiltonian system (4.1) under $\varepsilon = 0$.

Remark 4.11 To describe each $\{\overline{\boldsymbol{q}}^{0\prime}_{(i)}(-\bar{t}_0)\}$ in the original $x - y$ plane, it is necessary to transform each point on $\{\overline{\boldsymbol{q}}^{0\prime}_{(i)}(-\bar{t}_0)\}$ in $\bar{\sigma} - \bar{h}$ plane into $x - y$ plane. The transformation is performed as follows:

$$\begin{cases} I &= I^{m/n} + \sqrt{\varepsilon}\bar{h}, \\ \theta &= \bar{\sigma}, \end{cases} \tag{4.18}$$

and

$$\begin{cases} x &= T_x(I, \theta), \\ y &= T_y(I, \theta). \end{cases} \tag{4.19}$$

Remark 4.12 The criterion *approximately* represents the basin boundaries of the resonant solutions. It was obtained through the averaged system (4.14) which was derived by truncating the variational system (4.11). Although the phase structure of the averaged system (4.14) is identical to that of $\tilde{\mathscr{P}}_0^{\varepsilon}$ in the resonance band (4.9) qualitatively, it should be noted that the criterion provides us with the second order information about the basin boundaries of the resonant solutions. Additionally, Remark 3.10 again points out that it is inevitable to truncate each $\{\overline{\boldsymbol{q}}^{0\prime}_{(i)}(-\bar{t}_0)\}$ in a positive number $\overline{T}_0 \in \mathbb{R}$ such that $|\bar{t}_0| < \overline{T}_0$ to obtain a good estimation of the basin boundaries.

4.3 Illustrative examples

This section applies the derived criterion to concrete non-autonomous systems and exhibits both its effectiveness and application limits.

4.3.1 Greenspan and Holmes system

The criterion is applied to the following non-autonomous system [33, 35]:

$$\begin{cases} \dfrac{\mathrm{d}x}{\mathrm{d}t} &= y\{r-(x^2+y^2)\} &+ \varepsilon\{kx - x(x^2+y^2) + Bx\cos t\}, \\ \dfrac{\mathrm{d}y}{\mathrm{d}t} &= -x\{r-(x^2+y^2)\} &+ \varepsilon\{ky - y(x^2+y^2)\}. \end{cases} \tag{4.20}$$

The system (4.20) at $\varepsilon = 0$ is ODF Hamiltonian system with a Hamiltonian $\mathcal{H}$:

$$\mathcal{H}(x,y) = r\frac{x^2+y^2}{2} - \left(\frac{x^2+y^2}{2}\right)^2. \tag{4.21}$$

For $\varepsilon = 0$ the system (4.20) does not have any hyperbolic saddle point and associated homoclinic orbit. However, in the interior of the circle $\{(x,y) \mid x^2+y^2 = r\}$ the Hamiltonian system has a center at the origin and a family of periodic solutions satisfying Assumption 4.3. On the other hand, for $\varepsilon \neq 0$, $B = 0$, and $0 < k < r$, the system (4.20) has a non-resonant unstable focus at the origin and a stable limit cycle with the period $2\pi/(r-k)$.

We now consider 1/2–harmonic entrainment and associated basin boundary in system (4.20). The entrainment is mathematically represented by the resonance relation (4.9) at

$m = 2$ and $n = 1$. By using the following transformations:

$$\begin{cases} x &= \sqrt{2I}\sin\theta, \\ y &= \sqrt{2I}\cos\theta, \end{cases} \tag{4.22}$$

and

$$\begin{cases} \theta &= \dfrac{t}{2} + \sigma, \\ I &= \dfrac{\tilde{r}}{2} + \sqrt{\varepsilon}h, \end{cases} \tag{4.23}$$

where $\tilde{r} \triangleq r - 1/2$ and by averaging $\mathcal{O}(\varepsilon)$ terms, we obtain the second order averaged system as follows:

$$\begin{cases} \dfrac{\mathrm{d}\sigma}{\mathrm{d}t} &= \mu(-2h) &+ \varepsilon\dfrac{B}{4}\sin 2\sigma, \\ \dfrac{\mathrm{d}h}{\mathrm{d}t} &= \mu\tilde{r}\left(k - \tilde{r} - \dfrac{B}{4}\cos 2\sigma\right) &+ \varepsilon\left\{2(k - 2\tilde{r}) - \dfrac{B}{2}\cos 2\sigma\right\}h. \end{cases} \tag{4.24}$$

Now $\mu \triangleq \sqrt{\varepsilon}$, and all single bars are dropped. For $\varepsilon = 0$ the averaged system (4.24) is ODF Hamiltonian system with a Hamiltonian $\mathcal{K}$:

$$\mathcal{K}(\sigma, h) = \mu\left[-h^2 - \omega\left\{(k - \omega)\sigma - \frac{B}{8}\sin 2\sigma\right\}\right]. \tag{4.25}$$

A basin boundary of resonant solutions is now discussed under the following parameters [33]:

$$r = 1.0, \quad \varepsilon = 0.05, \quad k = 0.7, \quad B = 1.1. \tag{4.26}$$

The averaged system (4.24) under $\mu = \sqrt{0.05}$ and $\varepsilon = 0$ has two centers, two saddle points, and associated homoclinic orbits satisfying Assumptions 4.7 and 4.8. For $\varepsilon = 0.05$ the system (4.24) has two stable focuses associated with the two centers. The derived criterion can be therefore applied to the system (4.24).

Figure 4.2 shows the basin structure and the proposed criteria for the averaged system (4.24). In the figure, the *white* region denotes the basin of the stable focus ${}^1\mathsf{S}^1_{(1)}$, the *dark-gray* the basin of the stable focus ${}^1\mathsf{S}^1_{(2)}$, and the *light-gray* the basin of a limit cycle. The *black* solid lines in Fig. 4.2 represent the proposed criteria in Chapter 3 and are apparently close to the basin boundaries of ${}^1\mathsf{S}^1_{(i)}$ $(i = 1, 2)$. The proposed criteria are, however, far from the basin boundaries in the region $h < 0$. This is because the norm of the normal

vector $D\mathcal{K}(\overline{\boldsymbol{q}}^{0\prime}_{(i)}(-\bar{t}_0))$ is adopted to calculate the criteria, and the norm converges to zero as $\bar{t}_0 \to \pm\infty$ as mentioned in Remark 4.12.

Now we obtain the analytical criterion for the basin boundaries in the discrete dynamical system $\mathscr{P}_0^{\varepsilon}$ relative to the system (4.20) by transforming the proposed criteria on $\sigma - h$ plane into $x - y$ plane. Fig. 4.3 shows the basin structure and analytical criterion of $\mathscr{P}_0^{\varepsilon}$. In the figure, the *black* point, which is plotted at the origin, denotes the source ${}^1\mathsf{U}^1$ and QP the quasi-periodic solution. The *white* and *dark-gray* regions in Fig. 4.3 represent the basins of the two resonant periodic points ${}^1\mathsf{S}^2_{i\,(i=1,2)}$ and the *light-gray* region the basin of QP. The criterion is described with two *black* solid lines and precisely grasps a part of the basin boundaries of ${}^1\mathsf{S}^2_{i\,(i=1,2)}$. This example shows the effectiveness of the analytical criterion although it cannot clarify the detail of the basin boundaries of ${}^1\mathsf{S}^2_{i\,(i=1,2)}$.

4.3.2 Swing equation system

Next we next deal with the stability boundary analysis in the swing equation system:

$$\begin{cases} \mathcal{H}(\delta,\omega) &= \dfrac{1}{2}\omega^2 - b\cos\delta - \left(p_{\mathrm{m}} - p_{\mathrm{e(dc)}}\right)k, \\ g_1(\delta,\omega,t) &= 0, \\ g_2(\delta,\omega,t) &= -\tilde{D}\omega + a\cos\Omega t, \end{cases} \tag{4.27}$$

where the following parameters are set :

$$b = 0.7, \quad p_{\mathrm{m}} - p_{\mathrm{e(dc)}} = -0.1, \quad \varepsilon = 0.1, \quad \tilde{D} = 0.5, \quad a = 0.77, \quad \Omega = 0.7. \tag{4.28}$$

The parameter setting is based on the previous result in Chapter 2. Under the setting the system (4.27) has both non-resonant and resonant sinks.

The proposed approach is applied to the swing equation system (4.27). Fig. 4.4 shows the phase structure of the first order averaged system for the system (4.27). Here it is much difficult to perform the transformation and averaging process analytically. We therefore adopt a homoclinic orbit which exists in Fig. 4.4 as an valuation of the basin boundary of the resonant solution. In addition to this, the inverse transformation of (4.10) is hard to calculate analytically; its inverse is therefore numerically performed. Fig. 4.5 shows the basin portrait and the present evaluation in the discrete dynamical system $\mathscr{P}_0^{\varepsilon}$. In the

figure, the basin of the non-resonant sink ${}^1\mathsf{S}^1_{(1)}$ is denoted by the *white* region and the basin of the resonant sink ${}^1\mathsf{S}^1_{(2)}$ by the *black*. The finite points, marked by Our Present Approach in Fig. 4.5, are the transformed homoclinic orbit, that is, the present evaluation of the basin boundary of ${}^1\mathsf{S}^1_{(2)}$. The evaluation is included by the basin of ${}^1\mathsf{S}^1_{(2)}$. This implies that the present evaluation is a sufficient condition for the swing equation system (4.27) although the evaluation is conservative.

4.4 Summary

This chapter addressed the stability boundary analysis in the non-autonomous systems with the resonant solutions. An analytical criterion was derived for the basin boundaries of the resonant solutions. The criterion can be derived with the original ODF Hamiltonian system and is therefore effective for clarifying the basin boundaries analytically. In addition, the proposed criterion is applied to the concrete non-autonomous systems. In the case of Greenspan and Holmes system, the application illustrates the effectiveness of the proposed criterion. However, the swing equation system shows that the proposed criterion becomes a conservative and sufficient condition for the basin boundary of the resonant sink. It is much important to overcome the conservativeness in terms of the transient stability of the ac/dc power system. The problem should be attacked as a forthcoming research.

Appendix to Section 4.2: Derivation of averaged system (4.12) via second-order averaging

The following transformation is introduced based on the averaging theorem [35,39,108]:

$$\begin{cases} h &= \overline{h} + \sqrt{\varepsilon} \int \tilde{F}(I^{m/n}, \theta, t)\mathrm{d}t, \\ \sigma &= \overline{\sigma}, \end{cases} \tag{4.29}$$

where $\theta = \tilde{\Omega}(I^{m/n})t + \overline{\sigma}$. $\tilde{F}(I^{m/n}, \theta, t)$ is defined as follows:

$$\tilde{F}(I^{m/n}, \theta, t) \triangleq F(I^{m/n}, \theta, t) - \frac{1}{mT}\int_0^{mT} F(I^{m/n}, \tilde{\Omega}(I^{m/n})\tau + \overline{\sigma}, \tau)\mathrm{d}\tau. \tag{4.30}$$

That is, $\tilde{F}$ corresponds to an oscillating part of F. In addition, the averaged part of F is well-known as the following subharmonic Melnikov function:

$$\bar{\mathcal{M}}_1^{m/n}\left(\frac{\overline{\sigma}}{\tilde{\Omega}(I^{m/n})}\right) \triangleq \tilde{\Omega}(I^{m/n})\int_0^{mT} F(I^{m/n}, \tilde{\Omega}(I^{m/n})\tau + \overline{\sigma}, \tau)\mathrm{d}\tau. \tag{4.31}$$

The transformed system is then obtained as follows:

$$\begin{cases} \dfrac{\mathrm{d}\overline{h}}{\mathrm{d}t} &= \sqrt{\varepsilon}\dfrac{1}{2\pi n}\bar{\mathcal{M}}_1^{m/n}\left(\dfrac{\overline{\sigma}}{\tilde{\Omega}(I^{m/n})}\right) \\ &+ \varepsilon\left\{-\dfrac{\partial\tilde{\Omega}}{\partial I}(I^{m/n})\overline{h}\dfrac{\partial}{\partial\sigma}\int\tilde{F}(I^{m/n},\theta,t)\mathrm{d}t + \dfrac{\partial F}{\partial I}(I^{m/n},\theta,t)\overline{h}\right\} \\ &+ \mathcal{O}(\varepsilon^{3/2}), \\ \dfrac{\mathrm{d}\overline{\sigma}}{\mathrm{d}t} &= \sqrt{\varepsilon}\dfrac{\partial\tilde{\Omega}}{\partial I}(I^{m/n})\overline{h} \\ &+ \varepsilon\left\{\dfrac{\partial\tilde{\Omega}}{\partial I}(I^{m/n})\int\tilde{F}(I^{m/n},\theta,t)\mathrm{d}t + \dfrac{1}{2}\dfrac{\partial^2\tilde{\Omega}}{\partial I^2}(I^{m/n})\overline{h}^2 + G(I^{m/n},\theta,t)\right\} \\ &+ \mathcal{O}(\varepsilon^{3/2}), \end{cases} \tag{4.32}$$

where $\theta = \tilde{\Omega}(I^{m/n})t + \overline{\sigma}$. We apply the second order averaging to the transformed system (4.32), thereby obtaining the averaged system (4.12). Here, the second order averaging implicitly corresponds to the following transformations:

$$\begin{cases} \overline{h} &= \overline{\overline{h}} + \varepsilon v_h(\overline{\overline{\sigma}}, \overline{\overline{h}}, t), \\ \overline{\sigma} &= \overline{\overline{\sigma}} + \varepsilon v_\sigma(\overline{\overline{\sigma}}, \overline{\overline{h}}, t), \end{cases} \tag{4.33}$$

where v_σ and v_h are smooth functions and have the periodicity of $2\pi/\Omega$ for t. For simplicity, in the averaged system (4.12), the double bars of σ and h are replaced with the single bars.

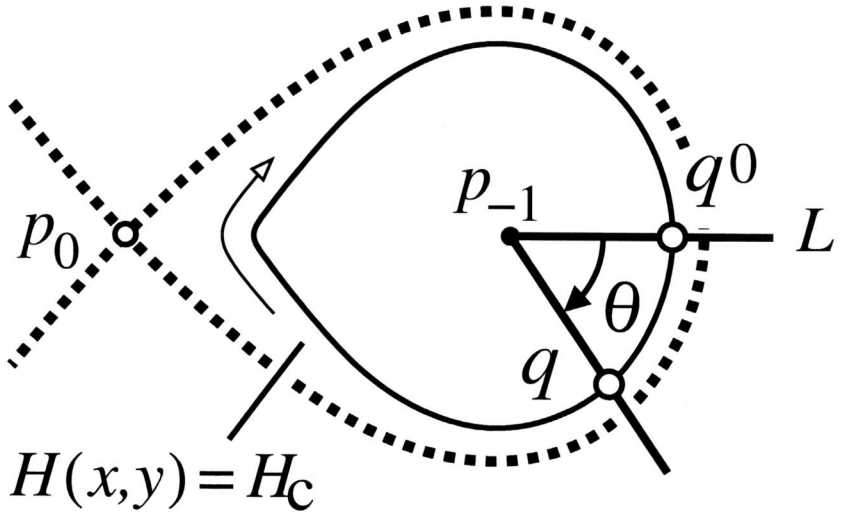

Figure 4.1 Conceptual diagram of action angle coordinates transformation in the Hamiltonian system

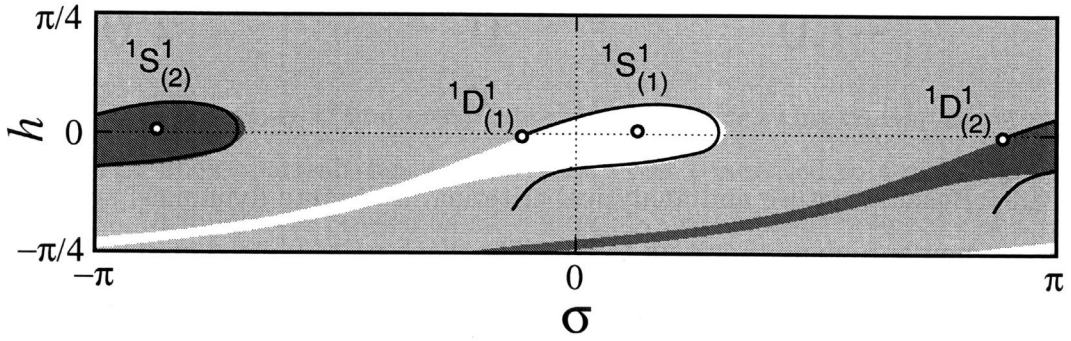

Figure 4.2 Basin structure and proposed criteria for averaged system (4.24). The basin of the stable focus $^1S^1_{(1)}$ is denoted by the *white* region, the basin of the stable focus $^1S^1_{(2)}$ by the *dark-gray*, and the basin of a second kind limit cycle by the *light-gray*. The *black* solid lines represent the proposed criteria in Chapter 3.

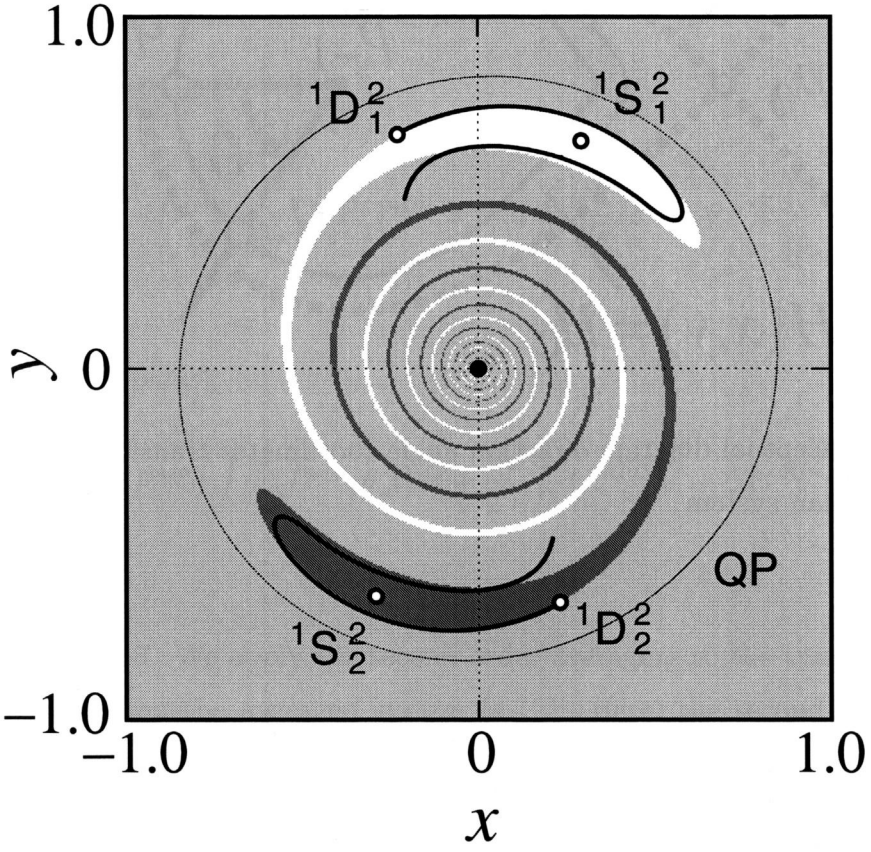

Figure 4.3 Basin structure and analytical criterion in discrete dynamical system $\mathscr{P}_0^{\varepsilon}$ for non-autonomous system (4.20). The *black* point plotted at the origin denotes the source $^1\mathsf{U}^1$. The *white* and *dark-gray* regions represent the basins of the two resonant periodic points $^1\mathsf{S}^2_{i\,(i=1,2)}$ and the *light-gray* region the basin of QP. The present criterion is described with the two *black* solid lines.

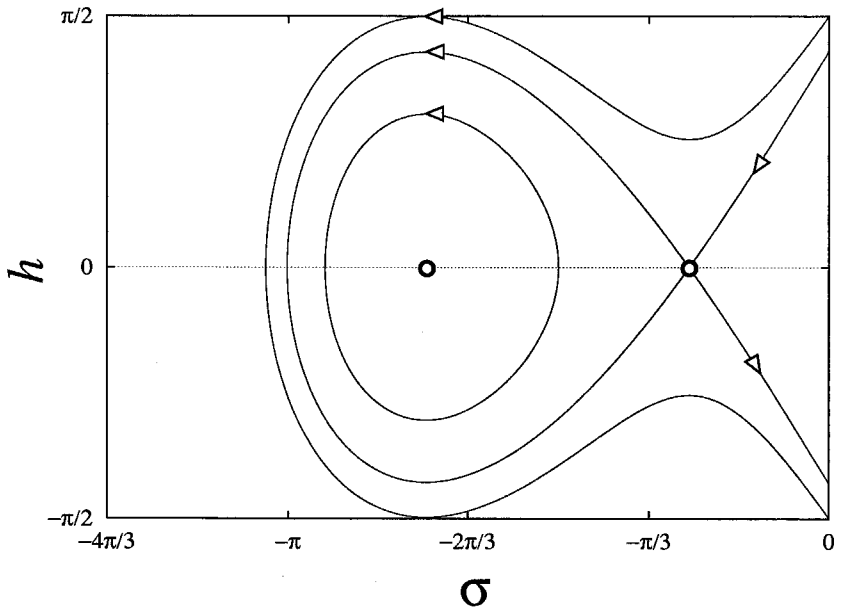

Figure 4.4 Phase structure of first order averaged system for swing equation system (4.27). The phase portrait has a homoclinic orbit connected to a saddle point. The homoclinic orbit is used as an evaluation of the basin boundary of a resonant sink.

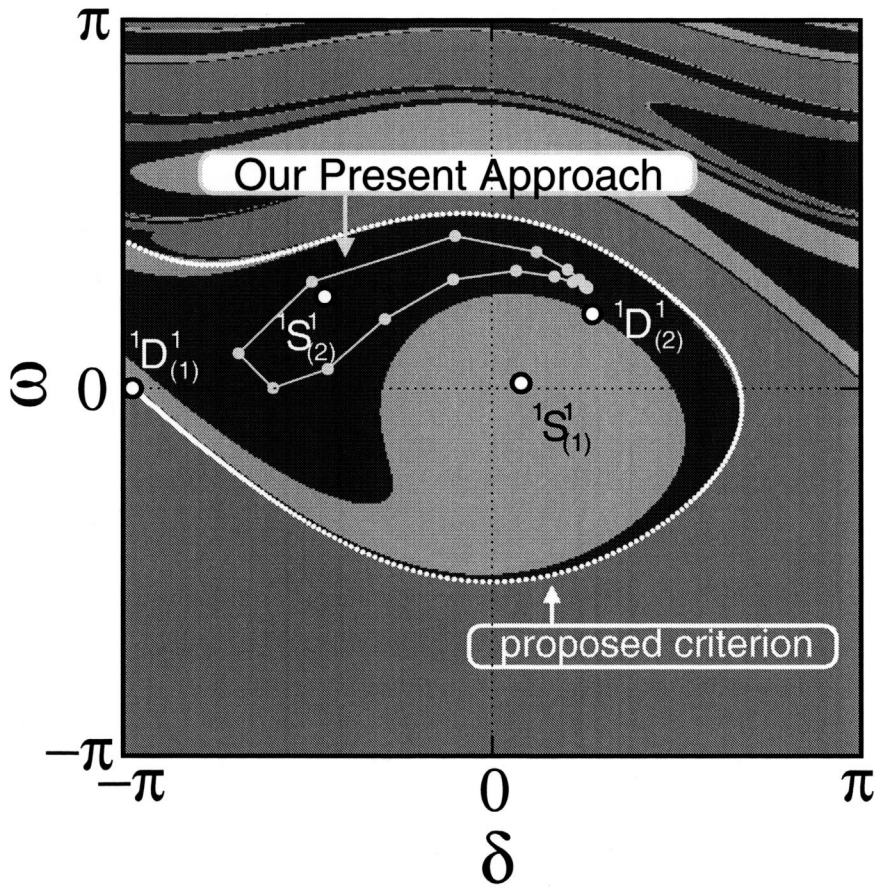

Figure 4.5 Basin structure and present evaluation in discrete dynamical system $\mathscr{P}_0^{\varepsilon}$ for swing equation system (4.27). The basin of the non-resonant solution $^1\mathsf{S}^1_{(1)}$ is colored with *light-gray* and the basin of the resonant solution $^1\mathsf{S}^1_{(2)}$ with *black*. The finite points, marked by Our Present Approach, show the present evaluation of the basin boundary of $^1\mathsf{S}^1_{(2)}$.

Chapter 5

Differential-algebraic equation system and stability boundary

The following chapter addresses transient dynamics and stability boundaries with considering dc system's operation and electric power relation between the ac and dc systems. Chapters 2–4 examined the swing equation system for the transient stability analysis of the ac/dc system. It was then assumed that the dc link was ideally operated and its electric power was constant. This assumption is, however, insufficient for considering transient stability involving dynamical characteristics of the dc link. In [21, 23, 30, 89, 98] the dc power modulation is proposed for damping power swings in ac transmission systems. The control strategy uses an effective characteristic in the rapid regulation of the electric power according to event disturbances. Thus, for practical stability estimation, it is inevitable to consider the transient dynamics and stability boundaries with taking the dc operation and the power balance relation into account.

A DAE system is here proposed for the analysis of the ac/dc power system in Fig. 1.1. The DAE system is described by a coupled system of differential and algebraic equations: the differential equation represents the dynamics of the generator and the dc link; while the algebraic equation describes the electric power relation between the ac and dc systems. The DAE system keeps the structural characteristics of power conversion and control setup in the dc link, and explicitly describes the power relationship. This chapter numerically investigates dynamical features of the DAE system. In particular, we examine a stability

boundary through several basin portraits and partly clarify its global structure in the solution space of the DAE system.

5.1 Differential-algebraic equation system

5.1.1 Derivation

This section derives a DAE system for the electric power system with dc transmission in Fig. 5.1. The figure shows the same configuration as Figs. 1.1 and 2.1. In the following discussion, all variables and parameters are in per unit except angles which are in radian. The detailed derivation of the DAE system is given in the appendix at the end of this chapter.

First, the dynamics of a generator is modeled based on the Park's theory [51, 76]:

$$\begin{cases} \dfrac{\mathrm{d}v'_q}{\mathrm{d}t} &= \dfrac{1}{T'_d}\left(\dfrac{L'_d}{L_d}V_0 + \dfrac{L_d - L'_d}{L_d}v_\mathrm{r}\cos\delta_\mathrm{r} - v'_q\right), \\ \dfrac{\mathrm{d}\delta}{\mathrm{d}t} &= \omega, \\ \dfrac{\mathrm{d}\omega}{\mathrm{d}t} &= \dfrac{1}{2H}(-D\omega + p_\mathrm{m} - p_\mathrm{g}), \end{cases} \tag{5.1}$$

where v'_q denotes the voltage source behind transient reactance, δ the rotor position with respect to synchronous reference axis, and ω the rotor speed deviation relative to system angular frequency. v_r and δ_r are defined for the ac bus voltage by

$$e_d \triangleq v_\mathrm{r}\sin\delta_\mathrm{r}, \quad e_q \triangleq v_\mathrm{r}\cos\delta_\mathrm{r}, \tag{5.2}$$

where e_d and e_q stand for the d-axis and q-axis terminal voltages. In the system (5.1), the parameters T'_d, L'_d, L_q, H, and D denote the characteristics of the generator, and V_0 is related to the input voltage to exciter. p_m represents the mechanical power input and p_g the electric power output:

$$p_\mathrm{g} \triangleq \frac{v'_q v_\mathrm{r}}{L'_d}\sin\delta_\mathrm{r} + \frac{v_\mathrm{r}^2}{2}\frac{L'_d - L_q}{L'_d L_q}\sin 2\delta_\mathrm{r}. \tag{5.3}$$

The system (5.1) is derived under the assumption that the sub-transient behavior is negligible. The effect of control systems, which are AVR, PSS, and so on, is also excluded in order to reveal the native dynamics and stability of the ac/dc system.

Second, the operation in ac-dc converters is modeled based on the averaged model [59, 67, 76]. It is here supposed that the ac-dc converters in Fig. 5.1 are ideally operated under normal conditions, and the harmonic components are completely filtered. The firing angle α of the rectifier is controlled according to

$$\alpha = G_\alpha(I_{\mathrm{dc(ref)}} - I_{\mathrm{dc}}), \tag{5.4}$$

where I_{dc} denotes the dc current, $I_{\mathrm{dc(ref)}}$ the reference dc current, and G_α the gain coefficient. On the other hand, the inverter is controlled with keeping the margin angle γ constant [59, 67, 76]. The output dc voltage of the rectifier $V_{\mathrm{dc(r)}}$ and the input one to the inverter $V_{\mathrm{dc(i)}}$ can be approximately given as follows:

$$\begin{cases} V_{\mathrm{dc(r)}} \approx K_V v_{\mathrm{r}} \cos\alpha - \dfrac{3}{\pi} X_{\mathrm{c}} I_{\mathrm{dc}}, \\ V_{\mathrm{dc(i)}} \approx K_V V_{\mathrm{i}} \cos\gamma - \dfrac{3}{\pi} X_{\mathrm{c}} I_{\mathrm{dc}}, \end{cases} \tag{5.5}$$

where K_V stands for the coupling coefficient between the ac bus and dc voltage, V_{i} the ac bus voltage at the inverter side, and X_{c} the commutating reactance of the rectifier or the inverter. The dynamics of the dc link is thus represented by

$$\frac{\mathrm{d}I_{\mathrm{dc}}}{\mathrm{d}t} = \frac{1}{L_{\mathrm{dc}}}\left(-R_{\mathrm{dc}} I_{\mathrm{dc}} + V_{\mathrm{dc(r)}} - V_{\mathrm{dc(i)}}\right), \tag{5.6}$$

where L_{dc} and R_{dc} denote the inductance and resistance in the dc line, which includes smoothing reactors, respectively.

Lastly, by considering the coupling relation between the ac and dc systems, we derive the DAE system for the transient stability analysis. The coupling relation is modeled based on the power balance equality. The electric power p_{g} is here called by *active power* as a matter of principle. The power relationship in the ac/dc system is now given by

$$\begin{cases} 0 = p_{\mathrm{g}} + p_{\mathrm{i}} - K_I v_{\mathrm{r}} I_{\mathrm{dc}} \cos\varphi_{\mathrm{r}}, \\ 0 = q_{\mathrm{g}} + q_{\mathrm{i}} - K_I v_{\mathrm{r}} I_{\mathrm{dc}} \sin\varphi_{\mathrm{r}}, \\ 0 = K_I v_{\mathrm{r}} I_{\mathrm{dc}} \cos\varphi_{\mathrm{r}} - \left(K_V v_{\mathrm{r}} \cos\alpha - \dfrac{3}{\pi} X_{\mathrm{c}} I_{\mathrm{dc}}\right) I_{\mathrm{dc}}, \end{cases} \tag{5.7}$$

where p_{i} denotes the active power which flows from the infinite bus, q_{g} the *reactive power* related to the generator, and q_{i} the one related to the infinite bus. The reactive power

relation is necessary for deriving the DAE system. These power terms are represented by

$$\begin{cases} p_{\rm i} & \triangleq & \dfrac{v_{\rm r}V_\infty}{L_\infty}\sin(\delta_{\rm r}-\delta), \\ q_{\rm g} & \triangleq & \dfrac{v'_q v_{\rm r}}{L'_d}\cos\delta_{\rm r} - \dfrac{v_{\rm r}^2}{2}\dfrac{L'_d+L_q}{L'_dL_q} + \dfrac{v_{\rm r}^2}{2}\dfrac{L'_d-L_q}{L'_dL_q}\cos 2\delta_{\rm r}, \\ q_{\rm i} & \triangleq & \dfrac{v_{\rm r}V_\infty}{L_\infty}\cos(\delta_{\rm r}-\delta) - \dfrac{v_{\rm r}^2}{L_\infty}, \end{cases} \tag{5.8}$$

where V_∞ denotes the infinite bus voltage and L_∞ the ac line inductance. The variable $\varphi_{\rm r}$ in the equation (5.7) is defined as a power factor angle of the rectifier, and K_I is equivalent to the coupling coefficient between the ac and dc current. In the equation (5.7), the first and second equations represent the active and reactive power balance in the ac system. The third equation represents the active power balance between the ac and dc systems. The derivation of the equation (5.7) is based on the averaged current relation at the rectifier side:

$$i_{\rm r} \approx K_I I_{\rm dc}, \tag{5.9}$$

where $i_{\rm r}$ denotes the amplitude of ac current. Hence, we obtain the following DAE system:

$$\begin{cases} \dfrac{{\rm d}\boldsymbol{x}}{{\rm d}t} &= \boldsymbol{f}(\boldsymbol{x},\boldsymbol{y};I_{\rm dc(ref)},\gamma), \\ \boldsymbol{0} &= \boldsymbol{g}(\boldsymbol{x},\boldsymbol{y};I_{\rm dc(ref)}), \end{cases} \tag{5.10}$$

where $\boldsymbol{x} \triangleq (v'_q,\delta,\omega,I_{\rm dc})^{\rm T} \in X = \mathbb{R}\times\mathbb{S}^1\times\mathbb{R}\times\mathbb{R}$, $\boldsymbol{y} \triangleq (v_{\rm r},\delta_{\rm r},\varphi_{\rm r})^{\rm T} \in Y = \mathbb{R}\times\mathbb{S}^1\times\mathbb{S}^1$, and $\boldsymbol{f}$ stands for the right-hand side of the systems (5.1) and (5.6), and $\boldsymbol{g}$ the right-hand side of the equation (5.7).

The DAE system (5.10) is regarded as a fruitful mathematical model for the transient stability analysis. The swing equation system (2.2) in Chapter 2 does not include the operation of the dc system. As mentioned before, it is important to clarify the transient stability with taking the dc operation into account. Thus we need to model the ac/dc system keeping the structural characteristics of power conversion and control setup. The precise modeling is not easy because of the interrupted operation of power devices. However, the difficulty can be avoided if we restrict our concerns to the rotor dynamics of the generator which is governed by the electric power balance in the ac and dc systems. Then the approximation

formulas (5.5) and (5.9) at the power conversion are relevant to deriving the power balance relation. From this standpoint, the DAE system (5.10) is regarded as an advanced formulation of the swing equation system (2.2). Similar DAE systems are also derived for voltage and transient stability analysis of general ac/dc power systems [11, 67, 68].

5.1.2 Reduction to swing equation system

The swing equation system (2.2) is naturally derived from the DAE system (5.10). For the derivation, we make some assumptions for the DAE system (5.10):

- The variables v'_q, v_r and δ_r related to the system voltages are constant in the transient period.
- The variable φ_r related to the reactive power balance is also constant.
- The dc current I_dc is constant.

The first and second assumptions are relevant for power system transient analysis [51]. The DAE system (5.10) is now reduced as follows:

$$\left\{\begin{array}{rcl} \dfrac{\mathrm{d}\delta}{\mathrm{d}t} &=& \omega, \\ \dfrac{\mathrm{d}\omega}{\mathrm{d}t} &=& \dfrac{1}{2H}\{-D\omega + p_\mathrm{m} - p_\mathrm{g}(\hat{v}'_q, \hat{v}_\mathrm{r}, \hat{\delta}_\mathrm{r})\}, \\ 0 &=& p_\mathrm{g}(\hat{v}'_q, \hat{v}_\mathrm{r}, \hat{\delta}_\mathrm{r}) + p_\mathrm{i}(\delta, \hat{v}_\mathrm{r}, \hat{\delta}_\mathrm{r}) - K_I \hat{v}_\mathrm{r} \hat{I}_\mathrm{dc} \cos\hat{\varphi}_\mathrm{r}, \end{array}\right. \tag{5.11}$$

where $\hat{v}'_q$ stands for the assumed constant value of v'_q. Now

$$p_\mathrm{g}(\hat{v}'_q, \hat{v}_\mathrm{r}, \hat{\delta}_\mathrm{r}) = -\frac{\hat{v}_\mathrm{r} V_\infty}{L_\infty} \sin(\hat{\delta}_\mathrm{r} - \delta) + p_\mathrm{dc}, \tag{5.12}$$

where $p_\mathrm{dc} \triangleq K_I \hat{v}_\mathrm{r} \hat{I}_\mathrm{dc} \cos\hat{\varphi}_\mathrm{r}$ is constant as a result of the assumptions. Hence we derive the following swing equation:

$$\left\{\begin{array}{rcl} \dfrac{\mathrm{d}\delta}{\mathrm{d}t} &=& \omega, \\ \dfrac{\mathrm{d}\omega}{\mathrm{d}t} &=& \dfrac{1}{2H}\left\{-D\omega + p_\mathrm{m} - p_\mathrm{dc} - \dfrac{\hat{v}_\mathrm{r} V_\infty}{L_\infty} \sin(\delta - \hat{\delta}_\mathrm{r})\right\}. \end{array}\right. \tag{5.13}$$

5.2 Fundamental concepts of differential-algebraic equation system

This section summarizes fundamental concepts of the DAE system (5.10). Since a structure preserving model was proposed in [8] for power system stability analysis, various DAE systems have been addressed for transient stability analysis [14, 15, 44, 45, 74, 90, 102, 103, 111] and voltage instability analysis [45, 86, 102, 103]. These previous works reveal basic characteristics of the DAE systems, based on which we can analyze the DAE system (5.10) in this dissertation. The present section arranges some of the concepts: dynamical system theory [15, 102, 103] and numerical methods [10, 38, 64].

5.2.1 Summarized theory as dynamical system

The following two sets L and S are defined for the DAE system (5.10) by

$$\begin{cases} L \triangleq \{(\boldsymbol{x}, \boldsymbol{y}) \in X \times Y \,;\, \boldsymbol{g}(\boldsymbol{x}, \boldsymbol{y}; I_{\mathrm{dc(ref)}}) = \boldsymbol{0}\}, \\ S \triangleq \{(\boldsymbol{x}, \boldsymbol{y}) \in L \,;\, \det(\mathrm{D}_y \boldsymbol{g})(\boldsymbol{x}, \boldsymbol{y}; I_{\mathrm{dc(ref)}}) = 0\}, \end{cases} \tag{5.14}$$

where $\mathrm{D}_y \boldsymbol{g}$ stands for the Jacobian of $\boldsymbol{g}$ with respect to $\boldsymbol{y}$. All solutions in the DAE system (5.10) exist on the constraint set L. S is called *singular surface* and decomposes L into several disjoint components Γ_i. If all the points on one component Γ_i are such that $\mathrm{D}_y \boldsymbol{g}$ has no eigenvalue with zero and positive real parts, then Γ_i is called *stable* component; it is denoted by Γ_{s}. The existence of Γ_{s} is important in order to discuss the DAE system (5.10) via the singular perturbation technique in Chapter 6.

An equilibrium point (EP) on $L \setminus S$ is said to be *hyperbolic* if and only if the stable map:

$$\mathscr{M} \triangleq \mathrm{D}_x \boldsymbol{f} - \mathrm{D}_y \boldsymbol{f} (\mathrm{D}_y \boldsymbol{g})^{-1} \mathrm{D}_x \boldsymbol{g}, \tag{5.15}$$

evaluated at the EP has no eigenvalue with zero real parts. A *type-k* EP for $0 \leq k \leq 4$ is a hyperbolic EP such that the stable map $\mathscr{M}$ evaluated at the EP has exactly k eigenvalues with positive real parts. A hyperbolic EP $(\boldsymbol{x}_{\mathrm{s}}, \boldsymbol{y}_{\mathrm{s}})$ is *asymptotically stable* if and only if $\mathscr{M}$ evaluated at $(\boldsymbol{x}_{\mathrm{s}}, \boldsymbol{y}_{\mathrm{s}})$ has no eigenvalue with zero and positive real parts. The *stability*

region of an asymptotically stable EP $(\boldsymbol{x}_s, \boldsymbol{y}_s)$ in a stable component Γ_s is defined as follows:

$$A(\boldsymbol{x}_s, \boldsymbol{y}_s) \triangleq \{(\boldsymbol{x}, \boldsymbol{y}) \in \Gamma_s ; \lim_{t \to +\infty} \phi_t(\boldsymbol{x}, \boldsymbol{y}) = (\boldsymbol{x}_s, \boldsymbol{y}_s)\}, \tag{5.16}$$

where $\phi_t(\cdot, \cdot)$ denotes the *flow* defined by the vector field on Γ_s. The boundary of $A(\boldsymbol{x}_s, \boldsymbol{y}_s)$ in Γ_s is called *stability boundary*, denoted by $\partial A(\boldsymbol{x}_s, \boldsymbol{y}_s)$. For a hyperbolic EP $(\hat{\boldsymbol{x}}, \hat{\boldsymbol{y}})$ of the DAE system (5.10), its *stable* and *unstable manifolds* $W^s(\hat{\boldsymbol{x}}, \hat{\boldsymbol{y}})$ and $W^u(\hat{\boldsymbol{x}}, \hat{\boldsymbol{y}})$ are defined by

$$\begin{cases} W^s(\hat{\boldsymbol{x}}, \hat{\boldsymbol{y}}) \triangleq \{(\boldsymbol{x}, \boldsymbol{y}) \in \Gamma_s ; \lim_{t \to +\infty} \phi_t(\boldsymbol{x}, \boldsymbol{y}) = (\hat{\boldsymbol{x}}, \hat{\boldsymbol{y}})\}, \\ W^u(\hat{\boldsymbol{x}}, \hat{\boldsymbol{y}}) \triangleq \{(\boldsymbol{x}, \boldsymbol{y}) \in \Gamma_s ; \lim_{t \to -\infty} \phi_t(\boldsymbol{x}, \boldsymbol{y}) = (\hat{\boldsymbol{x}}, \hat{\boldsymbol{y}})\}. \end{cases} \tag{5.17}$$

Two m-dimensional differentiable manifold M and n-dimensional differentiable manifold N are also said to intersect *transversally* if at every point $\boldsymbol{z} \in M \cap N$ the sum of the tangent spaces $T_z M$ and $T_z N$ equals $\mathbb{R}^{m+n}$.

5.2.2 Numerical methods

This subsection gives us two numerical methods for the DAE system (5.10). Since DAE systems are generally stiff [10,38,64], it is necessary to adopt implicit integration methods. The following two methods are now used to solve the DAE system (5.10). One is the 3rd-stage Radau IIA Implicit Runge-Kutta (IRK) method of order 5th [10,38]. The calculation scheme is given by

$$\begin{cases} \boldsymbol{X}_{ni} &= \boldsymbol{x}_n + h \sum_{j=1}^{3} a_{ij} \boldsymbol{f}(\boldsymbol{X}_{nj}, \boldsymbol{Y}_{nj}), \\ \boldsymbol{0} &= \boldsymbol{g}(\boldsymbol{X}_{ni}, \boldsymbol{Y}_{ni}), \\ \boldsymbol{x}_{n+1} &= \boldsymbol{X}_{n,3}, \\ \boldsymbol{y}_{n+1} &= \boldsymbol{Y}_{n,3}, \end{cases} \tag{5.18}$$

where $i = 1, 2, 3$; h represents the step size of the IRK and a_{ij} the factor of the matrix A in the Butcher table. Tab. 5.1 shows the Butcher table and parameters setting of the Radau IIA IRK method. The IRK method holds the global error $\mathcal{O}(h^5)$. The other is the 5th-stage backward differential formula (BDF) method [10, 64] which holds the following

scheme:

$$\begin{cases} \displaystyle\sum_{i=0}^{4} \alpha_i^{(5)} \boldsymbol{x}_{n-4+i} + \boldsymbol{x}_{n+1} &= h\beta^{(5)} \boldsymbol{f}(\boldsymbol{x}_{n+1}, \boldsymbol{y}_{n+1}) \\ \mathbf{0} &= \boldsymbol{g}(\boldsymbol{x}_{n+1}, \boldsymbol{y}_{n+1}) \end{cases} \tag{5.19}$$

The BDF method calculates the values of next step $\boldsymbol{x}_{n+1}$ and $\boldsymbol{y}_{n+1}$ via the previous steps $\boldsymbol{x}_{n-4+i}\,(i = 0, \ldots, 4)$. Tab. 5.2 denotes the parameters of the 5th-stage BDF method. The BDF method also holds the global error $\mathcal{O}(h^5)$.

5.3 Equilibrium points

Numerical simulations are performed through the parameters setting in Tab. 5.3. The setting is identical to that of the swing equation system (2.2). Fig. 5.2 shows the region for a post-fault steady state at $D = 0$ which corresponds to an asymptotically stable EP, indicated by EP#1, in the parameter plane $I_{\mathrm{dc(ref)}} - \gamma$. In the figure, each dashed line at constant γ represents the existence region of EP#1. Furthermore, the symbol $\times$ corresponds to a point at which the following equation is satisfied:

$$\cos\alpha = \cos\gamma, \tag{5.20}$$

In the right-side of the symbol $\times$,

$$\cos\alpha > \cos\gamma. \tag{5.21}$$

This implies that the practical system is usually operated in the right-side region of the symbol $\times$. In addition, the symbol $\bigcirc$ denotes an EP on the singular surface S. From the previous section, the stability cannot be defined on each point $\bigcirc$ via $\mathscr{M}$. Let us call another saddle-type EP EP#2. EP#1 and EP#2 collide at the right-end denoted by the symbol $\triangle$ in Fig. 5.2, and they extinct caused by the fold bifurcation. Tab. 5.4 shows the locations and stability of EP#1 and EP#2 under $D = 0$, $I_{\mathrm{dc(ref)}} = 1.0$, and $\gamma = 23.0°$. From the table, EP#2 has the three dimensional local stable manifold and one dimensional unstable manifold. The stable manifold therefore has the possibility of becoming one of the basic sets [7] of the basin boundary of EP#1. In addition, the value of imaginary part in eigenvalues 2 and 3 corresponds to almost 1.8 Hz in the practical time; the eigenvalue is regarded as the mode of power swing for the generator.

5.4 Global structure of stability boundary

This section focuses on the stability boundary of an asymptotically stable EP, denoted by EP#1, in the DAE system (5.10). In particular we consider its global structure in the solution space of the DAE system via several basin portraits. The following discussion is performed under the condition $D = 0$.

5.4.1 Basin portraits around equilibrium points

Figures 5.3 and 5.4 show the sectional basin portraits around EP#1 and EP#2. In the figures, initial conditions are set as follows: First v'_q is fixed at the EP's value: we use EP#1 in Fig. 5.3 and EP#2 in Fig. 5.4. Second $I_{\rm dc}$ is determined as follows: $I_{\rm dc}$ = (value at the EP) + $\Delta I_{\rm dc}$, where the deviation $\Delta I_{\rm dc}$ is arbitrary changed to clarify the global structure. Finally $(v_{\rm r}, \delta_{\rm r}, \phi_{\rm r})$ are set at the values which satisfy the algebraic constraint $\boldsymbol{g}(\boldsymbol{x}, \boldsymbol{y}; I_{\rm dc(ref)}) = \boldsymbol{0}$ for every initial condition (δ, ω). In the figures, 101 $\times$ 101 cells are used as initial conditions for numerical integration, and the initial conditions are classified as follows: the *white* region stands for the basin of EP#1 which represents an acceptable operating condition. The *gray* region describes the one from which any trajectory converges to the singular surface S. A trajectory which reaches the surface S is possibly discontinuous because the DAE system (5.10) does not satisfy the existence and uniqueness properties of solutions in S. The related phenomenon is called *jump behavior* [75,85]. Such discontinuous solutions would not be realized in the practical ac/dc system and is therefore due to modeling over-abstraction. However, since abstraction is inevitable for power system analysis, understanding the solution sand associated basin structures is much important, e.g. for examining the global structures of stability boundaries as seen below and developing a practical tool for the transient stability analysis using the DAE system.

5.4.2 Hyperbolic saddle point and stability boundary

EP#2 becomes one of the basic sets of the stability boundary of EP#1. We point out in Fig. 5.4(c) that the stable manifold of EP#2 forms a part of the boundary between *white* and *gray* regions, i.e., the stability boundary of EP#1. Furthermore, let us consider the

basin portraits around EP#2 in detail. The *gray* region can be now separated into two different regions based on transient behavior. Fig. 5.5 again shows the portraits around EP#2. Basin color for EP#1 is in Figs. 5.3 and 5.4. The *light-gray* and *dark-gray* basins in Fig. 5.5 are the undesirable regions; any trajectory from these regions converges to the singular surface S. The difference between these regions is characterized by transient behavior of solutions, that is, trajectories which start from every initial regions. Fig. 5.6 shows the transient behavior from the two initial conditions indicated by Fig. 5.5. The trajectory which starts from the initial point #2 in the *dark-gray* region converges to S much faster than that from #1 in the *light-gray* region. This is observed along the vertical boundary between these regions in Fig. 5.5. We here note in the figure that the decrease of $\Delta I_{\rm dc}$ raises the annihilation of the boundary, and the *white* region (basin of EP#1) also annihilates at an instant. This suggests that the vertical boundary is a part of the stable manifold of EP#2, and its manifold partially governs both the global structure of the stability boundary and the transient dynamics.

5.4.3 Global configuration of basin portraits

In addition, the basin in the vicinity of EP#1 has the same dynamical structure as that of EP#2. Fig. 5.3 shows that the *white* region annihilates as the derivation $\Delta I_{\rm dc}$ decreases. This is observed in Fig. 5.4 or 5.5. Here, the basin portrait in Fig. 5.3(e) has the similarity to that in Fig. 5.4(e). Fig. 5.7 shows the relationship between the initial conditions in Figs. 5.3(e) and 5.4(e). The figure indicates that both the initial conditions are close to each other in the solution space. In Fig. 5.4(e) the dc current at all initial conditions actually equals the value at EP#2; the difference therefore depends on the initial value v_q' only. Fig. 5.8 shows the configuration of all basin portraits in Figs. 5.3 and 5.4 via Number of Cells. Number of Cells is defined as the ratio of the basin for EP#1 on the initial conditions $(\delta, \omega) = [-\pi, \pi) \times [-0.02, 0.02]$. The figure implies that the sequences of the basin portraits around EP#1 and EP#2 are close to each other in the overall solution space. Hence we again suggest that the stable manifold of EP#2 governs the global structure of the stability boundary of EP#1.

The stability boundary indicates that the transient stability of the ac/dc system is

possibly determined by the stable manifold of EP#2. As introduced in Chapter 1, the transient stability can be discussed through the stability boundaries of the DAE system (5.10). Each solution of the DAE system corresponds to the system behavior due to an event disturbance which is added to the ac/dc system. If an initial condition is placed in the stability region of EP#1 that boundary is partly the stable manifold of EP#2, then the associated trajectory settles down EP#1 which coincides with an acceptable operating condition in the ac/dc system; otherwise, if an initial state is outside the stability region, the trajectory goes to the singular surface S, at which is an unsafe state of the ac/dc system. The stable manifold of EP#2 thus plays a key role in determining the transient stability.

5.5 Summary

This chapter addressed the transient dynamics and stability boundaries with considering the dc system's operation and the electric power balance. The DAE system was derived and investigated numerically for the present analysis. The stability boundary was particularly examined using several basin portraits around equilibrium points. The global structure of the stability boundary was partially clarified through the stable manifold of the hyperbolic saddle point. The obtained result reveals a dynamical aspect of the transient stability of the ac/dc system. Here we stress that the particular solutions are addressed which reach the singular surface S. The analysis of the solutions is crucial for clarifying the global structure. The next chapter will also focus on such solutions related to the singular surface S in the DAE system.

Appendix to Section 5.1: Detailed derivation of differential-algebraic equation system

Park's model of synchronous generator

The dynamics of a generator is modeled based on the Park's theory [51, 76]. The following discussion is expanded through the Park's transformation P:

$$\mathsf{P} = \frac{2}{3}\begin{pmatrix} \cos(\omega_{\mathrm{b}}t+\delta) & \cos\left(\omega_{\mathrm{b}}t+\delta-\frac{2\pi}{3}\right) & \cos\left(\omega_{\mathrm{b}}t+\delta+\frac{2\pi}{3}\right) \\ -\sin(\omega_{\mathrm{b}}t+\delta) & -\sin\left(\omega_{\mathrm{b}}t+\delta-\frac{2\pi}{3}\right) & -\sin\left(\omega_{\mathrm{b}}t+\delta+\frac{2\pi}{3}\right) \end{pmatrix}, \tag{5.22}$$

where ω_{b} denotes the system angular frequency and δ the rotor position with respect to synchronous reference axis. Fig. 5.9 shows the two-pole model of a synchronous generator. The direction of the phase currents is defined as positiveness in case the currents flow out of the generator. The relationship between the flux linkages and the currents is given by

$$\begin{cases} \phi_d &= -L_d i_d + M_{df} i_f, \\ \phi_q &= -L_q i_q, \\ \phi_f &= -\frac{3}{2} M_{df} i_d + L_f i_f, \end{cases} \tag{5.23}$$

where ϕ_d, ϕ_q, and ϕ_f denote the flux linkages of d-axis, q-axis, and field windings, respectively, L_d, L_q, and L_f the self-inductances of the d-axis, q-axis, and field windings, and M_{df} the mutual inductance between the d-axis and field windings. The terminal voltages e_d and e_q are related to the dynamics of the flux linkages in the following equations:

$$\begin{cases} e_d &= \frac{\mathrm{d}\phi_d}{\mathrm{d}t} - \omega\phi_q - R_{\mathrm{a}} i_d, \\ e_q &= \frac{\mathrm{d}\phi_q}{\mathrm{d}t} + \omega\phi_d - R_{\mathrm{a}} i_q, \\ e_f &= \frac{\mathrm{d}\phi_f}{\mathrm{d}t} + R_f i_f, \end{cases} \tag{5.24}$$

where e_f stands for the voltage source into the field winding, R_{a} the resistance of the armature winding, and R_f the resistance of the field winding. In addition, the rotor speed

ω satisfies

$$\omega = \omega_{\mathrm{b}} + \frac{\mathrm{d}\delta}{\mathrm{d}t}. \tag{5.25}$$

The rotor dynamics is now described by

$$\begin{cases} \dfrac{\mathrm{d}\delta}{\mathrm{d}t} = \omega - \omega_{\mathrm{b}}, \\ J\dfrac{\mathrm{d}\omega}{\mathrm{d}t} = \dfrac{p_{\mathrm{m}}}{\omega} - \dfrac{3}{2}\left(e_d i_d + e_q i_q\right), \end{cases} \tag{5.26}$$

where J denotes the rotor moment of inertia and p_{m} the mechanical input power.

Modeling of ac transmission line

The mathematical model of an ac transmission line is here considered. The three-phase infinite bus voltages $e_{a\infty}$, $e_{b\infty}$, and $e_{c\infty}$ are assumed in [76] as follows:

$$\begin{cases} e_{a\infty} \triangleq -V_\infty \sin \omega_{\mathrm{b}} t, \\ e_{b\infty} \triangleq -V_\infty \sin\left(\omega_{\mathrm{b}} t - \dfrac{2\pi}{3}\right), \\ e_{c\infty} \triangleq -V_\infty \sin\left(\omega_{\mathrm{b}} t + \dfrac{2\pi}{3}\right), \end{cases} \tag{5.27}$$

where V_∞ denotes the magnitude of the infinite bus voltages. The transformation P induces the following terminal voltages $e_{d\infty}$ and $e_{q\infty}$:

$$\begin{cases} e_{d\infty} = V_\infty \sin\delta, \\ e_{q\infty} = V_\infty \cos\delta. \end{cases} \tag{5.28}$$

The dynamics of the ac transmission line is thus represented as follows:

$$\begin{cases} V_\infty \sin\delta = e_{d\mathrm{r}} + R_\infty i_{d\infty} + L_\infty\left(\dfrac{\mathrm{d}i_{d\infty}}{\mathrm{d}t} - \omega i_{q\infty}\right), \\ V_\infty \cos\delta = e_{q\mathrm{r}} + R_\infty i_{q\infty} + L_\infty\left(\dfrac{\mathrm{d}i_{q\infty}}{\mathrm{d}t} + \omega i_{d\infty}\right), \end{cases} \tag{5.29}$$

where $e_{d\mathrm{r}}$ and $e_{q\mathrm{r}}$ denote the d-axis and q-axis voltages at the connecting point between the ac and dc systems.

Modeling of dc transmission system

The modeling of a dc link can be performed based on the averaged model [59, 67, 76]. The dynamics of converter transformers is here negligible. It is supposed that the ac-dc converters in Fig. 5.1 are ideally operated under normal conditions, and the harmonic components are completely filtered. In the following discussion, the dc link is assumed to be the bipolar-type with return conductor. The output dc voltage of the rectifier $V_{\mathrm{dc(r)}}$ and the input one to the inverter $V_{\mathrm{dc(i)}}$ are approximately given as follows:

$$\begin{cases} V_{\mathrm{dc(r)}} & \approx & \dfrac{3\sqrt{3}}{\pi} n v_{\mathrm{r}} \cos\alpha - \dfrac{3}{\pi} X_{\mathrm{c}} I_{\mathrm{dc}}, \\ V_{\mathrm{dc(i)}} & \approx & \dfrac{3\sqrt{3}}{\pi} n V_{\mathrm{i}} \cos\beta + \dfrac{3}{\pi} X_{\mathrm{c}} I_{\mathrm{dc}}, \end{cases} \tag{5.30}$$

where X_{c} is the commutating reactance and n the turn ratio of the converter transformers. v_{r} stands for the ac peak voltage to neutral at the rectifier side given by

$$v_{\mathrm{r}} \triangleq \sqrt{e_{d\mathrm{r}}^2 + e_{q\mathrm{r}}^2}. \tag{5.31}$$

In the formula (5.30), α denotes the lagging control angle of the rectifier, β the leading control angle of the inverter, I_{dc} the dc current, and V_{i} the ac peak voltage to neutral at the inverter side.

The well-known control setups of the reciter and the inverter are adopted based on [59, 67, 76]. The rectifier is equipped with the automatic current regulation:

$$\alpha = G_\alpha (I_{\mathrm{dc(ref)}} - I_{\mathrm{dc}}), \tag{5.32}$$

where $I_{\mathrm{dc(ref)}}$ stands for the reference dc current and G_α the gain factor of the controller to obtain the control angle α. On the other hand, the inverter is regulated with keeping the margin angle γ constant. The relation between the angles β and γ is then represented as follows:

$$\cos\beta = \cos\gamma - \frac{2}{\sqrt{3}} \frac{X_{\mathrm{c}} I_{\mathrm{dc}}}{n V_{\mathrm{i}}}. \tag{5.33}$$

The dc voltage $V_{\mathrm{dc(i)}}$ is given by

$$V_{\mathrm{dc(i)}} = \frac{3\sqrt{3}}{\pi} n V_{\mathrm{i}} \cos\gamma - \frac{3}{\pi} X_{\mathrm{c}} I_{\mathrm{dc}}. \tag{5.34}$$

By using $V_{\mathrm{dc(r)}}$ and $V_{\mathrm{dc(i)}}$ we describe the dynamics of the dc link as follows:

$$L_{\mathrm{dc}}\frac{\mathrm{d}I_{\mathrm{dc}}}{\mathrm{d}t} + R_{\mathrm{dc}}I_{\mathrm{dc}} = V_{\mathrm{dc(r)}} - V_{\mathrm{dc(i)}}, \tag{5.35}$$

where L_{dc} and R_{dc} denote the dc line reactance and resistance, respectively.

Per unit system

The well-known per unit system is next adopted to all the variables and parameters. For the ac system, the following relation is introduced between the base power $P_{\mathrm{b(ac)}}$ and voltage-ampere $V_{\mathrm{b(ac)}}I_{\mathrm{b(ac)}}$:

$$P_{\mathrm{b(ac)}} = \frac{3}{2}V_{\mathrm{b(ac)}}I_{\mathrm{b(ac)}}, \tag{5.36}$$

where $V_{\mathrm{b(ac)}}$ stands for the base voltage and $I_{\mathrm{b(ac)}}$ the base current. The base voltage $V_{\mathrm{b(ac)}}$ implies the generator and infinite bus peak rated voltage to neutral, $I_{\mathrm{b(ac)}}$ the generator and infinite bus peak rated current, and $P_{\mathrm{b(ac)}}$ the generator and infinite bus three-phase rated voltage-ampere. On the other hand, for the dc system, the following relationship is also imposed:

$$P_{\mathrm{b(dc)}} = 2V_{\mathrm{b(dc)}}I_{\mathrm{b(dc)}}, \tag{5.37}$$

where $P_{\mathrm{b(dc)}}$, $V_{\mathrm{b(dc)}}$, and $I_{\mathrm{b(dc)}}$ denote the dc ratings with respect to power, voltage, and current, respectively; this relation is based on the system construction. The normalized time t^* is given by

$$t^* = \omega_{\mathrm{b}}t. \tag{5.38}$$

All equations which describe the dynamics are now normalized. The dynamics of a step-up transformer is also negligible. When the step-up transformer is the star-star type[1], the normalization makes it possible to connect the variables e_d^*, $e_{d\mathrm{r}}^*$, e_q^*, and $e_{q\mathrm{r}}^*$ as follows:

$$e_d^* = e_{d\mathrm{r}}^*, \quad e_q^* = e_{q\mathrm{r}}^*, \tag{5.39}$$

where e_d^* stands for the normalized value of e_d. The above relation is also satisfied for the current variables.

[1]In practical systems, the connection is not realized. However, the setting is not essential in terms of the constraint dynamics based on the electric power relationship.

Active and reactive power relation

The active and reactive power relationship is constructed between the ac and dc systems. The following relations are easily derived:

$$\begin{cases} e_d^*\left(i_d^* + i_{d\infty}^*\right) + e_q^*\left(i_q^* + i_{q\infty}^*\right) &= v_{\mathrm{r}}^* i_{\mathrm{r}}^* \cos\varphi_{\mathrm{r}}, \\ e_q^*\left(i_d^* + i_{d\infty}^*\right) - e_d^*\left(i_q^* + i_{q\infty}^*\right) &= v_{\mathrm{r}}^* i_{\mathrm{r}}^* \sin\varphi_{\mathrm{r}}, \\ v_{\mathrm{r}}^* i_{\mathrm{r}}^* \cos\varphi_{\mathrm{r}} &= \dfrac{P_{\mathrm{b(dc)}}}{P_{\mathrm{b(ac)}}} V_{\mathrm{dc(r)}}^* I_{\mathrm{dc}}^*, \end{cases} \tag{5.40}$$

where φ_{r} stands for the power factor angle of the rectifier. v_{r}^* corresponds to the ac peak terminal voltage to neutral at the generator and is given as follows:

$$v_{\mathrm{r}}^* = \sqrt{e_d^{*2} + e_q^{*2}}. \tag{5.41}$$

The following formulas are introduced for the ac voltage v_{r}^*:

$$\begin{cases} e_d^* \triangleq v_{\mathrm{r}}^* \sin\delta_{\mathrm{r}}, \\ e_q^* \triangleq v_{\mathrm{r}}^* \cos\delta_{\mathrm{r}}, \end{cases} \tag{5.42}$$

where δ_{r} becomes one of the variables for the derived DAE system. i_{r}^* is defined by

$$i_{\mathrm{r}}^* \triangleq \sqrt{(i_d^* + i_{d\infty}^*)^2 + (i_q^* + i_{q\infty}^*)^2}, \tag{5.43}$$

where the relationship between i_{r}^* and I_{dc}^* is assumed from [76] as follows:

$$\begin{aligned} \sqrt{\left(\frac{i_d^*}{2n} + \frac{i_{d\infty}^*}{2n}\right)^2 + \left(\frac{i_q^*}{2n} + \frac{i_{q\infty}^*}{2n}\right)^2} &= \frac{i_{\mathrm{r}}^*}{2n}, \\ &\approx \frac{I_{\mathrm{b(dc)}}}{I_{\mathrm{b(ac)}}} \frac{2\sqrt{3}}{\pi} I_{\mathrm{dc}}^*, \end{aligned} \tag{5.44}$$

where n is the turn ratio of the converter transformer.

Differential-algebraic equation system

This dissertation mainly discusses the transient stability of the ac/dc power system. The following assumptions can be therefore adopted:

$$\begin{cases} \dfrac{\mathrm{d}\phi_d^*}{\mathrm{d}t^*} &= 0, \\ \dfrac{\mathrm{d}\phi_q^*}{\mathrm{d}t^*} &= 0, \\ R_{\mathrm{a}}^* &= 0, \\ \omega^* &\simeq 1, \\ \dfrac{\mathrm{d}i_{d\infty}^*}{\mathrm{d}t^*} &= 0, \\ \dfrac{\mathrm{d}i_{q\infty}^*}{\mathrm{d}t^*} &= 0, \\ R_{\infty}^* &= 0. \end{cases} \tag{5.45}$$

The following $v_q'^*$ and V_0^* are here defined as follows:

$$\begin{cases} v_q'^* &\triangleq \dfrac{M_{df}^*}{L_f^*}\phi_f^*, \\ V_0^* &\triangleq \dfrac{M_{df}^*}{R_f^*}e_f^*. \end{cases} \tag{5.46}$$

By the formula (5.42) the dynamics of the field winding is obtained:

$$T_d'^* \frac{\mathrm{d}v_q'^*}{\mathrm{d}t^*} = \frac{L_d'^*}{L_d^*}V_0^* + \frac{L_d^* - L_d'^*}{L_d^*}v_{\mathrm{r}}^* \cos\delta_{\mathrm{r}} - v_q'^*, \tag{5.47}$$

where $T_d'^*$ denotes the d-axis transient short-circuit time constant and $L_d'^*$ the d-axis transient, and they are defined as follows:

$$\begin{cases} T_d'^* &\triangleq \dfrac{L_f^*}{R_f^*} - \dfrac{M_{df}^{*2}}{R_f^* L_d^*}, \\ L_d'^* &\triangleq L_d^* - \dfrac{M_{df}^{*2}}{L_f^*}. \end{cases} \tag{5.48}$$

The active output power of the generator p_{g}^* is represented:

$$p_{\mathrm{g}}^* \triangleq e_d^* i_d^* + e_q^* i_q^* = \frac{v_q'^* v_{\mathrm{r}}^*}{L_d'^*}\sin\delta_{\mathrm{r}} + \frac{v_{\mathrm{r}}^{*2}}{2}\frac{L_d'^* - L_q^*}{L_d'^* L_q^*}\sin 2\delta_{\mathrm{r}}. \tag{5.49}$$

The swing equation system is now derived as follows:

$$\begin{cases} \dfrac{\mathrm{d}\delta}{\mathrm{d}t^*} &= \omega^* - 1, \\ 2H^* \dfrac{\mathrm{d}\omega^*}{\mathrm{d}t^*} &= p_{\mathrm{m}}^* - p_{\mathrm{g}}^* - D^*(\omega^* - 1), \end{cases} \tag{5.50}$$

where H^* is the inertia constant and D^* the damping coefficient in the generator. The reactive power related to the generator, denoted by q_{g}^*, is also given:

$$\begin{aligned} q_{\mathrm{g}}^* &\triangleq e_q^* i_d^* - e_d^* i_q^* \\ &= \frac{v_q'^* v_{\mathrm{r}}^*}{L_d'^*} \cos\delta_{\mathrm{r}} - \frac{v_{\mathrm{r}}^{*2}}{2} \frac{L_d'^* + L_q^*}{L_d'^* L_q^*} + \frac{v_{\mathrm{r}}^{*2}}{2} \frac{L_d'^* - L_q^*}{L_d'^* L_q^*} \cos 2\delta_{\mathrm{r}}. \end{aligned} \tag{5.51}$$

The active and reactive power related to the infinite bus, denoted by p_{i}^* and q_{i}^*, is given as follows:

$$\begin{cases} p_{\mathrm{i}}^* \triangleq e_d^* i_{d\infty}^* + e_q^* i_{q\infty}^* &= \dfrac{V_\infty^*}{L_\infty^*} \sin(\delta_{\mathrm{r}} - \delta), \\ q_{\mathrm{i}}^* \triangleq e_q^* i_{d\infty}^* - e_d^* i_{q\infty}^* &= \dfrac{v_{\mathrm{r}}^* V_\infty^*}{L_\infty^*} \cos(\delta_{\mathrm{r}} - \delta) - \dfrac{v_{\mathrm{r}}^{*2}}{L_\infty^*}, \end{cases} \tag{5.52}$$

In the end, the following algebraic relations hold:

$$\begin{cases} 0 &= p_{\mathrm{g}}^* + p_{\mathrm{i}}^* - K_I^* v_{\mathrm{r}}^* I_{\mathrm{dc}}^* \cos\varphi_{\mathrm{r}}, \\ 0 &= q_{\mathrm{g}}^* + q_{\mathrm{i}}^* - K_I^* v_{\mathrm{r}}^* I_{\mathrm{dc}}^* \sin\varphi_{\mathrm{r}}, \\ 0 &= K_I^* v_{\mathrm{r}}^* I_{\mathrm{dc}}^* \cos\varphi_{\mathrm{r}} - \left(K_V^* v_{\mathrm{r}}^* \cos\alpha - \dfrac{3}{\pi} X_{\mathrm{c}}^* I_{\mathrm{dc}}^* \right) I_{\mathrm{dc}}^*, \end{cases} \tag{5.53}$$

where

$$\begin{cases} \alpha &= G_\alpha^* \left(I_{\mathrm{dc(ref)}}^* - I_{\mathrm{dc}}^* \right), \\ K_V^* &\triangleq \dfrac{3\sqrt{3}}{\pi} \dfrac{V_{\mathrm{b(ac)}}}{V_{\mathrm{b(dc)}}} n, \\ K_I^* &\triangleq \dfrac{4\sqrt{3}}{\pi} \dfrac{I_{\mathrm{b(dc)}}}{I_{\mathrm{b(ac)}}} n. \end{cases} \tag{5.54}$$

The dynamics of the dc link is also determined by

$$L_{\mathrm{dc}}^* \frac{\mathrm{d}I_{\mathrm{dc}}^*}{\mathrm{d}t^*} + R_{\mathrm{dc}}^* I_{\mathrm{dc}}^* = K_V^* \left(v_{\mathrm{r}}^* \cos\alpha - V_{\mathrm{i}}^* \cos\gamma \right). \tag{5.55}$$

As a consequence we derive the DAE system which consists of the equations (5.47), (5.50), (5.53), and (5.55). Chapter 5 omits the symbol $*$ for simplicity. Additionally $\omega^* - 1$ in the system (5.50) is also replaced with ω^*.

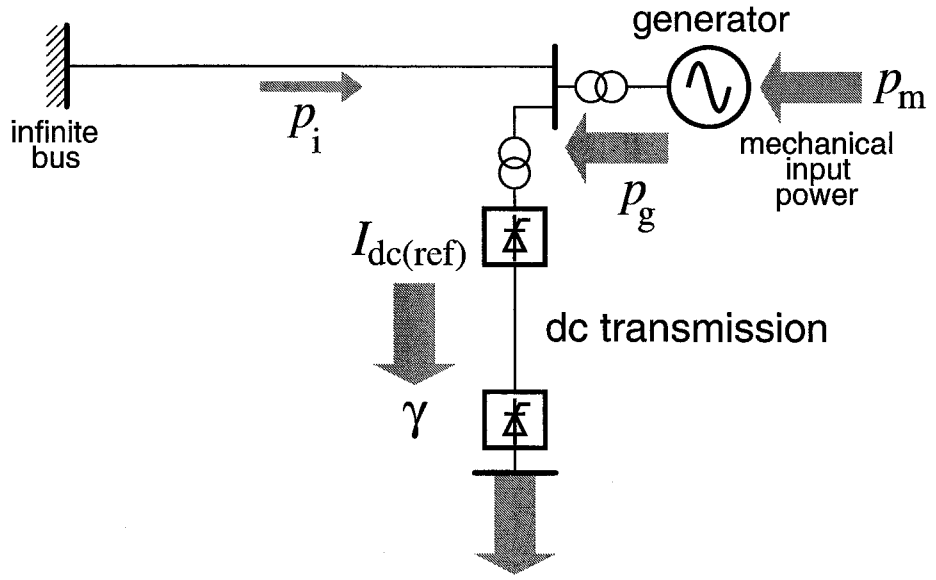

Figure 5.1 Configuration and power flow in ac/dc power system for the DAE system (5.10). The figure shows the same configuration as Figs. 1.1 and 2.1. The arrows in the figure denote the positive direction of active power.

Table 5.1 Butcher table and parameters setting of 3rd-stage Radau IIA implicit Runge-Kutta method of order 5

(a) Butcher table

$$\begin{array}{c|c} \boldsymbol{c} & \mathsf{A} \\ \hline & \boldsymbol{b}^{\mathrm{T}} \end{array}$$

(b) Parameters setting

$$\mathsf{A} = \begin{pmatrix} \frac{88-7\sqrt{6}}{360} & \frac{296-169\sqrt{6}}{1800} & \frac{-2+3\sqrt{6}}{225} \\ \frac{296+169\sqrt{6}}{1800} & \frac{88+7\sqrt{6}}{360} & \frac{-2-3\sqrt{6}}{225} \\ \frac{16-\sqrt{6}}{36} & \frac{16+\sqrt{6}}{36} & \frac{1}{9} \end{pmatrix}$$

$$\boldsymbol{b}^{\mathrm{T}} = \begin{pmatrix} \frac{16-\sqrt{6}}{36} & \frac{16+\sqrt{6}}{36} & \frac{1}{9} \end{pmatrix}$$

$$\boldsymbol{c}^{\mathrm{T}} = \begin{pmatrix} \frac{4-\sqrt{6}}{10} & \frac{4+\sqrt{6}}{10} & 1 \end{pmatrix}$$

Table 5.2 Parameters setting of 5th-order backward difference formula

$\alpha_0^{(5)}$	$\alpha_1^{(5)}$	$\alpha_2^{(5)}$	$\alpha_3^{(5)}$	$\alpha_4^{(5)}$	$\beta^{(5)}$
$-\frac{12}{137}$	$\frac{75}{137}$	$-\frac{200}{137}$	$\frac{300}{137}$	$-\frac{300}{137}$	$\frac{60}{137}$

Table 5.3 System parameters and base quantities in ac/dc power system for the DAE system (5.10). The parameters setting is basically identical to that of the swing equation system (2.2): see Tab. 2.3.

(a) Generator

rating		2.8 GVA
inertia constant	H	(0.89 s) $\times$ (120π s^{-1})
d-axis synchronous reactance	L_d	1.79
q-axis synchronous reactance	L_q	1.77
d-axis transient reactance	L'_d	0.34
d-axis transient short-circuit time constant	T'_d	(1.2 s) $\times$ (120π s^{-1})
exciter voltage refereed to armature circuit	V_0	1.7
mechanical input power	p_{m}	0.50

(b) AC line and dc link

ac line reactance	L_∞	0.883
infinite bus voltage	V_∞	1.0
dc line reactance	L_{dc}	4.2
dc line resistance	R_{dc}	0.014
ac bus voltage at inverter side	V_{i}	1.0
coupling coefficient between ac and dc systems	K_V	1.19
	K_I	1.19
commutating reactance	X_{c}	0.12
gain constant of rectifier controller	G_α	30.0

Table 5.3 (*continued*)

(c) Base quantities

	ac at generator side	ac at infinite bus side	dc
power	2.8 GVA	2.8 GVA	2.8 GVA
voltage	$\sqrt{\frac{2}{3}} \times (1.25 \times 10\ \text{kV})$	$\sqrt{\frac{2}{3}} \times (5.00 \times 10^2\ \text{kV})$	5.00×10^2 kV
current	1.828×10^2 kA	4.572 kA	2.800×10^3 A
impedance	$5.580 \times 10^{-2}\ \Omega$	$8.928 \times 10\ \Omega$	$1.785 \times 10^2\ \Omega$
time	$\frac{1}{120\pi}$ s	$\frac{1}{120\pi}$ s	$\frac{1}{120\pi}$ s

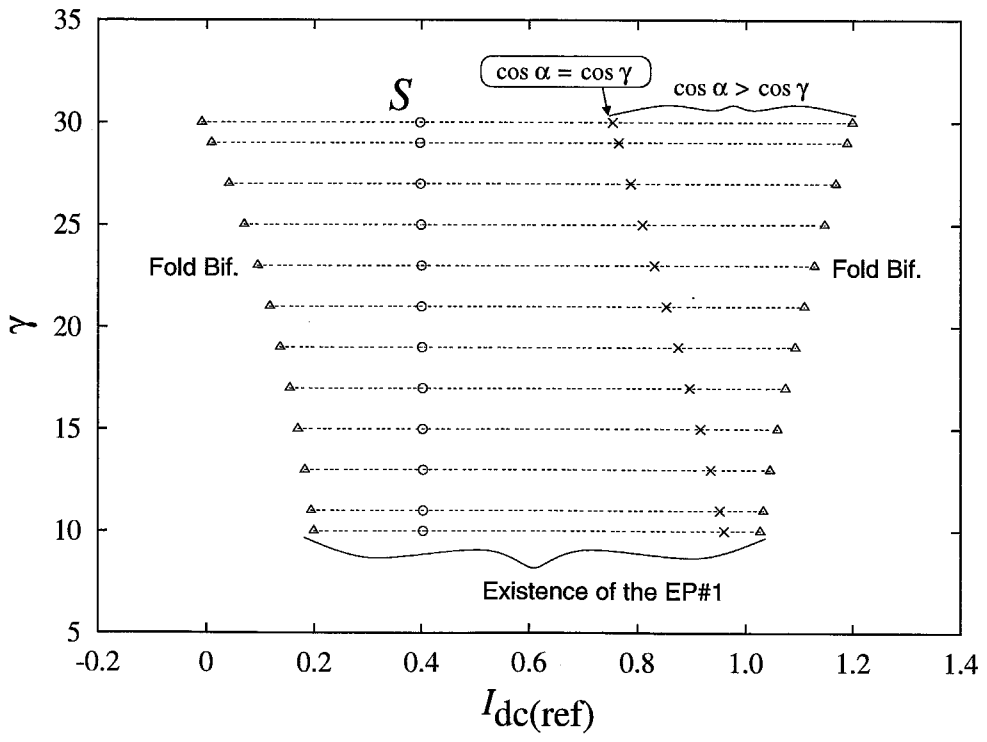

Figure 5.2 Region of steady state which corresponds to an asymptotically stable EP with $D = 0.0$. The stable EP is called EP#1 in the sequel.

Table 5.4 Locations and stability of equilibrium points under $D = 0.0$, $I_{\mathrm{dc(ref)}} = 1.0$, and $\gamma = 23.0°$

		EP#1	EP#2
v'_q		9.753214×10^{-1}	9.800746×10^{-1}
δ		4.749342×10^{-1}	4.884706×10^{-1}
ω		0.000000	0.000000
I_{dc}		5.899123×10^{-1}	5.716954×10^{-1}
v_{r}		9.606723×10^{-1}	9.655860×10^{-1}
δ_{r}		5.765143×10^{-1}	5.731841×10^{-1}
φ_{r}		4.365590×10^{-1}	4.436353×10^{-1}
α		$-1.511112 \times 10°$	$1.620139 \times 10°$
p_{g}		5.000000×10^{-1}	5.000000×10^{-1}
p_{i}		1.103255×10^{-1}	9.252590×10^{-2}
q_{g}		2.475875×10^{-1}	2.478743×10^{-1}
q_{i}		3.718883×10^{-2}	3.371123×10^{-2}
$\det(\mathrm{D}_y \boldsymbol{g})$		-2.121468	-2.123402
Eigenvalues	1	-7.244736×10^{-4}	-7.003787×10^{-4}
	2, 3	-1.580096×10^{-4} $\pm \mathrm{j}2.991998 \times 10^{-2}$	-1.275666×10^{-4} $\pm \mathrm{j}2.980325 \times 10^{-2}$
	4	-3.284533	3.371143

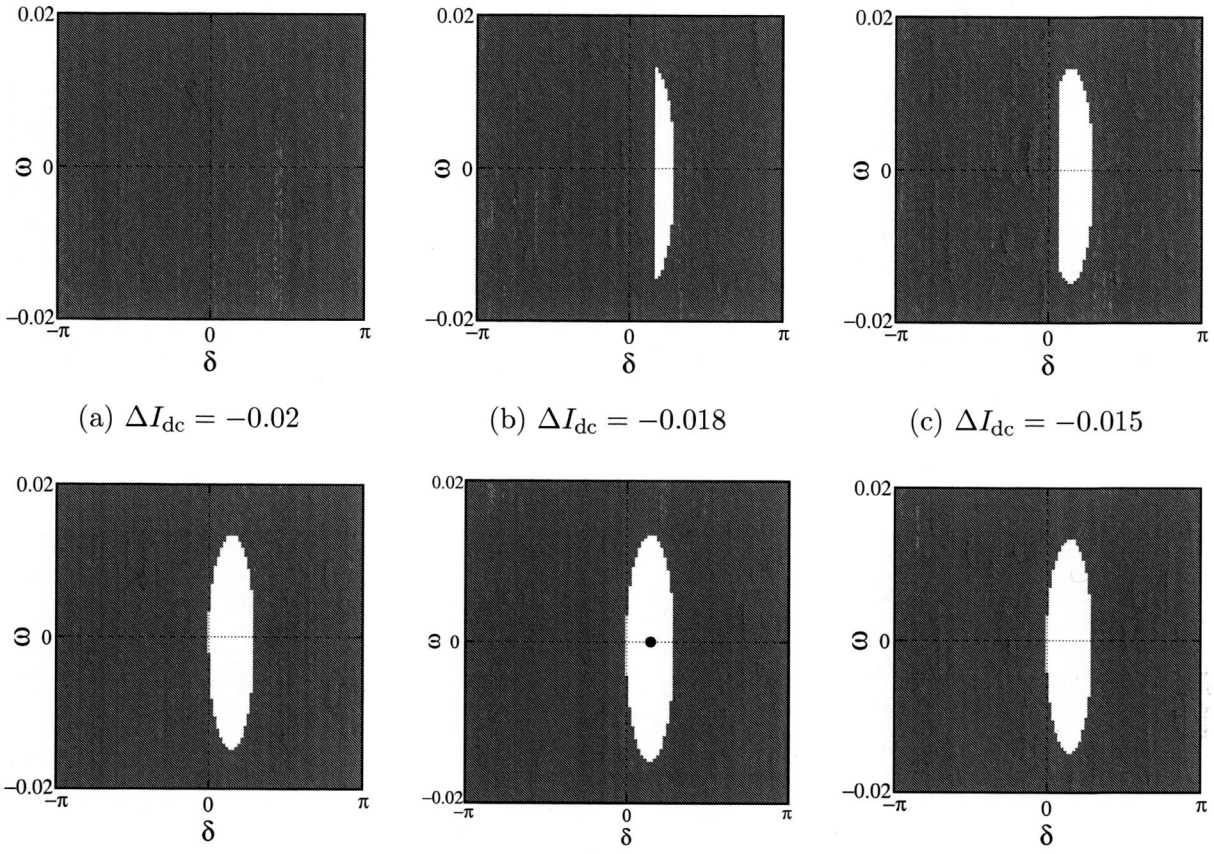

(a) $\Delta I_{\mathrm{dc}} = -0.02$ (b) $\Delta I_{\mathrm{dc}} = -0.018$ (c) $\Delta I_{\mathrm{dc}} = -0.015$

(d) $\Delta I_{\mathrm{dc}} = -0.01$ (e) $\Delta I_{\mathrm{dc}} = 0.0$ (f) $\Delta I_{\mathrm{dc}} = +0.01$

Figure 5.3 Sectional basin portraits around EP#1 in the DAE system (5.10) at $D = 0$. The symbol • in the figure (e) denotes EP#1. The initial conditions in the figure are classified as follows: the *white* region represents the basin of EP#1 and the *gray* region the one from which any trajectory converges to the singular surface S.

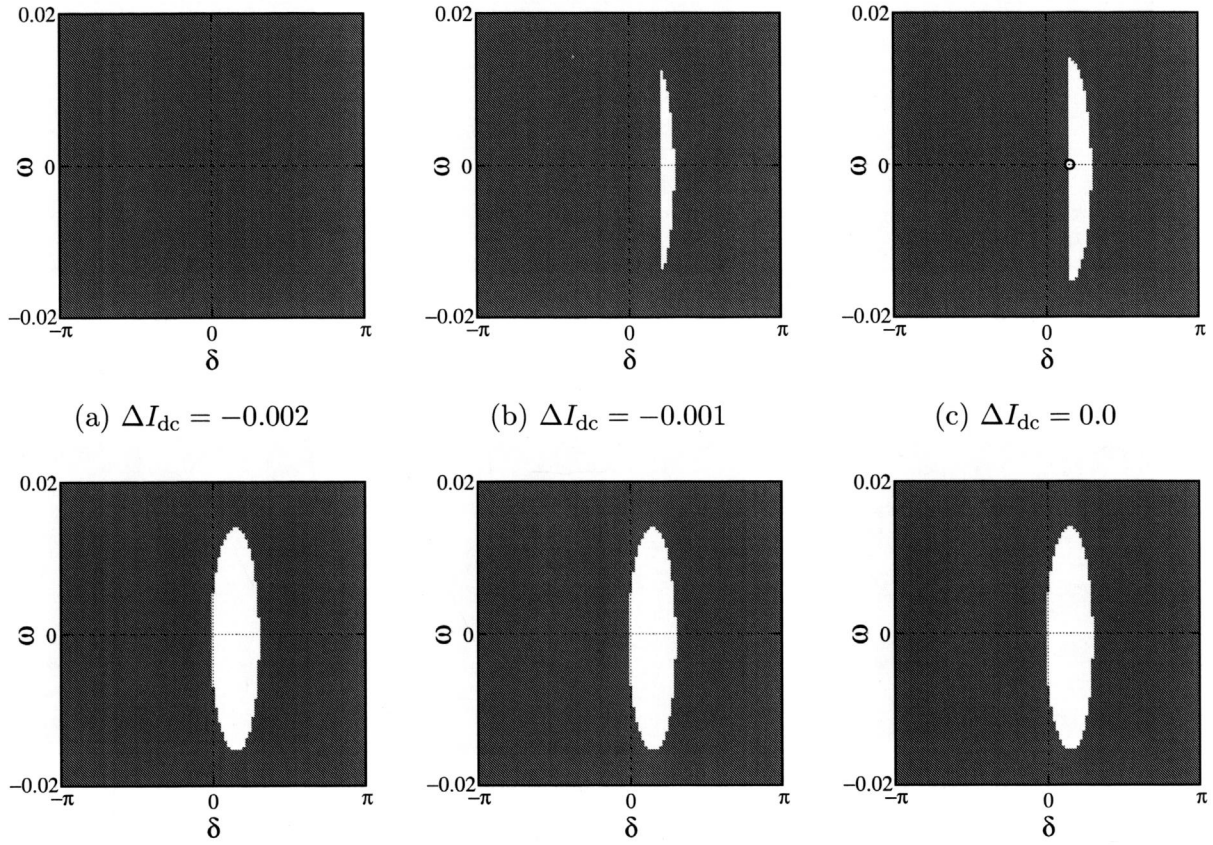

(a) $\Delta I_{\mathrm{dc}} = -0.002$ (b) $\Delta I_{\mathrm{dc}} = -0.001$ (c) $\Delta I_{\mathrm{dc}} = 0.0$

(d) $\Delta I_{\mathrm{dc}} = +0.01$ (e) $\Delta I_{\mathrm{dc}} = +0.018$ (f) $\Delta I_{\mathrm{dc}} = +0.02$

Figure 5.4 Sectional basin portraits around EP#2 in the DAE system (5.10) at $D = 0$. The symbol ○ in Fig. 5.4(c) stands for EP#2, and the basins are colored as the same way in Fig. 5.3.

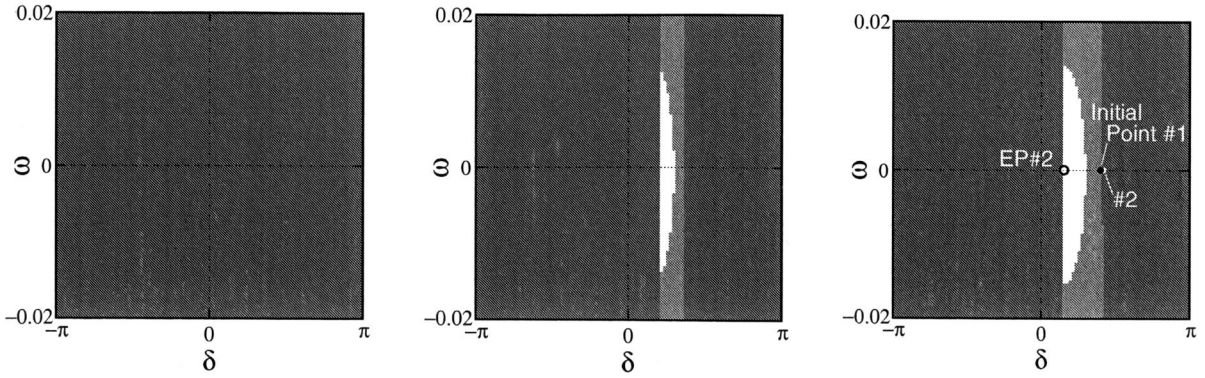

(a) $\Delta I_{\mathrm{dc}} = -0.002$ (b) $\Delta I_{\mathrm{dc}} = -0.001$ (c) $\Delta I_{\mathrm{dc}} = 0.0$

Figure 5.5 Basin portraits around EP#2 and its stable manifold. The *white* region corresponds to the basin of EP#1, and the *light-gray* and *dark-gray* regions the ones from which any trajectory converges to S. The difference between the two undesirable regions is characterized by transient behavior shown in Fig. 5.6.

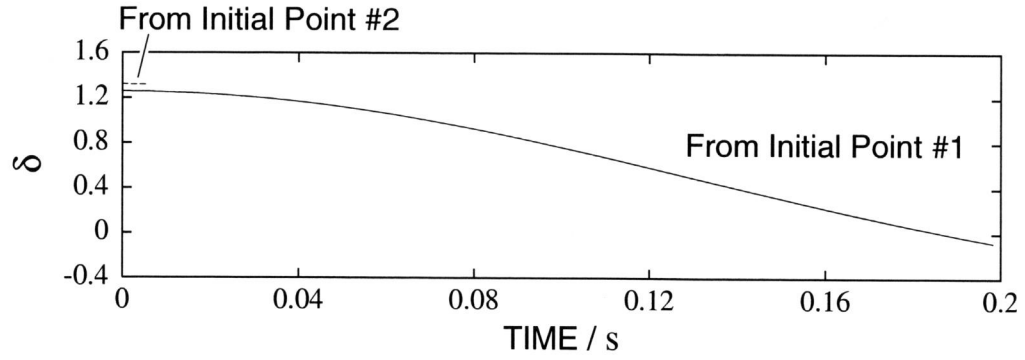

(a) Rotor position δ

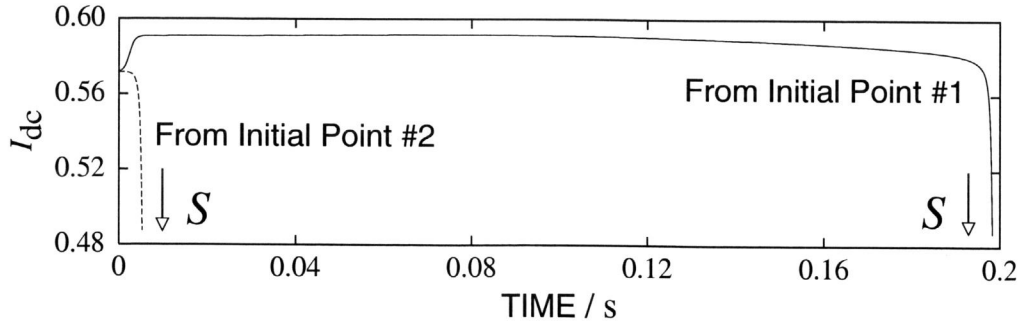

(b) DC current I_{dc}

Figure 5.6 Transient behavior from two different initial conditions indicated in Fig. 5.5(c)

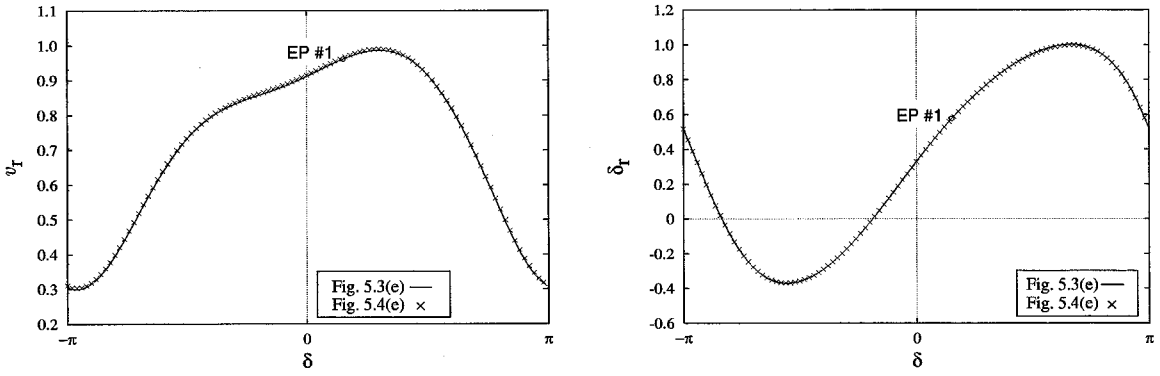

Figure 5.7 Relationship between initial conditions in neighborhood of EP#1

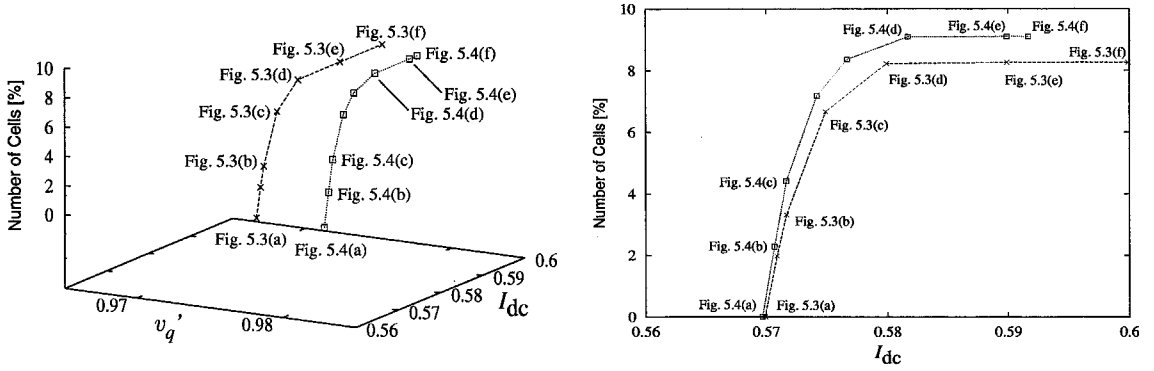

(a) The whole diagram

(b) Projection onto I_{dc}–Number of Cells plane

Figure 5.8 Configuration of basin portraits via Number of Cells. Number of Cells is defined as the ratio of the basin for EP#1 on the initial conditions $(\delta, \omega) = [-\pi, \pi) \times [-0.02, 0.02]$.

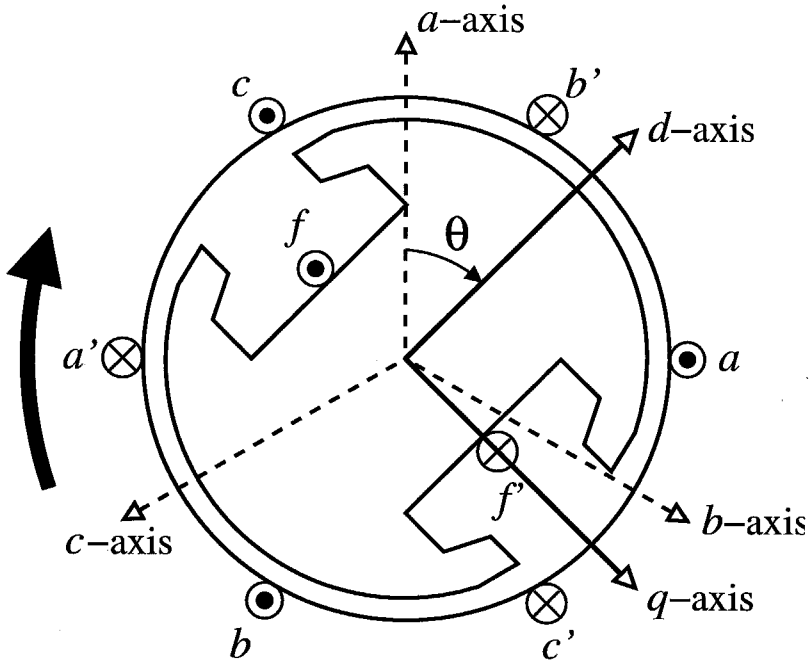

Figure 5.9 Two-pole model of synchronous generator. The direction of the phase currents is defined as positiveness in case the currents flow out of the generator.

Chapter 6

Stability boundaries and discontinuous dynamics

This chapter theoretically discusses stability boundaries and related dynamics in the DAE system. Chapter 5 analyzed a stability boundary numerically and showed that the stable manifold of the hyperbolic saddle point consisted of a part of the stability boundary. However, the entire global structure is not be clarified numerically and theoretically. In addition, the relationship is not examined between the stability boundary and possible system trajectories with respect to fault conditions. These understanding is inevitable for applying the obtained results in this dissertation to the practical stability estimation. The remaining problems are now studied as follows.

The first study is to characterize the stability boundaries using the singular perturbation technique. The singular perturbation plays an important role in studying multi-time scale dynamical systems: see e.g. [34,49,53]. The technique is also applied to power system transient analysis [14, 15, 18, 24, 74, 111]. In this chapter, we derive complete characterization of the stability boundaries via an energy function for an associated SP system. The derivation strongly relies on some fundamental results reported in [15]. The obtained characterization entirely shows global structures of the stability boundaries in the solution space of the DAE system. In addition, the characterization is examined via several numerical results on a stability boundary which is partially reported in Chapter 5.

The second work here is to discuss discontinuous trajectories caused by structural

change of the ac/dc network configuration. Chapters 5 and 6 examine the geometric and topological structures of the stability boundaries. To apply the obtained results to the practical stability estimation, it is necessary to consider discontinuous solutions of the DAE system with respect to practical fault conditions and reveal the relation between their solutions and the stability boundaries. In this chapter, we numerically and analytically examine several discontinuous solutions relative to two distinct fault conditions.

6.1 Preliminaries

This chapter also considers the following DAE system:

$$\left\{\begin{array}{rcl}
\dfrac{T'_{d0}}{L_d - L'_d}\dfrac{\mathrm{d}v'_q}{\mathrm{d}t} &=& \dfrac{V_0}{L_d - L'_d} + \dfrac{v_\mathrm{r}}{L'_d}\cos\delta_\mathrm{r} - \dfrac{L_d}{L'_d(L_d - L'_d)}v'_q, \\
\dfrac{\mathrm{d}\delta}{\mathrm{d}t} &=& \omega, \\
2H\dfrac{\mathrm{d}\omega}{\mathrm{d}t} &=& -D\omega + p_\mathrm{m} - \left(\dfrac{v'_q v_\mathrm{r}}{L'_d}\sin\delta_\mathrm{r} + \dfrac{v_\mathrm{r}^2}{2}\dfrac{L'_d - L_q}{L'_d L_q}\sin 2\delta_\mathrm{r}\right), \\
L_\mathrm{dc}\dfrac{\mathrm{d}I_\mathrm{dc}}{\mathrm{d}t} &=& -R_\mathrm{dc}I_\mathrm{dc} + K_V\left(v_\mathrm{r}\cos\alpha - V_\mathrm{i}\cos\gamma\right), \\
0 &=& \left(\dfrac{v'_q v_\mathrm{r}}{L'_d}\sin\delta_\mathrm{r} + \dfrac{v_\mathrm{r}^2}{2}\dfrac{L'_d - L_q}{L'_d L_q}\sin 2\delta_\mathrm{r}\right) \\
&& + \dfrac{v_\mathrm{r}V_\infty}{L_\infty}\sin(\delta_\mathrm{r} - \delta) - K_I v_\mathrm{r} I_\mathrm{dc}\cos\varphi_\mathrm{r}, \\
0 &=& \left(\dfrac{v'_q v_\mathrm{r}}{L'_d}\cos\delta_\mathrm{r} - \dfrac{v_\mathrm{r}^2}{2}\dfrac{L'_d + L_q}{L'_d L_q} + \dfrac{v_\mathrm{r}^2}{2}\dfrac{L'_d - L_q}{L'_d L_q}\cos 2\delta_\mathrm{r}\right) \\
&& + \left\{\dfrac{v_\mathrm{r}V_\infty}{L_\infty}\cos(\delta_\mathrm{r} - \delta) - \dfrac{v_\mathrm{r}^2}{L_\infty}\right\} - K_I v_\mathrm{r} I_\mathrm{dc}\sin\varphi_\mathrm{r}, \\
0 &=& K_I v_\mathrm{r} I_\mathrm{dc}\cos\varphi_\mathrm{r} - \left(K_V v_\mathrm{r}\cos\alpha - \dfrac{3}{\pi}X_\mathrm{c}I_\mathrm{dc}\right)I_\mathrm{dc},
\end{array}\right. \tag{6.1}$$

where $\alpha = G_\alpha(I_{\mathrm{dc(ref)}} - I_\mathrm{dc})$, $T'_{d0} \triangleq L_d T'_d / L'_d$, and we assume that $0 < v_\mathrm{r} < K$ for a sufficiently large positive number K: $(v'_q, \delta, \omega, I_\mathrm{dc})^\mathrm{T} \in X = \mathbb{R}\times\mathbb{S}^1\times\mathbb{R}\times\mathbb{R}$ and $(v_\mathrm{r}, \delta_\mathrm{r}, \varphi_\mathrm{r})^\mathrm{T} \in Y = \{v_\mathrm{r} \,|\, 0 < v_\mathrm{r} < K\}\times\mathbb{S}^1\times\mathbb{S}^1$.

The DAE system (6.1) is now rewritten via a structure preserving power system model [90]. The following variables transformations are introduced:

$$\theta_\mathrm{r} \triangleq \delta - \delta_\mathrm{r}, \quad V_\mathrm{r} \triangleq \ln v_\mathrm{r}. \tag{6.2}$$

We here define a smooth function $\mathcal{W}(v'_q, \delta, \omega, I_{\rm dc}, \theta_{\rm r}, V_{\rm r})$ by

$$\mathcal{W}(v'_q, \delta, \omega, I_{\rm dc}, \theta_{\rm r}, V_{\rm r}) \triangleq \frac{1}{2}(2H)\omega^2 + \mathcal{U}_{\rm ac}(v'_q, \delta, \omega, \theta_{\rm r}, V_{\rm r}) + \mathcal{U}_{\rm dc}(I_{\rm dc}), \tag{6.3}$$

where

$$\begin{cases} \mathcal{U}_{\rm ac} \triangleq -p_{\rm m}\delta - \dfrac{(L'_d - L_q)\cos 2(\delta - \theta_{\rm r}) - (L'_d + L_q)}{2L'_d L_q}\dfrac{{\rm e}^{2V_{\rm r}}}{2} - \dfrac{v'_q {\rm e}^{V_{\rm r}}}{L'_d}\cos(\delta - \theta_{\rm r}) \\ \qquad\qquad -\dfrac{{\rm e}^{V_{\rm r}}V_\infty}{L_\infty}\cos\theta_{\rm r} + \dfrac{{\rm e}^{2V_{\rm r}}}{2L_\infty} - \dfrac{V_0}{L_d - L'_d}v'_q + \dfrac{L_d}{L'_d(L_d - L'_d)}\dfrac{v'^2_q}{2}, \\ \mathcal{U}_{\rm dc} \triangleq \dfrac{1}{2}R_{\rm dc}I^2_{\rm dc}. \end{cases} \tag{6.4}$$

The original DAE system (6.1) is then re-formalized as follows:

$$\begin{cases} \dfrac{T'_{d0}}{L_d - L'_d}\dfrac{{\rm d}v'_q}{{\rm d}t} = -\dfrac{\partial \mathcal{W}}{\partial v'_q}, \\ \dfrac{{\rm d}\delta}{{\rm d}t} = \dfrac{1}{2H}\dfrac{\partial \mathcal{W}}{\partial \omega}, \\ 2H\dfrac{{\rm d}\omega}{{\rm d}t} = -D\omega - \dfrac{\partial \mathcal{W}}{\partial \delta}, \\ L_{\rm dc}\dfrac{{\rm d}I_{\rm dc}}{{\rm d}t} = -\dfrac{\partial \mathcal{W}}{\partial I_{\rm dc}} + \mu\tilde{K}_V({\rm e}^{V_{\rm r}}\cos\alpha - V_{\rm i}\cos\gamma), \\ 0 = -\dfrac{\partial \mathcal{W}}{\partial \theta_{\rm r}} - \mu\tilde{K}_I{\rm e}^{V_{\rm r}}I_{\rm dc}\cos\varphi_{\rm r}, \\ 0 = -\dfrac{\partial \mathcal{W}}{\partial V_{\rm r}} - \mu\tilde{K}_I{\rm e}^{V_{\rm r}}I_{\rm dc}\sin\varphi_{\rm r}, \\ 0 = \mu\left\{\tilde{K}_I{\rm e}^{V_{\rm r}}I_{\rm dc}\cos\varphi_{\rm r} - \left(\tilde{K}_V{\rm e}^{V_{\rm r}}\cos\alpha - \dfrac{3}{\pi}\tilde{X}_{\rm c}I_{\rm dc}\right)I_{\rm dc}\right\}, \end{cases} \tag{6.5}$$

where $\mu \geq 0$ is the perturbation parameter: $\mu\tilde{K}_V \triangleq K_V$, $\mu\tilde{K}_I \triangleq K_I$, and $\mu\tilde{X}_{\rm c} \triangleq X_{\rm c}$. For simplicity, the simple description of the transformed DAE system (6.5) is often used as follows:

$$\begin{cases} {\rm M}\dfrac{{\rm d}\boldsymbol{x}}{{\rm d}t} = \boldsymbol{f}(\boldsymbol{x}, \boldsymbol{y}), \\ \mathbf{0} = \boldsymbol{g}(\boldsymbol{x}, \boldsymbol{y}), \end{cases} \tag{6.6}$$

where $\boldsymbol{x} = (v'_q, \delta, \omega, I_{\rm dc})^{\rm T} \in X = \mathbb{R}\times\mathbb{S}^1\times\mathbb{R}\times\mathbb{R}$, $\boldsymbol{y} = (\theta_{\rm r}, V_{\rm r}, \varphi_{\rm r})^{\rm T} \in \mathbb{S}^1\times\{V_{\rm r} \,|\, V_{\rm r} < \ln K\}\times\mathbb{S}^1$, and $\boldsymbol{f}$ stands for the right-hand side of the differential equation in the DAE system (6.5)

and $\boldsymbol{g}$ the right-hand side of the algebraic equation. M is the positive-definite diagonal matrix:

$$\mathsf{M} \triangleq \mathsf{diag}\left(\frac{T'_{d0}}{L_d - L'_d}, 1, 2H, L_{\mathrm{dc}}\right). \tag{6.7}$$

6.2 Singular perturbation, energy function, and stability boundary

6.2.1 Singular perturbation technique

This chapter exploits the following SP system to examine the DAE system (6.6):

$$\begin{cases} \mathsf{M}\dfrac{\mathrm{d}\boldsymbol{x}}{\mathrm{d}t} &= \boldsymbol{f}(\boldsymbol{x},\boldsymbol{y}), \\ \varepsilon\dfrac{\mathrm{d}\boldsymbol{y}}{\mathrm{d}t} &= \boldsymbol{g}(\boldsymbol{x},\boldsymbol{y}), \end{cases} \tag{6.8}$$

where ε is small positive parameter. Obviously, the SP system corresponds to the DAE system (6.6) as $\varepsilon \to 0$. The SP system is a typical dynamical system described by an ordinary differential equation. In the following, several fundamental concepts of dynamical system theory (see e.g. [16, 35, 78, 108]) are adopted including hyperbolicity and type of EPs, stable and unstable manifolds, transversality, stability regions and boundaries. The concepts are almost the same as those for general DAE systems in Chapter 5.

Applying the variable transformation $1/s = \varepsilon/t$ to the SP system (6.8) gives us another SP system:

$$\begin{cases} \mathsf{M}\dfrac{\mathrm{d}\boldsymbol{x}}{\mathrm{d}s} &= \varepsilon\boldsymbol{f}(\boldsymbol{x},\boldsymbol{y}), \\ \dfrac{\mathrm{d}\boldsymbol{y}}{\mathrm{d}s} &= \boldsymbol{g}(\boldsymbol{x},\boldsymbol{y}), \end{cases} \tag{6.9}$$

By freezing $\varepsilon = 0$, we obtain the following boundary layer (BL) system:

$$\begin{cases} \mathsf{M}\dfrac{\mathrm{d}\boldsymbol{x}}{\mathrm{d}s} &= \boldsymbol{0}, \\ \dfrac{\mathrm{d}\boldsymbol{y}}{\mathrm{d}s} &= \boldsymbol{g}(\boldsymbol{x},\boldsymbol{y}), \end{cases} \tag{6.10}$$

The set of EPs in the BL system corresponds to L and the set of asymptotically stable EPs the union of stable components. This fact directly leads to the theoretical justification of

the discontinuous solutions in Section 6.5. We now refer to [50] for quantitative relation between the dynamics of the DAE system (6.6) and the corresponding SP system (6.8).

Theorem 6.1 [50] *Let $(\boldsymbol{x}(t,\varepsilon), \boldsymbol{y}(t,\varepsilon))$ represent the SP system* (6.8) *with the initial conditions $(\boldsymbol{x}(\varepsilon;t_0), \boldsymbol{y}(\varepsilon;t_0))$ at $t = t_0$. Assume that the following conditions are satisfied for all*

$$[t, \boldsymbol{x}, \boldsymbol{y}, \varepsilon] \in [0, t_1] \times D_x \times D_y \times [0, \varepsilon_0] \tag{6.11}$$

for some domains $D_x \subset X \subset \mathbb{R}^4$ and $D_y \subset Y \subset \mathbb{R}^3$, in which D_x is convex and D_y contains $(\boldsymbol{x}(0;t_0), \boldsymbol{y}(0;t_0))$, and $(\boldsymbol{x}_0, \boldsymbol{y}_0) \triangleq (\boldsymbol{x}(0;t_0), \boldsymbol{y}(0;t_0))$:

- *The functions $\boldsymbol{f}$, $\boldsymbol{g}$, and their first derivatives with respect to $(\boldsymbol{x}, \boldsymbol{y})$ are continuous; the Jacobian $\mathrm{D}_y\boldsymbol{g}$ has a continuous first partial derivative with respect to their arguments; the initial data $\boldsymbol{x}(\varepsilon;t_0)$ and $\boldsymbol{y}(\varepsilon;t_0)$ are smooth functions of ε.*

- *The solution $(\boldsymbol{x}(t), \boldsymbol{y}(t))$ of the DAE system* (6.6) *with the initial conditions $(\boldsymbol{x}_0, \boldsymbol{y}_0)$ is unique for $t \in [t_0, t_1]$, and $\boldsymbol{x}(t)$ is a member of a compact set of D_x.*

- *The point $\boldsymbol{y}_0$ is an exponentially stable EP of the BL system* (6.10)*, uniformly in $\boldsymbol{x}$; let Ω_y be a compact subset of the stability region of $\boldsymbol{y}_0$ of the system* (6.10).

Then, there exists a positive constant $\hat{\varepsilon} > 0$ such that for all $\boldsymbol{y} \in \Omega_y$ and $0 < \varepsilon < \hat{\varepsilon}$, the SP system (6.8) *has a unique solution $(\boldsymbol{x}(t,\varepsilon), \boldsymbol{y}(t,\varepsilon))$ on $[t_0, t_1]$, and*

$$\begin{cases} \boldsymbol{x}(t,\varepsilon) - \boldsymbol{x}(t) &= \boldsymbol{\mathcal{O}}(\varepsilon), \\ \boldsymbol{y}(t,\varepsilon) - \boldsymbol{y}(t) - \bar{\boldsymbol{y}}\left(\dfrac{t}{\varepsilon}\right) &= \boldsymbol{\mathcal{O}}(\varepsilon), \end{cases} \tag{6.12}$$

hold uniformly for $t \in [t_0, t_1]$, where $\bar{\boldsymbol{y}}(s)$ is the solution of the BL system (6.10).

The following result also provides us with invariant topological relationship between EPs in the DAE and SP systems:

Theorem 6.2 [18, 111] *Consider EPs on a stable component of the DAE system* (6.6). *There exists a positive constant $\hat{\varepsilon} > 0$ such that for all $0 < \varepsilon < \hat{\varepsilon}$,*

- $(\hat{\boldsymbol{x}}, \hat{\boldsymbol{y}})$ *is a hyperbolic EP of the DAE system* (6.6) *if and only if* $(\hat{\boldsymbol{x}}, \hat{\boldsymbol{y}})$ *is a hyperbolic EP of the corresponding SP system* (6.8);

- *for* $k \leq 4$, $(\hat{\boldsymbol{x}}, \hat{\boldsymbol{y}})$ *is a type-k EP*[1] *of the DAE system* (6.6) *if and only if* $(\hat{\boldsymbol{x}}, \hat{\boldsymbol{y}})$ *is a type-k EP of the corresponding SP system* (6.8).

6.2.2 Energy function and stability boundary

The definition of energy functions is now given for the corresponding SP system (6.8):

Definition 6.3 [13,14,17] A smooth function $\mathcal{W} : X \times Y \to \mathbb{R}$ is called *energy function* for the SP system (6.8) if the following three conditions are satisfied:

(i) The derivative of $\mathcal{W}$ along any system trajectory $(\boldsymbol{x}(t), \boldsymbol{y}(t))$ is non-positive, i.e.

$$\begin{aligned} \frac{\mathrm{d}\mathcal{W}}{\mathrm{d}t}(\boldsymbol{x}(t), \boldsymbol{y}(t)) &= (\mathrm{D}_x \mathcal{W})\mathsf{M}^{-1}\boldsymbol{f}(\boldsymbol{x}(t), \boldsymbol{y}(t)) + \frac{1}{\varepsilon}(\mathrm{D}_y \mathcal{W})\boldsymbol{g}(\boldsymbol{x}(t), \boldsymbol{y}(t)) \\ &\leq 0. \end{aligned} \tag{6.13}$$

(ii) If $(\boldsymbol{x}(t), \boldsymbol{y}(t))$ is a non-trivial trajectory (i.e. $(\boldsymbol{x}(t), \boldsymbol{y}(t))$ is not at any EP), then along the non-trivial trajectory $(\boldsymbol{x}(t), \boldsymbol{y}(t))$ the set

$$\left\{ t \in \mathbb{R}\,;\, \frac{\mathrm{d}\mathcal{W}}{\mathrm{d}t}(\boldsymbol{x}(t), \boldsymbol{y}(t)) = 0 \right\} \tag{6.14}$$

has measure zero in $\mathbb{R}$.

(iii) If a trajectory $(\boldsymbol{x}(t), \boldsymbol{y}(t))$ has a bounded value of $\mathcal{W}(\boldsymbol{x}(t), \boldsymbol{y}(t))$ for $t \in \mathbb{R}^+$, then the trajectory $(\boldsymbol{x}(t), \boldsymbol{y}(t))$ is also bounded.

The property (i) indicates that the energy is non-increasing along its trajectory, and, however, does not imply that the energy is strictly decreasing along its trajectory. There may exist a time interval $[t_1, t_2]$ such that $\mathrm{d}\mathcal{W}(\boldsymbol{x}(t), \boldsymbol{y}(t))/\mathrm{d}t = 0$. The properties (i) and (ii) imply that the energy is strictly decreasing along any trajectory. The property (iii) states that the energy function is a proper map [2] along a system trajectory. It should be also noted that the above properties do not depend on the positive parameter ε.

[1] A *type-k* EP is defined in Chapter 5.

The concept of the energy functions plays an important role in the characterization of stability boundaries in the SP system (6.8). In the following, we will show that for the SP system with an energy function the basic sets of a stability boundary consist of EPs only:

Theorem 6.4 [13, 14, 16] *If there exists an energy function for the SP system* (6.8), *then every trajectory on the stability boundary converges to one of the EPs on the stability boundary.*

The significance of the theorem is that it offers complete characterization of the stability boundary, denoted by ∂A_ε. To do this, we make the following three assumptions in the SP system (6.8):

Assumption 6.5 All the EPs on ∂A_ε are hyperbolic.

Assumption 6.6 The stable and unstable manifolds of the EPs on ∂A_ε satisfy the transversality condition.

Assumption 6.7 The SP system (6.8) has an energy function.

Assumptions 6.5 and 6.6 are well-known as generic properties for C^1 dynamical systems [16] although they are not easy to confirm. Assumption 6.7 is therefore crucial for the application of the next theorem. Theorem 6.8 now states that the stability boundary is the union of the stable manifolds of the unstable EPs:

Theorem 6.8 [16] *For the SP system* (6.8) *which satisfies Assumptions* 6.5–6.7, *let* $(\boldsymbol{x}_i, \boldsymbol{y}_i)$, $i = 1, 2, \ldots$, *be the EPs on the stability boundary* ∂A_ε *of an asymptotically stable EP. Then*

$$\partial A_\varepsilon = \bigcup_{(\boldsymbol{x}_i, \boldsymbol{y}_i) \in \partial A_\varepsilon} W_\varepsilon^{\mathrm{s}}(\boldsymbol{x}_i, \boldsymbol{y}_i), \tag{6.15}$$

where $W_\varepsilon^{\mathrm{s}}(\boldsymbol{x}_i, \boldsymbol{y}_i)$ *stands for the stable manifold of the EP* $(\boldsymbol{x}_i, \boldsymbol{y}_i)$ *in the SP system* (6.8).

Chiang and Fekih-Ahmed [15] clarify stability boundaries in the DAE system (6.6) using the singular perturbation technique. Theorem 6.2 implies that an asymptotically stable EP, which lies in a stable component, of the DAE system (6.6) persists in the corresponding SP system (6.8) under small perturbation ε. The following theorem establishes the relationship between the stable regions of the DAE and corresponding SP systems:

Theorem 6.9 [15] *Let $(\boldsymbol{x}_{\rm s}, \boldsymbol{y}_{\rm s}) \in \Gamma_{\rm s}$ be an asymptotically stable EP of the DAE system* (6.6)*, and assume that $\Gamma_{\rm s}$ is a stable component of the system* (6.6)*. Let A denote its stability region, and let A_ε be the stable region of the same EP in the corresponding SP system* (6.8)*. Then, there exists a positive constant $\hat{\varepsilon} > 0$ such that for all $0 < \varepsilon < \hat{\varepsilon}$*

$$A = A_\varepsilon \cap \Gamma_{\rm s}. \tag{6.16}$$

Furthermore, we can find the relationship between the stability boundaries of the DAE and corresponding SP systems:

Theorem 6.10 [15] *Let ∂A_ε and ∂A be the stability boundaries of the corresponding SP system* (6.8) *and the DAE system* (6.6)*, respectively, for an asymptotically EP $(\boldsymbol{x}_{\rm s}, \boldsymbol{y}_{\rm s})$ which lies on a stable component $\Gamma_{\rm s}$, and suppose that Assumption* 6.7 *is satisfied. Then*

$$\partial A = \partial A_\varepsilon \cap \Gamma_{\rm s}. \tag{6.17}$$

If Assumptions 6.5 *and* 6.6 *are satisfied further, then*

$$\partial A = \left\{ \bigcup_{(\boldsymbol{x}_i, \boldsymbol{y}_i) \in \partial A} W^{\rm s}(\boldsymbol{x}_i, \boldsymbol{y}_i) \right\} \cup \left\{ \bigcup_{(\boldsymbol{x}_i, \boldsymbol{y}_i) \in \partial A_\varepsilon \setminus \Gamma_{\rm s}} W^{\rm s}_\varepsilon(\boldsymbol{x}_i, \boldsymbol{y}_i) \cap \Gamma_{\rm s} \right\}. \tag{6.18}$$

The theorem states the global structure of the stability boundary as follows. ∂A consists of two parts: the first part is the set from which trajectories converge to EPs, and the second part contains points from which trajectories reach a singular surface S. In addition, the theorem suggests that the stability boundary ∂A is possibly examined through the corresponding SP system (6.8). The detailed structure of the second part is delineated in [102, 103] via the singular transformation.

6.3 Characterization of stability boundaries

The present section theoretically considers the stability boundaries in the DAE system (6.6). Unfortunately, any analytical expression of energy functions has not been derived for the corresponding SP system (6.8). To avoid the problem, we reduce the DAE system by eliminating the variable $\varphi_{\rm r}$ and characterize stability boundaries of the reduced DAE

system. The characterization here is performed through perturbation theory of vector fields. Thereby, this section indirectly clarifies the stability boundaries in the DAE system (6.6).

6.3.1 Reduction of DAE system

This section starts to derive a reduced DAE system for the present analysis. From the last equation of (6.5) (that it, (6.6)), we have

$$\begin{cases} \tilde{K}_I \mathrm{e}^{V_\mathrm{r}} I_\mathrm{dc} \cos\varphi_\mathrm{r} &= \left(\tilde{K}_V \mathrm{e}^{V_\mathrm{r}} \cos\alpha - \dfrac{3}{\pi} \tilde{X}_\mathrm{c} I_\mathrm{dc} \right) I_\mathrm{dc}, \\ \tilde{K}_I I_\mathrm{dc} \mathrm{e}^{V_\mathrm{r}} \sin\varphi_\mathrm{r} &= \sqrt{\tilde{K}_I^2 \mathrm{e}^{2V_\mathrm{r}} - (\tilde{K}_I \mathrm{e}^{V_\mathrm{r}} \cos\varphi_\mathrm{r})^2} \cdot I_\mathrm{dc}, \end{cases} \tag{6.19}$$

where it is here assumed that $I_\mathrm{dc} \neq 0$, $\sin\varphi_\mathrm{r} > 0$, and $\mu\tilde{K}_I > 0$ in the DAE system (6.5); this is relevant to considering the transient dynamics in the practical ac/dc system. Substituting (6.19) to (6.5) makes it possible to eliminate the variable φ_r from the DAE system (6.5). Now we derive the following reduced DAE system:

$$\begin{cases} \dfrac{T'_{d0}}{L_d - L'_d} \dfrac{\mathrm{d}v'_q}{\mathrm{d}t} &= -\dfrac{\partial \mathcal{W}}{\partial v'_q}, \\ \dfrac{\mathrm{d}\delta}{\mathrm{d}t} &= \dfrac{1}{2H} \dfrac{\partial \mathcal{W}}{\partial \omega}, \\ 2H \dfrac{\mathrm{d}\omega}{\mathrm{d}t} &= -D\omega - \dfrac{\partial \mathcal{W}}{\partial \delta}, \\ L_\mathrm{dc} \dfrac{\mathrm{d}I_\mathrm{dc}}{\mathrm{d}t} &= -\dfrac{\partial \mathcal{W}}{\partial I_\mathrm{dc}} &&+ \mu\tilde{K}_V(\mathrm{e}^{V_\mathrm{r}} \cos\alpha - V_\mathrm{i} \cos\gamma), \\ 0 &= -\dfrac{\partial \mathcal{W}}{\partial \theta_\mathrm{r}} &&- \mu \left(\tilde{K}_V \mathrm{e}^{V_\mathrm{r}} \cos\alpha - \dfrac{3}{\pi} \tilde{X}_\mathrm{c} I_\mathrm{dc} \right) I_\mathrm{dc}, \\ 0 &= -\dfrac{\partial \mathcal{W}}{\partial V_\mathrm{r}} &&- \mu \sqrt{\tilde{K}_I^2 \mathrm{e}^{2V_\mathrm{r}} - \left(\tilde{K}_V \mathrm{e}^{V_\mathrm{r}} \cos\alpha - \dfrac{3}{\pi} \tilde{X}_\mathrm{c} I_\mathrm{dc} \right)^2} \cdot I_\mathrm{dc}, \end{cases} \tag{6.20}$$

where $\boldsymbol{x} = (v'_q, \delta, \omega, I_\mathrm{dc})^\mathrm{T} \in X = \mathbb{R} \times \mathbb{S}^1 \times \mathbb{R} \times (\mathbb{R} \setminus \{I_\mathrm{dc} \,|\, I_\mathrm{dc} = 0\})$, $\boldsymbol{y} = (\theta_\mathrm{r}, V_\mathrm{r})^\mathrm{T} \in Y = \mathbb{S}^1 \times \{V_\mathrm{r} \,|\, V_\mathrm{r} < \ln K\}$. It should be noted that the dynamics of the reduced DAE system (6.20) is identical to that of the DAE system (6.5) at $\mu \neq 0$ under the following conditions: $I_\mathrm{dc} \neq 0$, $\sin\varphi_\mathrm{r} > 0$, and $\mu\tilde{K}_I > 0$. In addition, by introducing the small positive parameter

ε, we have the corresponding SP system:

$$\left\{\begin{array}{rcll} \dfrac{T'_{d0}}{L_d - L'_d}\dfrac{\mathrm{d}v'_q}{\mathrm{d}t} &=& -\dfrac{\partial \mathcal{W}}{\partial v'_q}, & \\ \dfrac{\mathrm{d}\delta}{\mathrm{d}t} &=& \dfrac{1}{2H}\dfrac{\partial \mathcal{W}}{\partial \omega}, & \\ 2H\dfrac{\mathrm{d}\omega}{\mathrm{d}t} &=& -D\omega - \dfrac{\partial \mathcal{W}}{\partial \delta}, & \\ L_{\mathrm{dc}}\dfrac{\mathrm{d}I_{\mathrm{dc}}}{\mathrm{d}t} &=& -\dfrac{\partial \mathcal{W}}{\partial I_{\mathrm{dc}}} & + \ \mu\tilde{K}_V(\mathrm{e}^{V_{\mathrm{r}}}\cos\alpha - V_{\mathrm{i}}\cos\gamma), \\ \varepsilon\dfrac{\mathrm{d}\theta_{\mathrm{r}}}{\mathrm{d}t} &=& -\dfrac{\partial \mathcal{W}}{\partial \theta_{\mathrm{r}}} & - \ \mu\left(\tilde{K}_V\mathrm{e}^{V_{\mathrm{r}}}\cos\alpha - \dfrac{3}{\pi}\tilde{X}_{\mathrm{c}}I_{\mathrm{dc}}\right)I_{\mathrm{dc}}, \\ \varepsilon\dfrac{\mathrm{d}V_{\mathrm{r}}}{\mathrm{d}t} &=& -\dfrac{\partial \mathcal{W}}{\partial V_{\mathrm{r}}} & - \ \mu\sqrt{\tilde{K}_I^2\mathrm{e}^{2V_{\mathrm{r}}} - \left(\tilde{K}_V\mathrm{e}^{V_{\mathrm{r}}}\cos\alpha - \dfrac{3}{\pi}\tilde{X}_{\mathrm{c}}I_{\mathrm{dc}}\right)^2}\cdot I_{\mathrm{dc}}. \end{array}\right. \tag{6.21}$$

The SP system (6.21) with a small parameter μ is regarded as a perturbed dynamical system described by an ordinary differential equation.

6.3.2 AC power system

Before examining the DAE system (6.20), this subsection performs the characterization of the stability boundaries in the DAE system (6.6) under $\mu = 0$. The present DAE system corresponds to the DAE system (6.20) as $\mu \to 0$: $\boldsymbol{x} = (v'_q, \delta, \omega, I_{\mathrm{dc}})^{\mathrm{T}} \in X = \mathbb{R}\times\mathbb{S}^1\times\mathbb{R}\times\mathbb{R}$ and $\boldsymbol{y} = (\theta_{\mathrm{r}}, V_{\mathrm{r}})^{\mathrm{T}} \in Y = \mathbb{S}^1 \times \{V_{\mathrm{r}} \,|\, V_{\mathrm{r}} < \ln K\}$. Then we can discuss the dynamics of the ac power system independently on the dc link. The setting at $\mu = 0$ therefore implies the characterization with the only ac system. Now let us confirm that the function $\mathcal{W}(\boldsymbol{x}, \boldsymbol{y})$ is an energy function for the corresponding SP system (6.8) at $\mu = 0$. By differentiating $\mathcal{W}$ along any trajectory of the SP system (6.8) at $\mu = 0$, we have

$$\begin{aligned} \frac{\mathrm{d}\mathcal{W}}{\mathrm{d}t} &= -\frac{L_d - L'_d}{T'_{d0}}\left(\frac{\partial \mathcal{U}_{\mathrm{ac}}}{\partial v'_q}\right)^2 - D\omega^2 - \frac{1}{L_{\mathrm{dc}}}\left(\frac{\partial \mathcal{U}_{\mathrm{dc}}}{\partial I_{\mathrm{dc}}}\right)^2 - \frac{1}{\varepsilon}\left(\frac{\partial \mathcal{U}_{\mathrm{ac}}}{\partial \theta_{\mathrm{r}}}\right)^2 - \frac{1}{\varepsilon}\left(\frac{\partial \mathcal{U}_{\mathrm{ac}}}{\partial V_{\mathrm{r}}}\right)^2 \\ &\leq 0, \end{aligned} \tag{6.22}$$

where $(L_d - L'_d)/T'_{d0}$ and L_{dc} are positive in practical situations, and D is assumed to be positive. The property (i) of the energy function is therefore satisfied. Suppose that there is an interval $t \in [t_1, t_2]$ such that $\mathrm{d}\mathcal{W}(\boldsymbol{x}(t), \boldsymbol{y}(t))/\mathrm{d}t = 0$. It follows from the SP

system (6.8) at $\mu = 0$ and the inequality (6.22) that $\omega(t) = 0$, $I_{\rm dc}(t) = 0$, $\mathrm{d}v'_q(t)/\mathrm{d}t = 0$, $\mathrm{d}\delta(t)/\mathrm{d}t = 0$, $\mathrm{d}\theta_{\rm r}(t)/\mathrm{d}t = 0$, and $\mathrm{d}V_{\rm r}(t)/\mathrm{d}t = 0$ for $t \in [t_1, t_2]$. Then it follows that the SP system (6.8) at $\mu = 0$ is at an EP. Thus the property (ii) of the energy function also holds. In addition, we can confirm by the same way as [18,19] that if $v'_q(t)$, $\theta_{\rm r}(t)$, and $V_{\rm r}(t)$ are bounded for every nontrivial trajectory $(\boldsymbol{x}(t), \boldsymbol{y}(t))$ with a bounded function $\mathcal{W}(\cdot,\cdot)$, then $\mathcal{W}(\boldsymbol{x}(t), \boldsymbol{y}(t))$ satisfies the property (iii). Hence the function $\mathcal{W}(\boldsymbol{x}, \boldsymbol{y})$ is an energy function for the corresponding SP system (6.8) at $\mu = 0$. The above discussion results in the following proposition:

Proposition 6.11 *If $v'_q(t)$, $\theta_{\rm r}(t)$, and $V_{\rm r}(t)$ are bounded for every nontrivial trajectory $(\boldsymbol{x}(t), \boldsymbol{y}(t))$ with a bounded function $\mathcal{W}(\cdot,\cdot)$, then the function $\mathcal{W}(\boldsymbol{x}, \boldsymbol{y})$ becomes an energy function for the corresponding SP system* (6.8) *at $\mu = 0$.*

The proposition is also given as the slightly different version in [18]. Furthermore, the following proposition is obtained with the characterization of a stability boundary:

Proposition 6.12 *Suppose that the function $\mathcal{W}(\boldsymbol{x}, \boldsymbol{y})$ is an energy function for the corresponding SP system* (6.8) *at $\mu = 0$. If Assumptions* 6.5 *and* 6.6 *are satisfied for the SP system* (6.8) *at $\mu = 0$, then a stability boundary ∂A of an asymptotically stable EP $(\boldsymbol{x}_{\rm s}, \boldsymbol{y}_{\rm s})$ in a stable component $\Gamma_{\rm s}$ in the DAE system* (6.6) *at $\mu = 0$ is given by the formula* (6.18).

6.3.3 AC/DC power system

On the other hand, this subsection characterizes stability boundaries in the DAE system (6.20) under sufficiently small perturbation μ. The characterization is based on perturbation theory of vector fields. Here we state the following two theorems in [13] to investigate both EPs and their types on stability boundaries under small perturbation of general vector fields:

Theorem 6.13 [13] *Let $f : M \to E$ be a C^1 vector field. M is an open set in the vector space E, and $V(M)$ the set of all C^1 vector fields on M. Let $\hat{x}$ be a type-k hyperbolic EP on the stability boundary $\partial A_f(x_{\rm s})$ satisfying the transversality condition. Then, for any $\eta > 0$, there exist a ξ-neighborhood $R \subset V(M)$ of f and a neighborhood of $U \subset M$ of $\hat{x}$ such that for any $g \in R$,*

- *there is a unique type-k hyperbolic EP* $\hat{x}^g$ *of the vector field* g *such that* $||\hat{x}^g - \hat{x}|| < \eta$; *moreover,*

- $\hat{x}^g$ *is on the stability boundary* $\partial A_g(\hat{x}^g_{\rm s})$, *where* $\hat{x}^g_{\rm s}$ *is an asymptotically EP of vector field* g *and* $||\hat{x}^g_{\rm s} - \hat{x}_{\rm s}|| < \eta$.

Theorem 6.14 [13] *Let* $x_{\rm s}$ *be an asymptotically stable EP of the vector field* f *and let* x_i, $i = 1, 2, \ldots, k$, *be the hyperbolic EPs on* $\partial A_f(x_{\rm s})$ *and the intersection between an unstable manifold* $W^{\rm u}_f(x_i)$ *of* x_i *and a stable manifold* $W^{\rm s}_f(x_{\rm s})$ *of* $x_{\rm s}$ *satisfies the transversality condition and* $\partial A_f(x_{\rm s}) = \bigcup_{x_i \in \partial A_f(x_{\rm s})} W^{\rm s}_f(x_i)$. *There exists a positive number* η *such that, for any vector field* g *which is a* $\eta - C^1$ *perturbation of* f, *the EPs* $h(x_i)$, $i = 1, 2, \ldots, k$, *are also on the stability boundary of* $h(x_{\rm s})$, *and* $\partial A_g(h(x_{\rm s})) = \bigcup_{h(x_i) \in \partial A_g(h(x_{\rm s}))} W^{\rm s}_g(h(x_i))$, *where* $h(\cdot)$ *is an one-to-one correspondence and* $h(x_{\rm s})$ *is an asymptotically EP of the vector field* g.

Applying Theorems 6.13 and 6.14 to the SP system (6.21) results in the following proposition:

Proposition 6.15 *Suppose that the SP system* (6.8) *at* $\mu = 0$ *holds Assumptions* 6.5–6.7, *and the intersection between a stability region* A_ε *of an asymptotically stable EP* $(\boldsymbol{x}_{\rm s}, \boldsymbol{y}_{\rm s})$ *and an unstable manifolds* $W^{\rm u}_\varepsilon(\boldsymbol{x}_i, \boldsymbol{y}_i)$ *of* $(\boldsymbol{x}_i, \boldsymbol{y}_i)$, $i = 1, 2, \ldots, k$, *on the stability boundary* ∂A_ε *satisfies the transversality condition. Then, for any* $\eta > 0$, *there exists a positive number* $\xi > 0$ *such that for any* $(\mu/\varepsilon) < \xi$, *there is a unique asymptotically stable EP* $(\boldsymbol{x}^\mu_{\rm s}, \boldsymbol{y}^\mu_{\rm s})$ *of the SP system* (6.21) *with* $||(\boldsymbol{x}^\mu_{\rm s}, \boldsymbol{y}^\mu_{\rm s}) - (\boldsymbol{x}_{\rm s}, \boldsymbol{y}_{\rm s})|| < \eta$, *and for each* $(\boldsymbol{x}_i, \boldsymbol{y}_i)$ *there is a unique hyperbolic EP* $(\boldsymbol{x}^\mu_i, \boldsymbol{y}^\mu_i)$ *of the SP system* (6.21) *with* $||(\boldsymbol{x}^\mu_i, \boldsymbol{y}^\mu_i) - (\boldsymbol{x}_i, \boldsymbol{y}_i)|| < \eta$. *In addition, there is no other EP than* $(\boldsymbol{x}^\mu_i, \boldsymbol{y}^\mu_i)$, $i = 1, 2, \ldots, k$, *on the stability boundary* $\partial A^\mu_\varepsilon$ *of* $(\boldsymbol{x}^\mu_{\rm s}, \boldsymbol{y}^\mu_{\rm s})$, *and*

$$\partial A^\mu_\varepsilon = \bigcup_{(\boldsymbol{x}^\mu_i, \boldsymbol{y}^\mu_i) \in \partial A^\mu_\varepsilon} W^{\rm s}_\varepsilon(\boldsymbol{x}^\mu_i, \boldsymbol{y}^\mu_i). \tag{6.23}$$

Hence, by considering a stable component $\Gamma^\mu_{\rm s}$ of the DAE system (6.20), and for a sufficiently small positive number μ, taking a positive number $\hat{\varepsilon}$ such that $\mu/\xi < \hat{\varepsilon}$ holds in

Theorems 6.1 and 6.2, we obtain the characterization of a stability boundary in the DAE system (6.20):

Proposition 6.16 *Suppose that the corresponding SP system* (6.8) *at* $\mu = 0$ *holds Assumptions* 6.5–6.7, *and the intersection between a stability region* A_ε *of an asymptotically stable EP* $(\boldsymbol{x}_{\rm s}, \boldsymbol{y}_{\rm s})$ *and an unstable manifolds* $W^{\rm u}_\varepsilon(\boldsymbol{x}_i, \boldsymbol{y}_i)$ *of* $(\boldsymbol{x}_i, \boldsymbol{y}_i)$, $i = 1, 2, \ldots, k$, *on the stability boundary* ∂A_ε *satisfies the transversality condition. Then, for any* $\eta > 0$, *there exists a positive number* $\xi > 0$ *such that for any* $(\mu/\varepsilon) < \xi$, *there is a unique asymptotically stable EP* $(\boldsymbol{x}^\mu_{\rm s}, \boldsymbol{y}^\mu_{\rm s})$ *of the SP system* (6.21) *with* $||(\boldsymbol{x}^\mu_{\rm s}, \boldsymbol{y}^\mu_{\rm s}) - (\boldsymbol{x}_{\rm s}, \boldsymbol{y}_{\rm s})|| < \eta$, *and for each* $(\boldsymbol{x}_i, \boldsymbol{y}_i)$ *there is a unique hyperbolic EP* $(\boldsymbol{x}^\mu_i, \boldsymbol{y}^\mu_i)$ *of the SP system* (6.21) *with* $||(\boldsymbol{x}^\mu_i, \boldsymbol{y}^\mu_i) - (\boldsymbol{x}_i, \boldsymbol{y}_i)|| < \eta$. *Furthermore, for sufficiently small* μ, *suppose that there exists a stable component* $\Gamma^\mu_{\rm s}$ *of the DAE system* (6.20) *such that the EP* $(\boldsymbol{x}^\mu_{\rm s}, \boldsymbol{y}^\mu_{\rm s})$ *is a member of* $\Gamma^\mu_{\rm s}$. *Then, the stability boundary* ∂A^μ *of* $(\boldsymbol{x}^\mu_{\rm s}, \boldsymbol{y}^\mu_{\rm s})$ *for the DAE system* (6.20) *is given by the same formula as* (6.18), *that is,*

$$\partial A^\mu = \left\{ \bigcup_{(\boldsymbol{x}^\mu_i, \boldsymbol{y}^\mu_i) \in \partial A^\mu} W^{\rm s}(\boldsymbol{x}^\mu_i, \boldsymbol{y}^\mu_i) \right\} \cup \left\{ \bigcup_{(\boldsymbol{x}^\mu_i, \boldsymbol{y}^\mu_i) \in \partial A^\mu_\varepsilon \setminus \Gamma^\mu_{\rm s}} W^{\rm s}_\varepsilon(\boldsymbol{x}^\mu_i, \boldsymbol{y}^\mu_i) \cap \Gamma^\mu_{\rm s} \right\}. \quad (6.24)$$

The above result completely describes the global structure of the stability boundary in the electric power system with dc transmission; the stability boundary consists of the two parts including the sets from which trajectories converge to the EPs and the singular surface. Namely, the dynamical feature of the stability boundary persists under the small perturbation that corresponds to the interaction between the ac and dc systems. Moreover, the obtained characterization makes it possible to apply the controlling UEP method [14, 15, 111], which is an effective and practical method for estimating the transient stability of ac power systems, to the ac/dc power system in Fig. 5.1.

6.4 Concrete structure of stability boundary: Numerical results revisited

This section revisits the numerical results on a stability boundary. Chapter 5 numerically analyzed a stability boundary under the parameters $D = 0$, $\mu\tilde{K}_V = \mu\tilde{K}_I = 1.19$, and

$\mu\tilde{X}_c = 0.12$; other parameters setting is shown in Tab. 5.3. We now confirm the obtained characterization (6.24) based on the numerical results.

6.4.1 Hyperbolic saddle point in differential-algebraic equation system

A stability boundary ∂A^μ of EP#1 is first considered via the basin portrait around EP#2 in Fig. 5.4(c). The same basin portrait is shown in Fig. 6.1(b). Here we note that all the initial conditions are included by one stable component. The initial conditions are classified in Fig. 6.1 as follows: the *white* region represents the basin of EP#1 and the *gray* region the one from which any trajectory converges to the singular surface S. This figure shows that the stable manifold of EP#2 coincides with a part of the stability boundary ∂A^μ; EP#2 is one of the basic sets of the stability boundary ∂A^μ. This structure of the stability boundary coincides with the first term of the obtained characterization (6.24).

6.4.2 Periodic orbit in singularly perturbed system

Next let us consider another part of the stability boundary ∂A^μ shown in Figs. 5.3(e) and 5.4(c) based on the SP system (6.8). The same portraits are also described by Fig. 6.1. The dynamics of the SP system (6.8) has the similarity to that of the DAE system (6.1) in one stable component; this property is validated by Theorem 6.1. Fig. 6.2 shows the transient behavior of the DAE system (6.1) and the SP system (6.8). All solutions in the figure start from the same initial conditions. In Fig. 6.2 the solution of the DAE system (6.1) converges to the singular surface S. On the other hand, all solutions of the SP system (6.8) converge to another stable EP, called by EP#3. Fig. 6.2 implies that all solutions of the SP system (6.8) show the same behavior as that of the DAE system (6.1) before its solution reaches S. Thus the stability boundary ∂A^μ can be examined through the SP system (6.8).

We now examine basic sets related to the part of stability boundary in Fig. 6.1 by the straddle orbit method [7] for the SP system (6.8). In principle any straddle orbit goes to one of the basic sets whose stable manifold is a part of the stability boundary. Fig. 6.1 also shows the initial conditions which are fixed to calculate the straddle orbits. In each

condition, one point exists in the basin of EP#1, and another point in the basin of EP#3 for the SP system (6.8). Fig. 6.3 shows the obtained straddle orbits at $\varepsilon = 0.5$ for the SP system (6.8). Each straddle orbit is described by being projected onto the $\delta - \omega$ and $\omega - I_{\rm dc}$ planes. In Fig. 6.3, all straddle orbits converge to a periodic orbit in Fig. 6.3(c); the periodic orbit is one of the basic sets of the stability boundary $\partial A_{\varepsilon}^{\mu}$ in the SP system (6.8).

6.4.3 Remarks and discussion

To discuss the above numerical results, we now need to remark two non-trivial relationships between the theoretical and numerical results. The value of the damping coefficient D is fixed at zero in Chapter 5 and this section. On the other hand, in Section 6.3, the positiveness of D is necessary to consider the existence of energy functions for the associated SP system (6.21). This is the first relationship which we need to examine numerically. However, it is numerically confirmed that the numerical results at $D = 0$ are identical to those at $D = 0.05$. Thus the numerical results are tractable for the following discussion in this subsection.

The last relationship is that the dynamics of the SP system (6.8) is not strictly consistent with that of the associated SP system (6.21) with the DAE system (6.20). This section numerically discussed the SP system (6.8) and confirmed the existence of the periodic solution. On the other hand, Section 6.3 theoretically clarified the dynamics of the SP system (6.21). To integrate the numerical and theoretical results, we therefore need to discuss whether the dynamics of the SP systems (6.8) and (6.21) are qualitatively equivalent or not. Unfortunately, this equivalence is not trivial and not clarified analytically. Here, we can point out how to attack the problem: an application of Theorem 6.1 to the present analysis by regarding the SP system (6.21) as a degenerate limit of the SP system (6.8). In the following discussion it is implicitly assumed that the dynamics of the SP systems (6.8) and (6.21) are qualitatively equivalent.

The existence of the periodic orbit possibly shows that the obtained characterization (6.24) is not applicable to the DAE system (6.1) under the present parameters. The above subsection confirmed the obtained characterization via the numerical results on the stability

boundary ∂A^{μ}. It is shown that a periodic orbit exists on the stability boundary $\partial A^{\mu}_{\varepsilon}$ in the SP system (6.8). By assuming the above consistency of the dynamics, this implies that the phase structure of the SP system (6.8) at $\mu = 0$ does not persist under the existence of the perturbation terms. The perturbation implies the interaction between the ac and dc systems. Namely, this result suggests that the theoretical result in Section 6.3 is inadequate to clarify the stability boundary in the DAE system (6.1) under the present parameters in Tab. 5.3.

An important question we will address is how to confirm the numerical results on the stability boundary theoretically. It is important to clarify the stability boundary in terms of the planning and operation of the ac/dc power system. Here it is stated as a contraposition of Theorem 6.4 that if a trajectory on $\partial A^{\mu}_{\varepsilon}$ of the SP system (6.8) converges to an periodic solution as time increases, then there exists no energy function for the SP system (6.8). The numerical results in Section 6.4 therefore show one of the application limits of the characterization based on the present energy function. To confirm the numerical results in this chapter, we need to explore a comprehensive energy function theory of stability boundaries in the DAE system (6.1).

6.5 Discontinuous solutions and transient stability

The rest of this chapter focuses on discontinuous trajectories in the DAE system (6.1) which are due to structural change of the ac/dc network configuration. Discontinuous solutions have been reported for power system transient analysis using structure-preserving models in [14,15,18,74,111]. As mentioned in Section 5.4, none of such discontinuous state change would be strictly observed in practical power systems. However, the solutions themselves are of paramount importance, because the DAE system (6.1) has the potential to be embedded into power system simulators as a detailed transient analysis model. In this chapter, we numerically and analytically examine several discontinuous solutions in the DAE system (6.1) using the singular perturbation technique.

6.5.1 Faults setting and external jump

Two fault cases which we now adopt are as follows: one is a three-phase fault in the ac transmission line, and the generator operates as a result onto the dc link only during the sustained fault. The other is a three-phase fault at the infinite bus, and thereby the infinite bus voltage is fixed at zero in the fault duration. Suppose that the system is at a known asymptotically stable EP at $t = 0^-$, the fault duration is confined to the time $[0^+, t_{\rm cl}^-]$, and the fault is cleared at a time $t = t_{\rm cl}$. It is assumed for simplicity that the post-fault DAE system is identical to the pre-fault DAE one. The above two cases are mathematically formulated in the DAE system (6.1) for $t \in [0^+, t_{\rm cl}^-]$: $1/L_\infty = 0$ (case-1) and $V_\infty = 0$ (case-2), respectively.

Two constraint sets are apparently different between the pre-fault (or post-fault) and fault-on DAE systems. The difference generates discontinuous solutions of the DAE system (6.1) at $t = 0$ and $t_{\rm cl}$; they are called *external jumps* [18, 111]. Such jump behaviors or discontinuous solutions have been discussed for constrained dynamical systems in [18, 74, 75, 85, 111]. Their previous works define the discontinuous solutions based on associated BL systems. In particular, when the BL systems are gradient [78], the discontinuous solutions are simply characterized based on the orbit structures of the BL systems. In the following, we use some previous results in [18, 74] to validate numerical discontinuous solutions (external jumps) in the DAE system (6.1).

6.5.2 Numerical simulations

Numerical simulations are performed for the DAE system (6.1). The parameters setting is identical to Tab. 5.3. The value of D is fixed at 0.05. The 3rd-stage Radau-IIA implicit Runge-Kutta method [10, 38] is here adopted to integrate the DAE system numerically. Since the numerical scheme is the one-step type, we possibly obtain numerical discontinuous solutions although they do not generally hold the uniqueness properties.

Figure 6.4 shows the transient behavior of ω, $I_{\rm dc}$, $V_{\rm r}(= \ln v_{\rm r})$, and electric power with setting the case-1 fault at $t_{\rm cl}/(120\pi\ {\rm s}^{-1}) = 140$ ms. In the figures, $\square$ denotes the initial condition, which coincides with the pre-fault steady state EP#1 in Chapter 5, and $\bullet$ the state at each $t = 0^+$, $t_{\rm cl}^-$, or $t_{\rm cl}^+$. The solution in the figure converges to EP#1, which

is a post-fault asymptotically stable EP, as time goes to infinity. In Fig. 6.4, ω and $I_{\rm dc}$, which are two of the variables related to the differential equation, are continuous; while $V_{\rm r}(=\ln v_{\rm r})$, which is one of the variables related to the algebraic equation, is discontinuous at $t/(120\pi\ {\rm s}^{-1}) = 0$ s and 140 ms. The numerical result will be discussed in the next subsection. Fig. 6.4(d) also shows the active power swing in the ac/dc system. During the fault duration, the active power output of the infinite bus is zero, and the generator output is therefore identical to the dc power input. Since the generator output during the fault duration is greater than the constant mechanical power input $p_{\rm m} = 0.5$, the generator is decelerated as shown in Fig. 6.4(a). After the fault is cleared at $t = t_{\rm cl}$, both the generator and infinite bus output show the oscillatory motions and converge to the corresponding values to EP#1 as shown in Fig. 5.4.

The case-2 fault solution is shown in Fig. 6.5. The solution converges to the singular surface S of the fault-on DAE system. The solution which reaches S is possibly discontinuous as noted in Chapter 5; the discontinuity here is qualitatively different from external jumps [18, 111]. This result implies an application limit of the DAE system (6.1) for the transient stability analysis. We state in Chapter 1 that the transient stability is determined by the dynamics of *post-fault* dynamical systems. The transient behavior in Fig. 6.5 therefore suggests that the present DAE system (6.1) is not relevant to clarifying the transient stability problem relative to the case-2 fault. To overcome the limitation, it is necessary to model the transient dynamics in detail with taking some equipments of the ac/dc system into account: AVR, shunt capacitors at converter stations, and so on.

6.5.3 Discontinuous solutions and boundary layer systems

Next we discuss the discontinuous solution of the case-1 fault setting through the SP system (6.8). As discussed before, the SP system (6.8) plays a key role in validating numerical simulations for the DAE system (6.1). Fig. 6.6 shows the projected trajectories of the DAE and associated SP systems onto $\theta_{\rm r} - V_{\rm r}$ plane. The perturbation parameter ε is set at 0.5. The *solid* line denotes the trajectory of the DAE system (6.1) and the *dotted* line that of the SP system (6.8) which initial condition is identical to that for the DAE system (6.1). The figure implies that the trajectory of the SP system (6.8) traces the

discontinuous solution of the DAE system (6.1) although the details of the external jumps are not confirmed. Thus the SP system (6.8) provides us with an overall approximation of the discontinuous solution.

The external jumps of the case-1 fault are now analytically justified based on a BL system. To confirm the projected discontinuous solution shown in Fig. 6.6, we adopt the following BL system which is derived from the reduced DAE system (6.20):

$$\begin{cases} \dfrac{\mathrm{d}\theta_{\mathrm{r}}}{\mathrm{d}s} &= -\dfrac{\partial \mathcal{W}}{\partial \theta_{\mathrm{r}}}\left(v_q', \delta, \theta_{\mathrm{r}}, V_{\mathrm{r}}\right) - \mu\left(\tilde{K}_V \mathrm{e}^{V_{\mathrm{r}}}\cos\alpha - \dfrac{3}{\pi}\tilde{X}_{\mathrm{c}} I_{\mathrm{dc}}\right) I_{\mathrm{dc}}, \\ \dfrac{\mathrm{d}V_{\mathrm{r}}}{\mathrm{d}s} &= -\dfrac{\partial \mathcal{W}}{\partial V_{\mathrm{r}}}\left(v_q', \delta, \theta_{\mathrm{r}}, V_{\mathrm{r}}\right) \\ & \quad -\mu\sqrt{\tilde{K}_I^2 \mathrm{e}^{2V_{\mathrm{r}}} - \left(\tilde{K}_V \mathrm{e}^{V_{\mathrm{r}}}\cos\alpha - \dfrac{3}{\pi}\tilde{X}_{\mathrm{c}} I_{\mathrm{dc}}\right)^2}\cdot I_{\mathrm{dc}}, \end{cases} \tag{6.25}$$

where $\alpha = G_\alpha(I_{\mathrm{dc(ref)}} - I_{\mathrm{dc}})$. It should be noted that the dynamics of the reduced DAE system (6.20) is identical to that of the DAE system (6.1) under the following conditions: $0 < v_{\mathrm{r}} < K$, $I_{\mathrm{dc}} \neq 0$, $\sin\varphi_{\mathrm{r}} > 0$, and $\mu\tilde{K}_I > 0$. Here we state from [18, 74] that if the DAE system (6.1) admits of the external jump at $t = t_*$, then the trajectory of the BL system (6.25) with the initial condition $(\theta_{\mathrm{r}}(t_*^-), V_{\mathrm{r}}(t_*^-))$ converges to the point $(\theta_{\mathrm{r}}(t_*^+), V_{\mathrm{r}}(t_*^+))$ satisfying $\boldsymbol{x}(t_*^-) = \boldsymbol{x}(t_*^+)$; the coincident property holds in Figs. 6.4(a) and (b). This follows that the point $(\theta_{\mathrm{r}}(t_*^-), V_{\mathrm{r}}(t_*^-))$ is on a stable manifold of the EP $(\theta_{\mathrm{r}}(t_*^+), V_{\mathrm{r}}(t_*^+))$ in the BL system (6.25). Fig. 6.7 definitely describes the trajectories of the pre- and post-BL systems and the projected discontinuous solution of the DAE system (6.1), for which we here use the transformations $\theta_{\mathrm{r}} = \delta - \delta_{\mathrm{r}}$ and $V_{\mathrm{r}} = \ln v_{\mathrm{r}}$. In the figure, all trajectories of the BL systems converge to asymptotically stable EPs of the BL systems, and the EPs coincide with the starting points of the external jumps at $t = 0$ and t_{cl}. Hence, we conclude that the numerical discontinuous solution including the external jumps is valid in the analytical sense.

6.5.4 Discussion

This section analyzed several discontinuous solutions of the DAE system (6.1) numerically. The discontinuous solutions were also analytically justified using the BL system. The discontinuous solutions provide us with several information about the transient dynamics

of the ac/dc system: in case-1 fault (i) the dc system remains at a pre-fault state during the sustained fault; (ii) the generator is decelerated to supply the demanded power by the dc system; and in case-2 fault (iii) the present DAE system (6.1) is not relevant to the transient stability analysis.

The discontinuous dynamics here is closely related to the transient stability. Chapters 5 and 6 show that the stability is governed by the global structure of the stability boundary. Fig. 6.8 shows the transient behavior of the DAE system (6.1) with the case-1 fault at $t_{\rm cl}/(120\pi\ {\rm s}^{-1}) = 140$ ms and 170 ms. The discontinuous solution at $t_{\rm cl}/(120\pi\ {\rm s}^{-1}) = 140$ ms converges to EP#1, while the solution with $t_{\rm cl}/(120\pi\ {\rm s}^{-1}) = 170$ ms reaches the singular surface S of the post-fault DAE system. The difference between these solutions is clarified based on the global structure shown in Chapters 5 and 6. Fig. 6.9 describes the transient behavior of the SP system (6.8) with the case-1 fault; the initial condition equals the one in Fig. 6.8. In the figure, the solution at $t_{\rm cl}/(120\pi\ {\rm s}^{-1}) = 140$ ms settles down EP#1, while the solution at $t_{\rm cl}/(120\pi\ {\rm s}^{-1}) = 170$ ms goes to EP#3 which appears in Section 6.4. These figures imply that the solutions of the SP system (6.8) give us the good approximations of the solutions in the DAE system (6.1) until the trajectory at $t_{\rm cl}/(120\pi\ {\rm s}^{-1}) = 170$ ms reaches S. Furthermore, the solutions in Fig. 6.9 qualitatively coincide with those in Fig. 6.2 which are used for the stability boundary analysis in Section 6.4. These numerical simulations suggest that the mechanism behind the different transient behavior possibly originates from the periodic orbit and associated stability boundary of EP#1 in Chapter 6. Thus we can discuss the transient stability analytically by investigating both the stability boundary and the discontinuous solutions.

6.6 Summary

This chapter addressed the stability boundaries of the DAE system (6.1). Section 6.3 completely characterized the stability boundaries of the DAE system. The theoretical result describes the entire global structures of the stability boundaries in the solution space of the DAE system. Moreover, the characterization makes it possible to apply the controlling UEP method [14, 15, 111] to the ac/dc power system. Section 6.5 analyzed the discontinuous solutions of the DAE system with respect to some event disturbances. The

obtained results provide us with the information about the transient dynamics of the ac/dc system and reveal the fault condition under which the present DAE system is not relevant to the transient stability analysis.

Throughout this chapter, we show how the dc link strongly affects the stability boundary of the ac/dc system. As seen in Section 6.3, the stability boundary of the ac system consists of both the stable manifolds of EPs and the particular trajectories which reach the singular surface. The obtained characterization in Section 6.3 then shows that the dynamical feature of the stability boundary persists under the small perturbation that corresponds the interaction between the ac and dc systems. On the other hand, Section 6.4 shows that a periodic orbit exists on the stability boundary of the associated SP system (6.8) under the parameters setting in Tab. 5.3. This possibly implies that the existence of the dc link changes the dynamical feature of the stability boundary under the present parameters. The boundary structure sheds a new insight on the transient stability for the ac/dc power system.

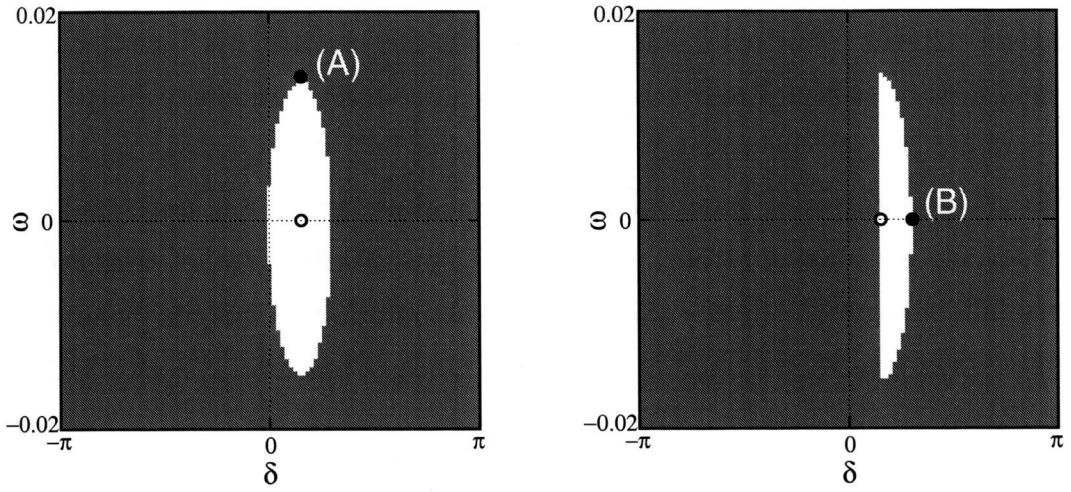

(a) Fig. 5.3(e)

(b) Fig. 5.4(c)

Figure 6.1 Basin portraits around EP#1 and EP#2 in the DAE system (6.1) with $D = 0$. The portraits (a) and (b) are the same ones as Figs. 5.3(e) and 5.4(c), respectively. The symbols ○ in the figures (a) and (b) denote EP#1 and EP#2, respectively. The initial conditions are classified as follows: the *white* region represents the basin of EP#1 and the *gray* region the one from which any trajectory converges to the singular surface S. The two points (A) and (B) in the figures also stand for the initial conditions of the straddle orbit method for the SP system (6.8).

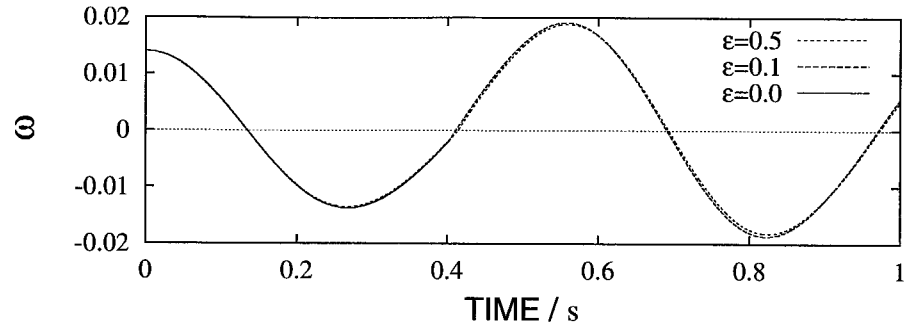

(a) Rotor speed deviation ω

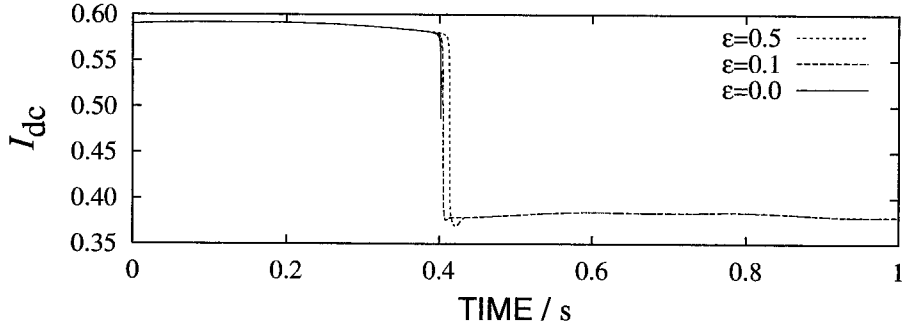

(b) DC current I_{dc}

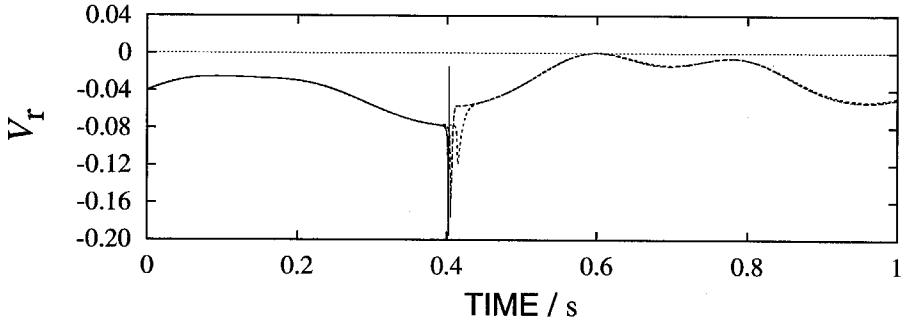

(c) The related value V_r to ac voltage v_r: $V_r = \ln v_r$

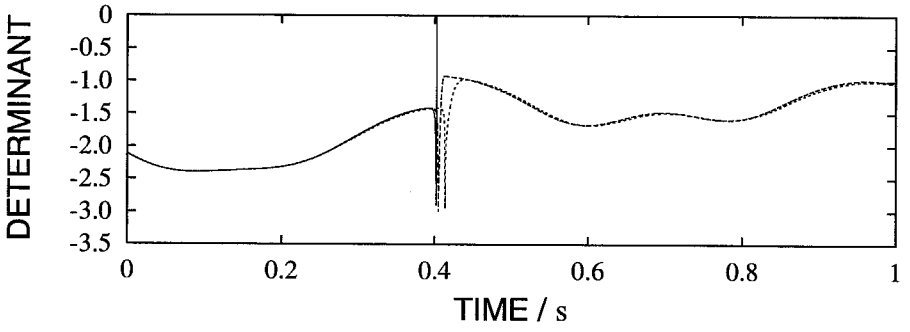

(d) Determinant $D_y g$ for the DAE system (5.10) or (6.1)

Figure 6.2 Transient behavior of the DAE system (6.1) and the SP system (6.8). All solutions in the figure start from the same initial condition: the value of ω is 1.4×10^{-2}, and the other values equal those at EP#1.

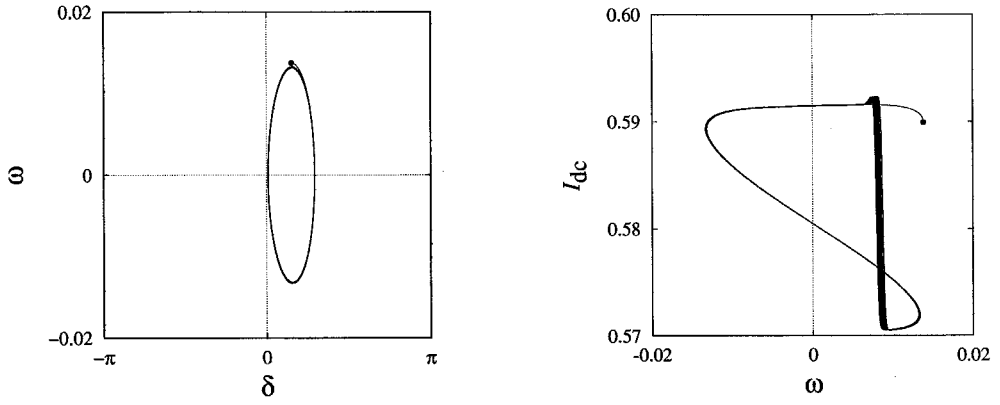

(a) From the points (A)

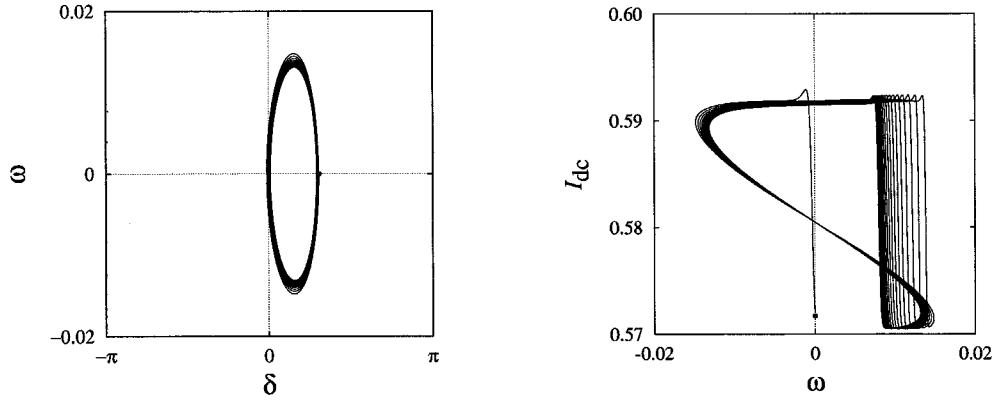

(b) From the points (B)

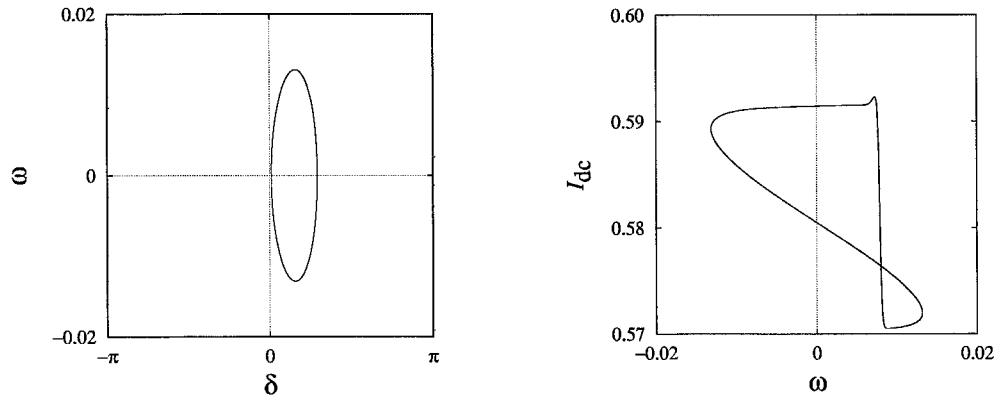

(c) Periodic orbit

Figure 6.3 Projected straddle orbits and periodic orbit in the SP system (6.8) at $\varepsilon = 0.5$

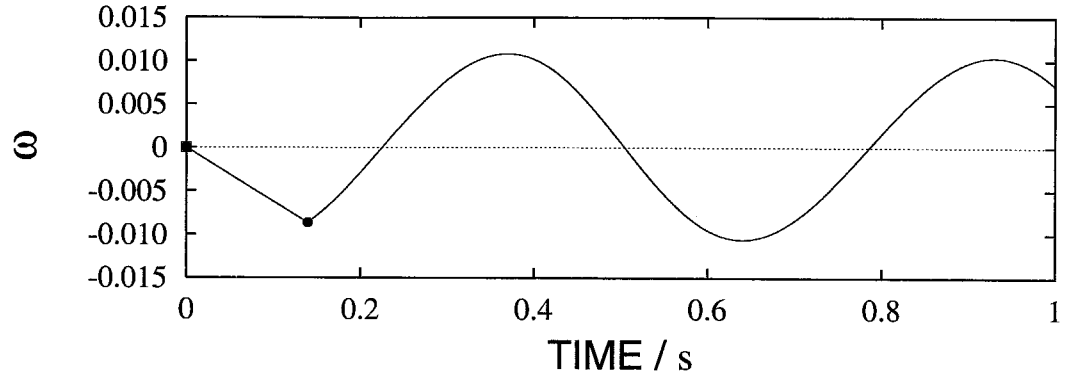

(a) Rotor speed deviation ω

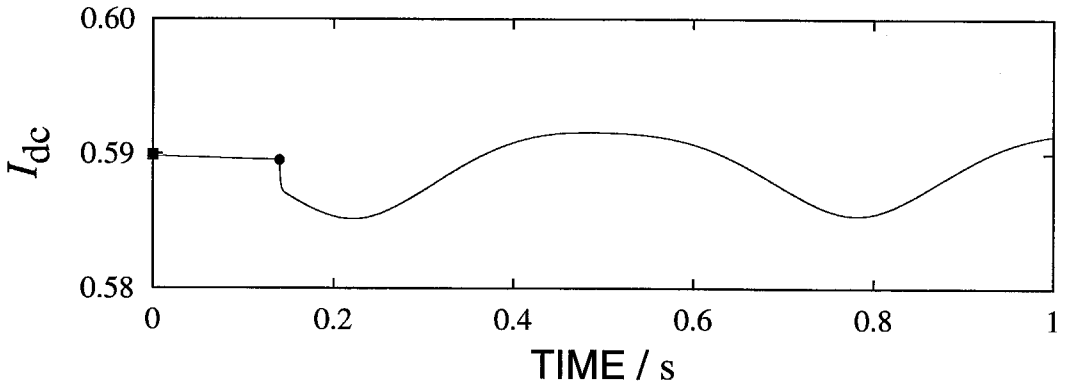

(b) DC current I_{dc}

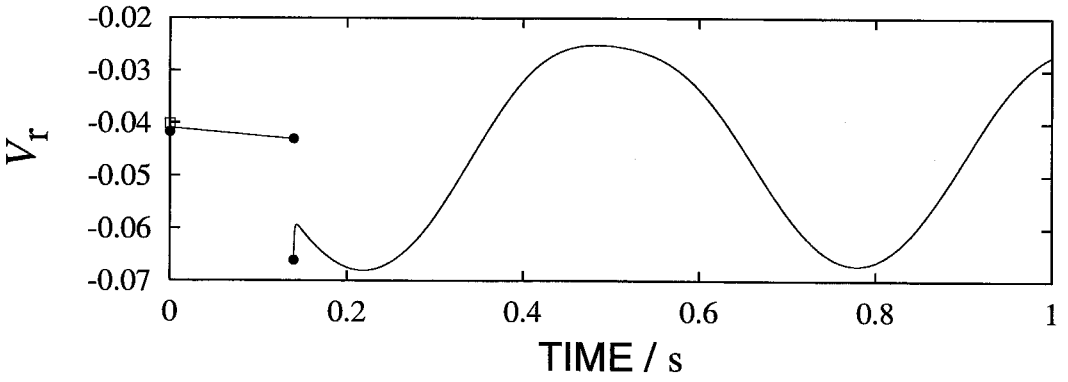

(c) The related value V_r to ac voltage v_r: $V_r = \ln v_r$

Figure 6.4 Transient behavior and discontinuous solution of the DAE system (6.1) with case-1 fault setting. The fault-clearing time $t_{cl}/(120\pi\ \mathrm{s}^{-1})$ is fixed at 140 ms. The solution in the figure converges to EP#1 which is a post-fault asymptotically stable EP.

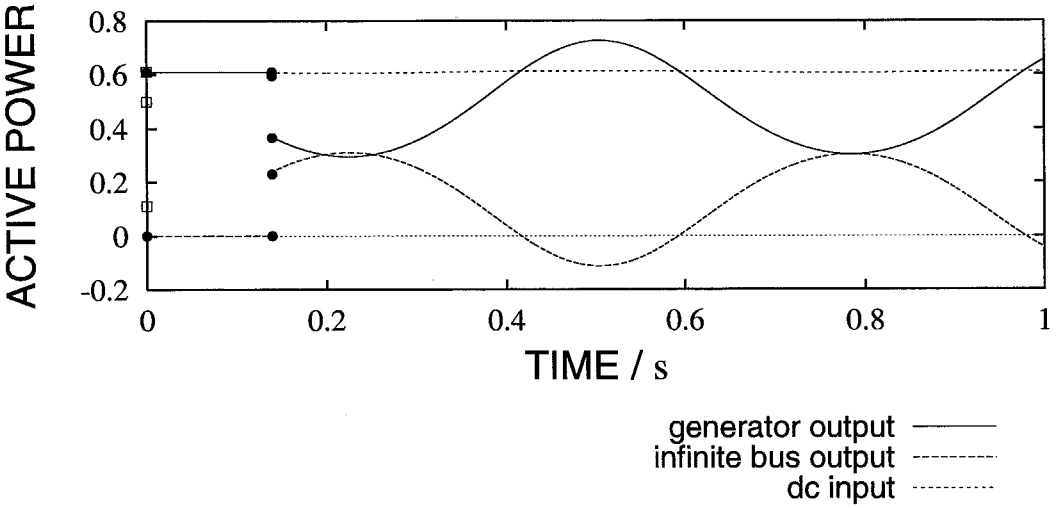

(d) Active power

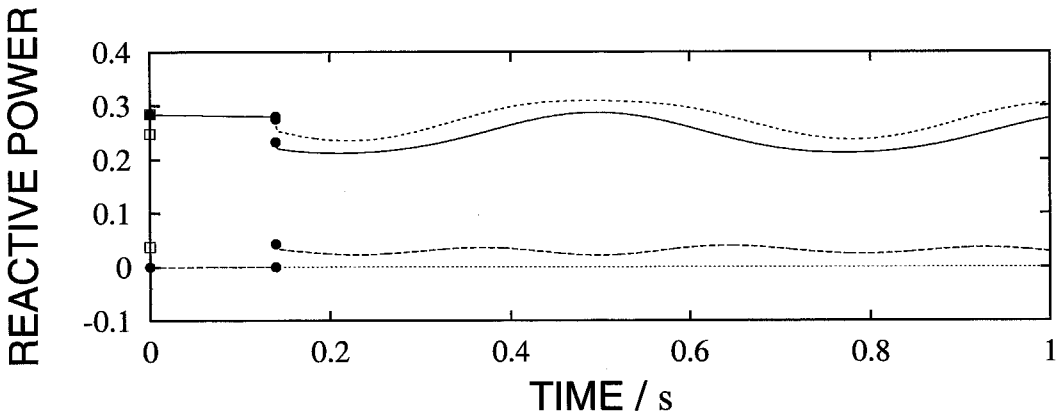

(e) Reactive power

Figure 6.4 (*continued*)

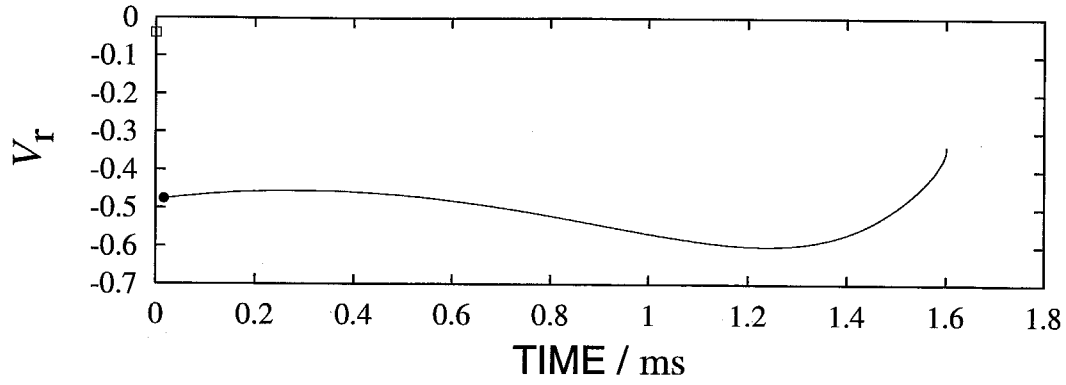

(a) The related value V_r to ac voltage v_r: $V_r = \ln v_r$

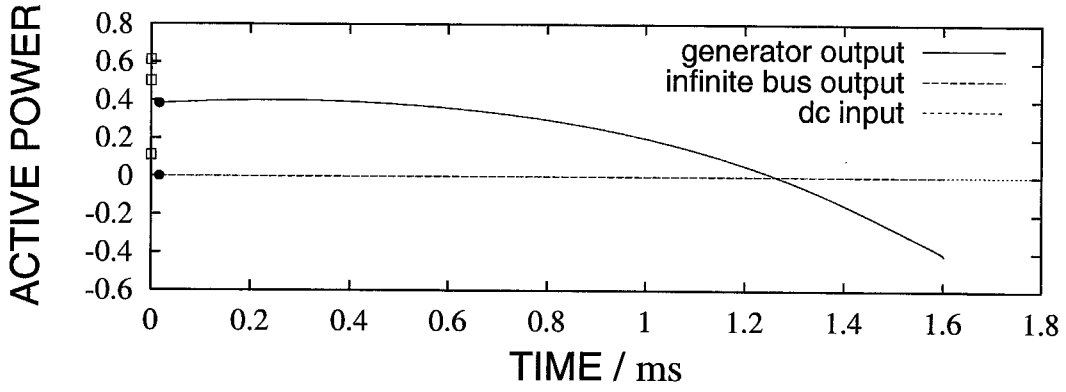

(b) Active power

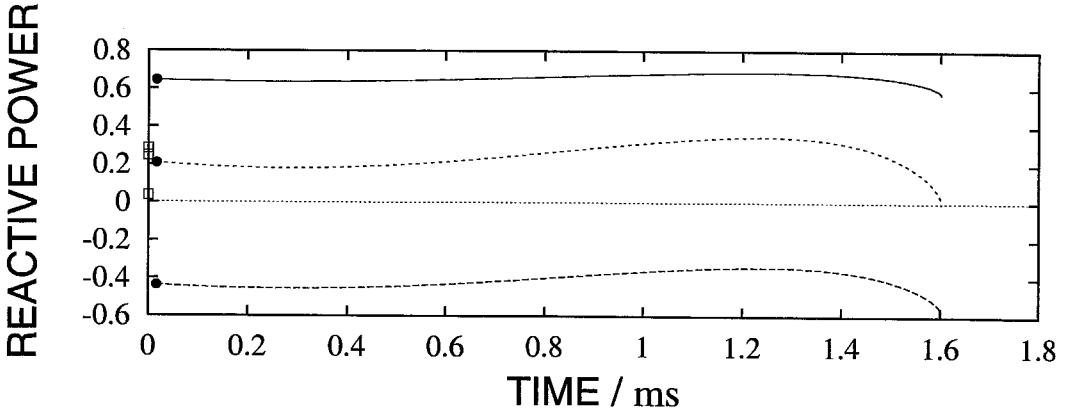

(c) Reactive power

Figure 6.5 Transient behavior and discontinuous solution of the DAE system (6.1) with case-2 fault setting. The solution converges to the singular surface of the fault-on DAE system.

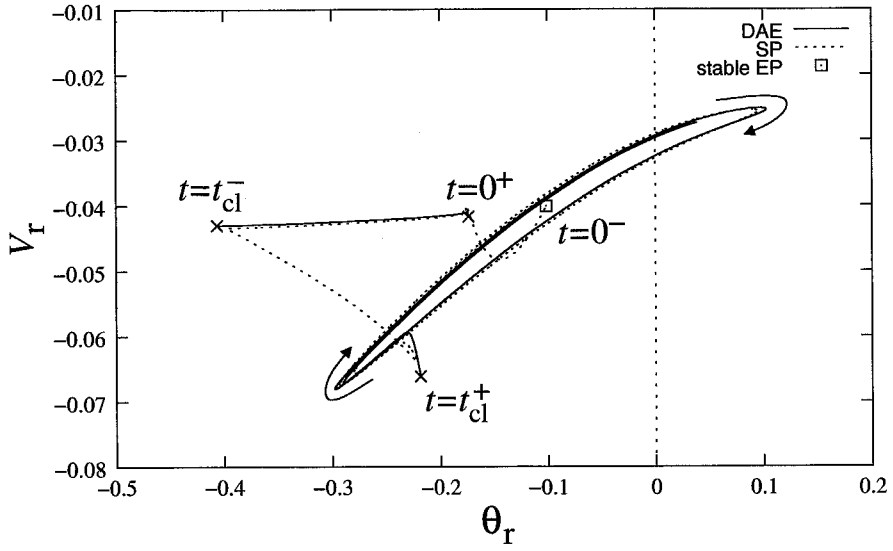

Figure 6.6 Projected trajectories of the DAE and SP systems with case-1 fault setting onto $\theta_r - V_r$ plane. The perturbation parameter ε is set at 0.5. The *solid* line denotes the trajectory of the DAE system (6.1) shown in Fig. 6.4, for which we here use the transformations $\theta_r = \delta - \delta_r$ and $V_r = \ln v_r$, and the *dotted* line that of the SP system (6.8).

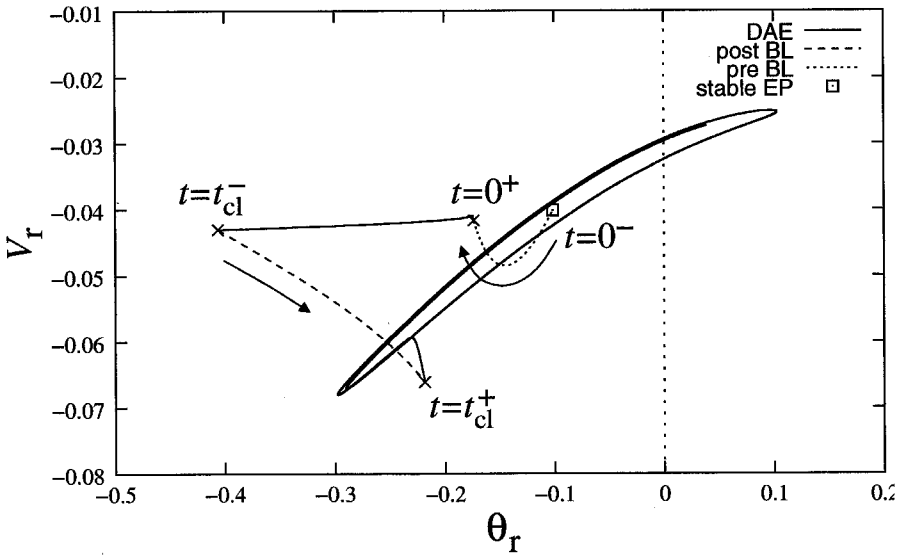

Figure 6.7 Projected discontinuous solution and trajectories of the pre- and post-BL systems with case-1 fault setting onto $\theta_r - V_r$ plane. The *solid* line denotes the trajectory of the DAE system (6.1) shown in Fig. 6.4, for which we here use the transformations $\theta_r = \delta - \delta_r$ and $V_r = \ln v_r$, and the *dotted* and *broken* lines those of the BL systems (6.25) at $t = 0$ and t_{cl}.

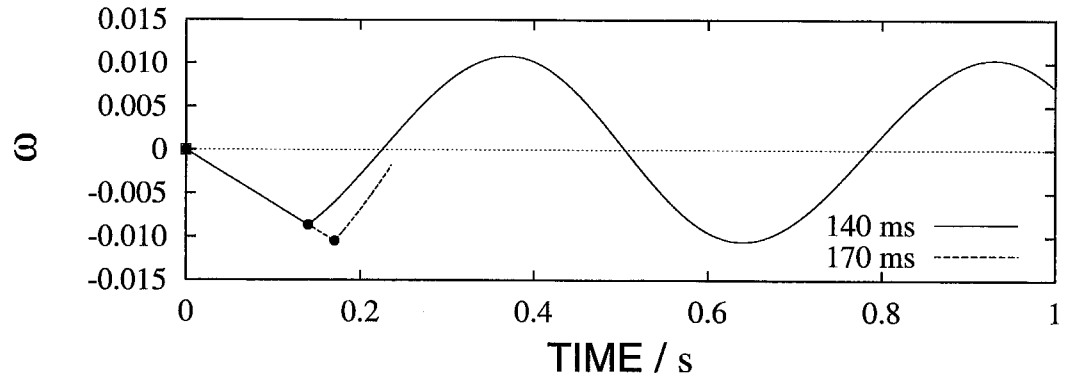

(a) Rotor speed deviation ω

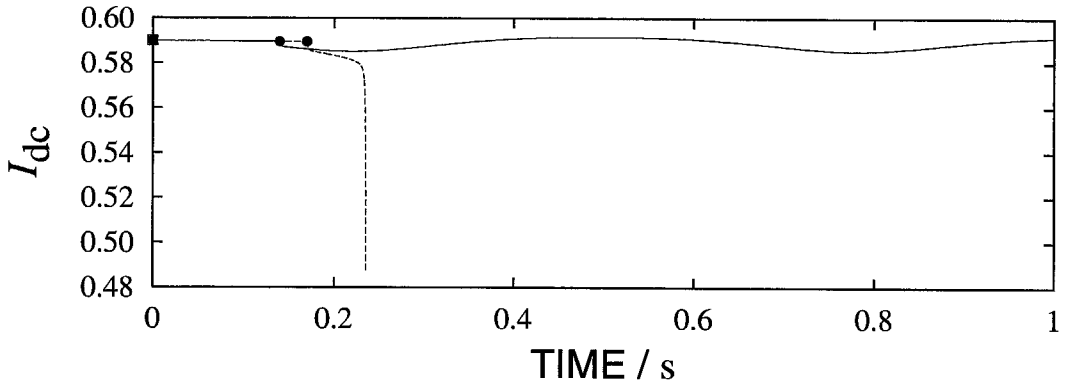

(b) DC current I_{dc}

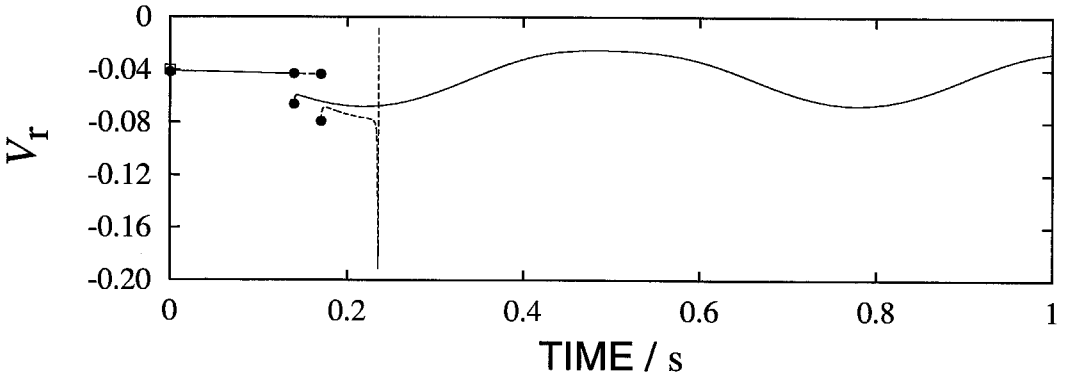

(c) The related value V_r to ac voltage v_r: $V_r = \ln v_r$

Figure 6.8 Transient behavior of the DAE system (6.1) with setting case-1 fault at $t_{cl}/(120\pi\ \mathrm{s}^{-1}) = 140$ ms and 170 ms. The discontinuous solution with $t_{cl}/(120\pi\ \mathrm{s}^{-1}) = 140$ ms is identical to that in Fig. 6.4 and converges to EP#1. The solution with $t_{cl}/(120\pi\ \mathrm{s}^{-1}) = 170$ ms converges to the singular surface of the post-fault DAE system.

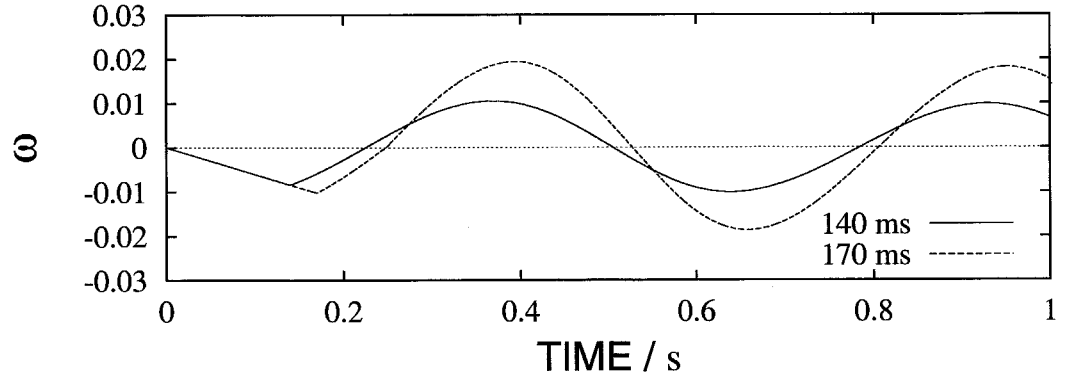

(a) Rotor speed deviation ω

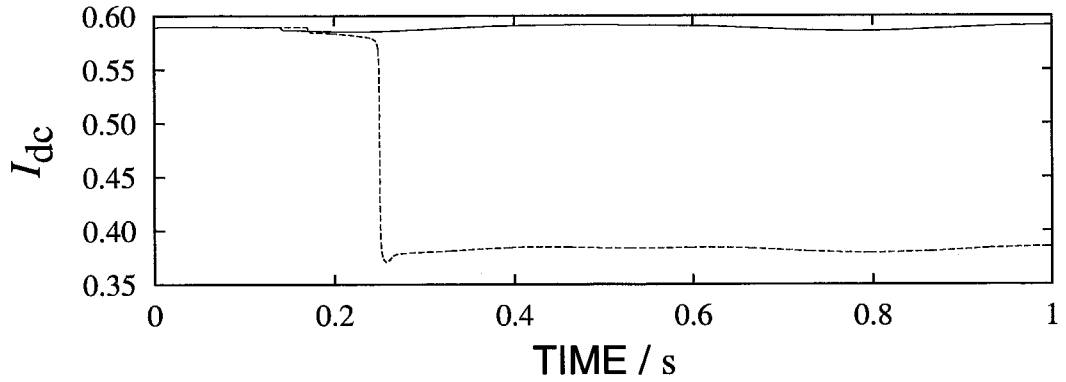

(b) DC current I_{dc}

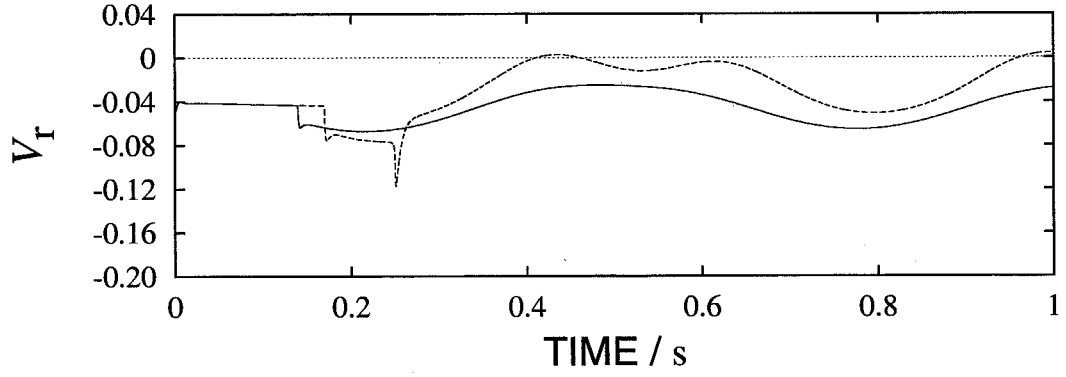

(c) The related value V_r to ac voltage v_r

Figure 6.9 Transient behavior of the SP system (6.8) with setting case-1 fault at $t_{cl}/(120\pi\ s^{-1}) = 140$ ms and 170 ms. The solution with $t_{cl}/(120\pi\ s^{-1}) = 140$ ms is identical to that in Fig. 6.6 and converges to EP#1. The solution with $t_{cl}/(120\pi\ s^{-1}) = 170$ ms converges to EP#3.

Chapter 7

Conclusion

This dissertation was devoted to analysis of transient dynamics and stability boundaries in an electric power system with dc transmission. The analysis was performed based on two mathematical models: swing equation and DAE systems. The dynamical systems were derived through an actual ac/dc power system. In the following, we summarize the obtained results in this dissertation and collect future research directions.

Chapter 2 analyzed transient dynamics and stability boundaries affected by constant electric power which flows into the dc link. We here derived and examined the unsymmetrical swing equation system. The system has the dc external force which corresponds to the constant dc power. As an important feature of the dynamical behavior, it is shown that the fractal structure grows in a stability boundary caused by the dc external forcing. The fractal boundary indicates that the system behavior becomes unpredictable depending on the dc operation.

In Chapter 3 we proposed an analytical criterion for stability boundaries of the swing equation system. The criterion was derived based on the Melnikov's perturbation method for ODF time-periodic perturbed Hamiltonian systems. The proposed criterion can be analytically calculated with the corresponding integrable Hamiltonian systems. The criterion was also applied to the analysis of the stability boundaries in the swing equation system. The application shows the effectiveness of the proposed criterion for the analysis of the ac/dc power system.

Chapter 4 focused on basin boundaries of resonant solutions in the swing equation sys-

tem. We here proposed an analytical criterion for the basin boundaries of the resonant solutions based on the subharmonic Melnikov function and related theories. This chapter also applied the proposed criterion to the stability boundary analysis of the swing equation system. The obtained results illustrate not only its effectiveness but also its conservativeness for the stability estimation. This problem remains to be solved as a forthcoming research topic.

Chapters 5 and 6 discussed transient dynamics and stability boundaries with considering dc system's operation and power balance relation between the ac and dc systems. The analysis was based on the DAE system. The DAE system keeps the structural characteristics of power conversion and control setup in the dc link, and explicitly describes the power relation between the ac and dc systems. Chapter 5 clarified some dynamical features of the DAE system. In particular, a stability boundary was numerically examined via several basin portraits. We here show that there exists a hyperbolic saddle point on the stability boundary, and its stable manifold partially governs the global structure of the stability boundary. The structure motivates the theoretical characterization of the stability boundaries in Chapter 6. Furthermore, this chapter points out that the singular surface and associated trajectories are crucial for clarifying the global structure.

In Chapter 6 we theoretically examined stability boundaries and related trajectories of the DAE system. Complete characterization of the stability boundaries was derived using an energy function for an associated SP system. The theoretical result reveals the entire global structures of the stability boundaries. In addition, the characterization was examined via some numerical results with a stability boundary in Chapter 5. The numerical simulation shows that there exists a periodic orbit in an associated SP system under the present parameters, and the characterization is therefore possibly inadequate for the present ac/dc power system. The boundary structure itself sheds a new insight on the transient stability for the ac/dc system, although the structure is a disappointing message for the theoretical characterization. This result also implies the requirement of fundamental studies on stability boundaries in the DAE system. Furthermore, this chapter numerically and theoretically discussed several discontinuous solutions of the DAE system with respect to practical fault conditions. The analysis provides us with several information about the transient dynamics and reveals a fault condition under which the DAE system is not

relevant to the transient stability analysis.

This dissertation proposes future research directions in power system analysis and control, nonlinear dynamics, and so on. Some of them are arranged below.

We have worked on synthesis of dc controllers to improve the transient dynamics of the ac/dc power system. This dissertation shows that the dc link strongly affects the transient dynamics and stability boundaries. On the contrary, this suggests that the dc link has a potential to stabilize ac power systems. The dc power modulation is proposed in [21, 23, 30, 89, 98] for damping power swings in ac transmission systems. In addition, dc control schemes are considered in [22, 58, 105, 106] for enhancement of transient stability of ac/dc power systems. Unfortunately, they are not established through control theories. The control strategies are much interesting in terms of power balance utilization for power system control.

We are also exploring a comprehensive energy function theory of the DAE system involving periodic orbits. The obtained results in Chapter 6 imply the requirement of further studies on stability boundaries of the DAE system. The present definition of energy functions in Chapter 6 does not admit any existence of periodic orbits. To overcome this difficulty, it is necessary to construct an alternative energy function theory with taking periodic orbits into account. The research topic is important for not only clarifying the numerical results in this dissertation but also considering network-reduction power system models with small transfer conductances [1, 12, 13].

Another direction is in experimental studies on the transient dynamics and stability of the electric power system with dc transmission. The analysis in this dissertation was performed numerically and theoretically. It is inevitable to confirm the obtained results experimentally to apply them to the practical stability estimation. The results will be discussed via a hybrid-type power system simulator [84].

In closing, the author would like to remark that we are now in a position to construct comprehensive system theories about complex power networks. Needless to say, power networks have become fairly complicated in terms of their size, configuration, dynamics, and control [4, 29, 81]. This actually appears as some large blackouts in the world. In such power networks, conventional power engineering is not effective because of its classical basis. This raises the requirement of novel system theories about the power networks, by

which we can analyze and synthesize the complexity. To achieve this, we need to reveal the dynamics of the complex networks, one of which is the synchronization through electric power transmission. In addition to the dynamical aspect, it is inevitable to propose how to tame the complexity of the power supply. Then, the dc-based power apparatuses have a great potential to control the complex power networks. Their important dynamics and control play an essential role in the planning and operation of the present and future power networks. Thus this dissertation focused on the analysis of the transient dynamics and stability of the electric power system with dc transmission. The obtained results herein provide us with a clue so as to the dynamics and control of the electric power networks involving dc apparatuses, although the research is restricted to the simple network. The author believes that this dissertation is a first challenge towards the establishment of the comprehensive theories about the complex power networks.

Bibliography

[1] E. H. Abed and P. P. Varaiya. Nonlinear oscillations in power systems. *Electrical Power & Energy Systems*, 6(1):37–43, January 1984.

[2] R. H. Abraham, J. E. Marsden, and T. Ratiu. *Manifolds, Tensor Analysis, and Applications*, volume 75 of *Applied Mathematical Sciences*. Springer-Verlag, New York, 2nd edition, 1988.

[3] R. H. Abraham and C. D. Show. *Dynamics: The Geometry of Behavior*. Studies in Nonlinearity. Addison-Wesley, Redwood City, 2nd edition, 1992.

[4] R. Albert and A. -L. Barabási. Statistical mechanics of complex networks. *Reviews of Modern Physics*, 74:47–97, January 2002.

[5] B. Anderson and C. Barker. A new era in HVDC? *IEE Review*, 46(2):33–39, March 2000.

[6] V. I. Arnold. *Mathematical Methods of Classical Mechanics*, volume 60 of *Graduate Texts in Mathematics*. Springer-Verlag, New York, second edition, 1989.

[7] P. M. Battelino, C. Grebogi, E. Ott, J. A. Yorke, and E. D. Yorke. Multiple coexisting attractors, basin boundaries and basic sets. *Physica D*, 32:296–305, 1988.

[8] A. R. Bergen and D. J. Hill. A structure preserving model for power system stability analysis. *IEEE Transactions on Power Apparatus and Systems*, PAS-100(1):25–35, January 1981.

[9] G. D. Birkhoff. *Collected Mathematical Papers*, volume II. Dover Publications, New York, 1968.

[10] K. E. Brenan, S. L. Campbell, and L. R. Petzold. *Numerical Solution of Initial-Value Problems in Differential-Algebraic Equations.* Elsevier Science Publishing, New York, 1989.

[11] C. A. Cañizares, F. L. Alvarado, C. L. DeMarco, I. Dobson, and W. F. Long. Point of collapse methods applied to ac/dc power systems. *IEEE Transactions on Power Systems*, 7(2):673–683, May 1992.

[12] H. -D. Chiang. Study of the existence of energy functions for power systems with losses. *IEEE Transactions on Circuits and Systems*, 36(11):1423–1429, November 1989.

[13] H. -D. Chiang and C. -C. Chu. Theoretical foundation of the BCU method for direct stability analysis of network-reduction power system models with small transfer conductances. *IEEE Transactions on Circuits and Systems-I: Fundamental Theory and Applications*, 42(5):252–265, May 1995.

[14] H. -D. Chiang, C. -C. Chu, and G. Cauley. Direct stability analysis of electric power systems using energy functions: Theory, applications, and perspective. *Proceedings of the IEEE*, 83(11):1497–1529, November 1995.

[15] H. -D. Chiang and L. Fekih-Ahmed. On the direct method for transient stability analysis of power system structure preserving models. In *Proceedings of the International Symposium on Circuits and Systems*, pages 2545–2548, 1992.

[16] H. -D. Chiang, M. W. Hirsch, and F. F. Wu. Stability regions of nonlinear autonomous dynamical systems. *IEEE Transactions on Automatic Control*, 33(1):16–27, January 1988.

[17] H. -D. Chiang, F. F. Wu, and P. P. Varaiya. Foundation of direct methods for power system transient stability analysis. *IEEE Transactions on Circuits and Systems*, CAS-34(2):160–173, February 1987.

[18] C. -C. Chu. *Transient dynamics of electric power systems: Direct stability assessment and chaotic motions.* PhD dissertation, Cornell University, January 1996.

[19] C. -C. Chu and H. -D. Chiang. Constructing analytical energy functions for lossless network-reduction power system models: Framework and new developments. *Circuits, Systems, and Signal Processing*, 18(1):1–16, 1999.

[20] CIGRÉ and IEEE FACTS Working Groups. *FACTS Overview*, IEEE Catalog #95-TP-108, 1995.

[21] R. L. Cresap, D. N. Scott, W. A. Mittelstadt, and C. W. Tailor. Operating experience with modulation of The Pacific HVDC Intertie. *IEEE Transactions on Power Apparatus and Systems*, PAS-97(4):1053–1059, July/August 1978.

[22] P. K. Dash, B. Puthal, O. P. Malik, and G. S. Hope. Transient stability and optimal control of parallel a.c.-d.c. power systems. *IEEE Transactions on Power Apparatus and Systems*, PAS-95(3):811–820, May/June 1976.

[23] S. Dechanupaprittha, A. Patanapakdee, and I. Ngamroo. An hvdc-based controller design for stabilization of frequency oscillation. In *Proceedings of the International Symposium on Circuits and Systems*, volume III, pages 379–382, 2003.

[24] C. L. DeMarco and A. R. Bergen. Application of singular perturbation techniques to power system transient stability analysis. In *Proceedings of the International Symposium on Circuits and Systems*, pages 597–601, 1984.

[25] D. D'humeieres, M. R. Beasley, B. A. Huberman, and A. Libchaber. Chaotic states and routes to chaos in the forced pendulum. *Physical Review A*, 26(6):3483–3496, November 1982.

[26] I. Dobson and H. -D. Chiang. Towards a theory of voltage collapse in electric power systems. *Systems & Control Letters*, 13:253–262, 1989.

[27] T. Endo and L. O. Chua. Chaos from phase-locked loops. *IEEE Transactions on Circuits and Systems*, 35(8):987–1003, August 1988.

[28] T. Endo and L. O. Chua. Bifurcation diagrams and fractal basin boundaries of phase-locked loop circuits. *IEEE Transactions on Circuits and Systems*, 37(4):534–540, April 1990.

[29] P. Fairley. The unruly power grid. *IEEE Spectrum*, 41(8):22–27, August 2004.

[30] T. Fujiwara, K. Matsuno, Y. Inoue, and T. Hayashi. Study of power modulation and fast margin angle control in Kii Channel HVDC Link. In *Proceedings of the CIGRÉ Tokyo Symposium*, 1995. paper #410-05.

[31] C. Grebogi, E. Ott, and J. A. Yorke. Basin boundary metamorphoses: Changes in accessible boundary orbits. *Physica D*, 24:243–262, 1987.

[32] B. Greenspan and P. Holmes. Homoclinic orbits, subharmonics and global bifurcations in forced oscillations. In G. I. Barenblatt, G. Iooss, and D. D. Joseph, editors, *Nonlinear Dynamics and Turbulence*, chapter 10. Pitman, London, 1983.

[33] B. Greenspan and P. Holmes. Repeated resonance and homoclinic bifurcation in a periodically forced family of oscillators. *SIAM Journal on Mathematical Analysis*, 15(1):69–97, January 1984.

[34] J. Guckenheimer. Toward a global theory of singularly perturbed dynamical systems. *Progress in Nonlinear Differential Equations and Their Applications*, 19:213–225, 1996.

[35] J. Guckenheimer and P. Holmes. *Nonlinear Oscillations, Dynamical Systems, and Bifurcations of Vector Fields*, volume 42 of *Applied Mathematical Sciences*. Springer-Verlag, New York, 1983.

[36] E. G. Gwinn and R. M. Westervelt. Intermittent chaos and low-frequency noise in the driven damped pendulum. *Physical Review Letters*, 54(15):1613–1616, April 1985.

[37] K. Hackett and P. Holmes. Josephson's junction, annulus maps, Birkhoff attractors, horseshoes and rotation sets. *Ergodic Theory and Dynamical Systems*, 6:205–239, 1986.

[38] E. Hairer and G. Wanner. *Solving Ordinary Differential Equations 2. Stiff and Differential-Algebraic Problems*, volume 14 of *Springer Series in Computational Mathematics*. Springer-Verlag, Berlin Heidelberg, second revised edition, 1996.

[39] J. K. Hale. *Ordinary Differential Equations*, volume XXI of *Pure and Applied Mathematics*. John Wiley & Sons, New York, 1969.

[40] T. J. Hammons, D. Woodford, J. Loughtan, M. Chamia, J. Donahoe, D. Povh, B. Bisewski, and W. Long. Role of hvdc transmission in future energy development. *IEEE Power Engineering Review*, 20(2):10–15, February 2000.

[41] T. Hasegawa, M. Sakai, and K. Yamaji. Design of ±500 kV compact converter stations of The Kii Channel HVDC Link. In *Proceedings of the CIGRÉ Tokyo Symposium*, 1995. paper #420-05.

[42] Y. Hasegawa and Y. Ueda. Global basin structure of attraction of two degrees of freedom swing equation system. *International Journal of Bifurcation and Chaos*, 9(8):1549–1569, 1999.

[43] C. Hayashi. *Nonlinear Oscillations in Physical Systems*. McGraw-Hill Electrical and Electronic Engineering Series. McGraw-Hill, New York, 1964.

[44] D. J. Hill and I. M. Y. Mareels. Stability theory for differential/algebraic systems with application to power systems. *IEEE Transactions on Circuits and Systems*, 37(11):1416–1423, November 1990.

[45] I. A. Hiskens and D. J. Hill. Energy functions, transient stability and voltage behavior in power systems with nonlinear loads. *IEEE Transactions on Power Systems*, 4(4):1525–1533, October 1989.

[46] C. Holmes and P. Holmes. Second order averaging and bifurcations to subharmonics in Duffing's equation. *Journal of Sound and Vibration*, 78(2):161–174, 1981.

[47] C. S. Hsu. *Cell-to-Cell Mapping: A Method of Global Analysis for Nonlinear Systems*, volume 64 of *Applied Mathematical Sciences*. Springer-Verlag, New York, 1987.

[48] B. A. Huberman, J. P. Crutchifield, and H. Packard. Noise phenomena in Josephson junctions. *Applied Physics Letters*, 37(8):750–752, October 1980.

[49] J. Kevorkian and J. D. Cole. *Multiple Scale and Singular Perturbation Methods*, volume 114 of *Applied Mathematical Sciences*. Springer-Verlag, New York, 1996.

[50] H. K. Khalil. *Nonlinear Systems*. Prentice Hall, New Jersey, third edition, 2002.

[51] E. W. Kimbark. *Power System Stability*, volume I and III. John Wiley & Sons, New York, 1947 and 1956.

[52] E. W. Kimbark. *Direct Current Transmission*, volume I. John Wiley & Sons, New York, 1971.

[53] P. V. Kokotović, H. K. Khalil, and J. O'Reilly. *Singular Perturbation Methods in Control: Analysis and Design*. Academic Press, London, 1986.

[54] N. Kopell and R. B. Washburn Jr. Chaotic motions in the two-degree-of-freedom swing equations. *IEEE Transactions on Circuits and Systems*, CAS-29(11):738–746, November 1982.

[55] Y. Kuramoto. *Chemical Oscillations, Waves, and Turbulence*. Dover Publications, New York, 2003.

[56] J. La Salle and S. Lefschetz. *Stability by Liapunov's direct method: with Applications*. Academic Press, New York, 1961.

[57] N. Levinson. Transformation theory of non-linear differential equations of the second order. *Annals of Mathematics*, 45(4):723–737, October 1944.

[58] T. Machida. Improving transient stability of ac system by joint usage of dc system. *IEEE Transactions on Power Apparatus and Systems*, PAS-85(3):226–232, March 1966.

[59] T. Machida, editor. *DC Transmission Engineering*. Tokyo Denki University Press, Tokyo, 1999. (in Japanese).

[60] J. Machowski, J. W. Bialek, and J. R. Bumby. *Power System Dynamics and Stability*. John Wiley & Sons, England, 1997.

[61] S. W. McDonald, C. Grebogi, E. Ott, and J. A. Yorke. Fractal basin boundaries. *Physica D*, 17:125–153, 1985.

[62] V. K. Melnikov. On the stability of the center for time periodic perturbations. *Transactions on Moscow Mathematical Society*, 12:1–56, 1963.

[63] M. Minorsky. *Introduction to Non-Linear Mechanics.* Edwards Brothers, Michigan, 1947.

[64] T. Mitsui. *Numerical Solution of Ordinary Differential Equations.* Iwanami-Shoten, Tokyo, 2003. (in Japanese).

[65] F. C. Moon and G. X. Li. Fractal basin boundaries and homoclinic orbits for periodic motion in a two-well potential. *Physical Review Letters*, 55(14):1439–1442, September 1985.

[66] W. Ohno, T. Endo, and Y. Ueda. Extinction and intermittency of the chaotic attractor via crisis in phase-locked loop equation with periodic external forcing term. *The Transactions of the IEICE A*, J82-A(5):627–636, May 1999. (in Japanese).

[67] K. R. Padiyar. *HVDC Power Transmission Systems: Technology and System Interactions.* Wiley Eastern, New Delhi, 1990.

[68] K. R. Padiyar and H. S. Y. Sastry. A structure-preserving energy function for stability analysis of ac/dc systems. *Sādhanā: Academy Proceedings in Engineering Science*, 18(5):787–799, September 1993.

[69] M. A. Pai. *Power System Stability: Analysis by the Direct Method of Lyapunov.* North-Holland, Amsterdam, 1981.

[70] M. A. Pai, K. R. Padiyar, and C. Radhakrishna. Transient stability analysis of multimachine ac/dc power systems via energy-function method. *IEEE Transactions on Power Apparatus and Systems*, PAS-100(12):5027–5035, December 1981.

[71] D. Povh. Use of HVDC and FACTS. *Proceedings of the IEEE*, 88(2):235–245, February 2000.

[72] F. M. A. Salam, J. E. Marsden, and P. P. Varaiya. Arnold diffusion in the swing equations of a power system. *IEEE Transactions on Circuits and Systems*, CAS-31(8):673–688, August 1984.

[73] F. M. A. Salam and S. S. Sastry. Dynamics of the forced Josephson junction circuit: The regions of chaos. *IEEE Transactions on Circuits and Systems*, CAS-32(8):784–796, August 1985.

[74] S. Sastry and P. Varaiya. Hierarchical stability and alert steering control of interconnected power systems. *IEEE Transactions on Circuits and Systems*, CAS-27(11):1102–1112, November 1980.

[75] S. S. Sastry and C. A. Desoer. Jump behavior of circuits and systems. *IEEE Transactions on Circuits and Systems*, CAS-28(12):1109–1124, December 1981.

[76] Y. Sekine. *Transient Analysis of Electric Power System.* Ohm-sha, Tokyo, 1984. (in Japanese).

[77] Y. Sekine, S. Kato, T. Motoki, and S. Ito. Kii Channel HVDC Link between Shikoku and Kansai Electric Power Companies by submarine cables. In *Proceedings of the CIGRÉ Tokyo Symposium*, 1995. paper #220-04.

[78] S. Smale. Differentiable dynamical systems. *Bulletin of the American Mathematical Society*, 73:747–817, 1967.

[79] M. S. Soliman and J. M. T. Thompson. Basin organization prior to a tangled saddle-node bifurcation. *International Journal of Bifurcation and Chaos*, 1(1):107–118, 1991.

[80] Status quo and future perspective in power quality. *Electrical Cooperative Research*, 55(3), 2000. (in Japanese).

[81] S. Strogatz. Exploring complex networks. *Nature*, 410:268–276, March 2001.

[82] V. Szebehely. Review of concepts of stability. *Celestial Mechanics*, 34:49–64, 1984.

[83] J. Takagi. History and future problems in research on synchronization phenomena. In *1974 Joint Convention Record of Four Institutes of Electrical Engineers, Japan*, volume 6, pages 97–100, October 1974. (in Japanese).

[84] Y. Takama, Y. Susuki, T. Funaki, and T. Hikihara. Development and validation of hybrid-type power system simulator. Technical Report CAS2004-36/NLP2004-48, IEICE, 2004. (in Japanese).

[85] F. Takens. Constrained equations; A study of implicit differential equations and their discontinuous solutions. In *Structural Stability, the Theory of Catastrophes, and Applications in the Sciences*, volume 525 of *Lecture Notes in Mathematics*, pages 143–234. Springer-Verlag, 1976.

[86] Y. Tamura, H. Mori, and S. Iwamoto. Relationship between voltage instability and multiple load flow solutions in electric power systems. *IEEE Transactions on Power Apparatus and Systems*, PAS-102(5):1115–1123, May 1983.

[87] Technical Committee on Transmission System for Tachibana-bay Thermal Power Station, ed., Technical Report on Transmission System for Tachibana-bay Thermal Power Station [Omnibus Version], November 1994. (in Japanese).

[88] J. M. T. Thompson and H. B. Stewart. *Nonlinear Dynamics and Chaos.* John Wiley & Sons, England, second edition, 2002.

[89] K. Tomiyama, M. Sato, K. Yamaji, M. Sekita, and M. Goto. Power swing damping control by hvdc power modulation in ac/dc hybrid transmission system. *The Transactions of the IEEJ*, 117-B(7):938–944, 1997. (in Japanese). *Electrical Engineering in Japan*, 124(3):10–18, 1998.

[90] N. A. Tsolas, A. Arapostathis, and P. P. Varaiya. A structure preserving energy function for power system transient stability analysis. *IEEE Transactions on Circuits and Systems*, CAS-32(10):1041–1049, October 1985.

[91] Y. Ueda. Explosion of strange attractors exhibited by Duffing's equation. *Nonlinear Dynamics, Annals of the New York Academy of Sciences*, 357:422–434, 1980. *The Road to Chaos-II.* pages 133–146.

[92] Y. Ueda. Personal communication, 1999.

[93] Y. Ueda. *The Road to Chaos-II.* Aerial Press, Santa Cruz, 2001.

[94] Y. Ueda, T. Enomoto, and H. B. Stewart. Chaotic transients and fractal structures governing coupled swing dynamics. In J. H. Kim and J. Stringer, editors, *Applied Chaos*, chapter 8. John Wiley & Sons, London, 1992.

[95] Y. Ueda and M. Hirano. On synchronization phenomena between electric power systems. Technical Reports NLP98-65, NLP98-82, and NLP98-99, IEICE, 1998. (in Japanese).

[96] Y. Ueda and J. Ogawa. On basins of synchronization phenomena between electric power systems. Technical Report NLP99-170, IEICE, 2000. (in Japanese).

[97] Y. Ueda, Y. Ueda, H. B. Stewart, and R. H. Abraham. Nonlinear resonance in basin portraits of two coupled swings under periodic forcing. *International Journal of Bifurcation and Chaos*, 8(6):1183–1197, 1998.

[98] E. Uhlmann. Stabilisation of an a.c. link by a parallel d.c. link. *Direct Current*, 9(3):89–94, August 1964.

[99] U.S.-Canada Power System Outage Task Force, ed. Final Report on the August 14, 2003 Blackout in the United States and Canada: Causes and Recommendations, April 2004.

[100] B. van der Pol. Forced oscillations in a circuit with non-linear resistance (Reception with reactive triode). *The London, Edinburgh, and Dublin Philosophical Magazine and Journal of Science*, 3:65–80, 1927.

[101] M. Varghese and J. S. Thorp. An analysis of truncated fractal growths in the stability boundaries of three-node swing equation. *IEEE Transactions on Circuits and Systems*, 35(7):825–834, July 1988.

[102] V. Venkatasubramanian. *A taxonomy of the dynamics of large differential algebraic systems such as the power system.* PhD dissertation, Washington University, 1992.

[103] V. Venkatasubramanian, H. Schättler, and J. Zaborszky. Dynamics of large constrained nonlinear systems–A taxonomy theory. *Proceeding of the IEEE*, 83(11):1530–1561, November 1995.

[104] A. J. Viterbi. *Principles of Coherent Communication.* McGraw-Hill Series in Systems Science. McGraw-Hill, New York, 1966.

[105] N. A. Vovos and G. D. Galanos. Transient stability of ac-dc systems. *IEEE Transactions on Power Apparatus and Systems*, PAS-98(4):1375–1383, July/August 1979.

[106] N. A. Vovos and G. D. Galanos. Enhancement of the transient stability of integrated ac/dc systems using active and reactive power modulation. *IEEE Transactions on Power Apparatus and Systems*, PAS-104(7):1696–1702, July 1985.

[107] S. Wiggins. *Global Bifurcations and Chaos: Analytical Methods*, volume 73 of *Applied Mathematical Sciences.* Springer-Verlag, New York, 1988.

[108] S. Wiggins. *Introduction to Applied Nonlinear Dynamical Systems and Chaos*, volume 2 of *Texts in Applied Mathematics.* Springer-Verlag, New York, 1990.

[109] N. Yorino, K. Mori, and Y. Tamura. On the relationship between power system stability and parametric resonance. *The Transactions of the IEEJ*, 105-B(1):15–22, 1985. (in Japanese).

[110] J. Zaborszky, G. Huang, B. Zheng, and T. -C. Leung. On the phase portrait of a class of large nonlinear dynamic systems such as the power system. *IEEE Transactions on Automatic Control*, 33(1):4–15, January 1988.

[111] Y. Zou, M. -H. Yin, and H. -D. Chiang. Theoretical foundation of the controlling UEP method for direct transient-stability analysis of network-preserving power system models. *IEEE Transactions of Circuits and Systems-I: Fundamental Theory and Applications*, 50(10):1324–1336, October 2003.

Published papers

The published papers, which contain most parts of this dissertation, by the author are listed below.

Archival journal articles

- Y. Susuki and T. Hikihara. An analytical criterion for stability boundaries of non-autonomous systems based on Melnikov's method. *Transactions of the ISCIE*, 15(11):586–592, November 2002.

- Y. Susuki, T. Hikihara, and H. -D. Chiang. Stability boundaries analysis of electric power system with dc transmission based on differential-algebraic equation system. *IEICE Transactions on Fundamentals of Electronics, Communications and Computer Sciences*, E87-A(9):2339–2346, September 2004.

- Y. Susuki and T. Hikihara. Transient dynamics in electric power system with dc transmission: Fractal growth in stability boundary. *IEE Proceedings–Circuits, Devices & Systems*, 2005. (accepted for publication).

- Y. Susuki and T. Hikihara. Stability boundaries in non-autonomous systems with resonant solutions: A subharmonic Melnikov function approach. (in review).

- Y. Susuki, T. Hikihara, and H. -D. Chiang. Transient stability and discontinuous solutions in electric power system with dc transmission: A differential-algebraic equation approach. (in review).

International conference proceedings

- Y. Susuki and T. Hikihara. Swing phenomena and global structures of solution space in an electric power system with dc transmission. In *Proceedings of the ninth workshop on Nonlinear Dynamics of Electronic Systems*, pages 133–136, Delft University of Technology, The Netherlands, June 21–23 2001.

- Y. Susuki and T. Hikihara. Stability region in electric power system with dc transmission based on differential-algebraic equation. In *Proceedings of the 37th International Universities Power Engineering Conference*, volume 2, pages 745–749, Staffordshire University, Great Britain, September 9–11 2002.

- Y. Susuki and T. Hikihara. An analysis with differential-algebraic equation in electric power system with dc transmission. In *Proceedings of the IEEE/PES Transmission and Distribution Conference and Exhibition 2002 Asia Pacific*, volume 3, pages 1933–1936, Pacifico Yokohama, Japan, October 6–10 2002.

- Y. Susuki and T. Hikihara. Stability boundaries analysis of non-autonomous systems with resonant solutions based on subharmonic Melnikov functions. In *Proceedings of the 2004 American Control Conference*, pages 1743–1748, Boston Sheraton Hotel, USA, June 30–July 2 2004.

- Y. Susuki, T. Hikihara, and H. -D. Chiang Transient stability and discontinuous solution in electric power system with dc transmission: A study with DAE system. In *Proceedings of the 2004 International Conference in Nonlinear Theory and its Applications*, ACROS Fukuoka, Japan, November 29–December 3 2004. (accepted).

Domestic conference proceedings and technical reports

- T. Hikihara and Y. Susuki. A study on swing phenomena in electric power system with dc transmission. In *Proceedings of the 2000 Engineering Sciences Society Conference of IEICE*, Nagoya Institute of Technology, Japan, October 3 2000. paper #A-2-12.

- T. Hikihara and Y. Susuki. Swing phenomena and basin structure in electric power system with dc transmission. Technical Report NLP2000-69, IEICE, October 20 2000.

- T. Hikihara and Y. Susuki. Region for stable operation in electric power system with dc transmission. In *Record of the 2000 Kansai-section Joint Convention of Institutes of Electrical Engineering, Japan*, Osaka Electro-Communication University, Japan, November 25 2000. paper #G6-4.

- Y. Susuki and T. Hikihara. A study on stability region in an electric power system with dc transmission. In *Proceedings of the 45th Annual Conference of the ISCIE*, Hotel Awina Osaka, Japan, May 10 2001. paper #2043.

- Y. Susuki and T. Hikihara. Stability analysis of an electric power system with dc transmission based on a differential-algebraic equation. In *Proceedings of the twelfth Annual Conference of Power and Energy Society, IEEJ*, Tohoku University, Japan, August 3 2001. paper #A04-127.

- Y. Susuki and T. Hikihara. Modeling and its numerical examination of electric power system with dc transmission based on differential-algebraic equation. In *Resume of the Joint Seminar on Power Engineering and Power System Engineering, IEEJ*, Kyodai-Kaikan, Japan, October 3 2001. paper #PE-01-24/PSE-01-18.

- Y. Susuki and T. Hikihara. Transient waveforms related to stability boundary in electric power system with dc transmission based on differential-algebraic equation. In *Proceedings of the 2002 Annual Conference of IEEJ*, Kogakuin University, Japan, March 26 2002. paper #A06-013.

- Y. Susuki and T. Hikihara. A study on global structure of stability region in electric power system with dc transmission based on differential-algebraic equation. In *Proceedings of the 46th Annual Conference of the ISCIE*, International Conference Center Kobe, Japan, May 16 2002. paper #3035.

- Y. Susuki and T. Hikihara. A study on power swing damping control via dc transmission in ac/dc power system based on differential-algebraic equation. In *Proceedings*

of the 2002 Annual Conference of IEEJ, Tohoku Gakuin University, Japan, March 18 2003. paper #A06-024 (in Japanese).

- Y. Susuki and T. Hikihara. Stability boundaries in non-autonomous systems with resonant solutions: An analytical approach via subharmonic Melnikov function. In *Proceedings of the 47th Annual Conference of the ISCIE*, Kyoto Terrsa, Japan, May 14 2003. paper #2009.

- Y. Susuki, H. -D. Chiang, and T. Hikihara. Characterization of stability boundaries in ac/dc power system based on differential-algebraic equation system. In *Proceedings of the 48th Annual Conference of the ISCIE*, Kyoto Terrsa, Japan, May 19 2004. paper #3011.

- Y. Susuki, T. Hikihara, and H. -D. Chiang. Transient dynamics due to discontinuous solutions in electric power system with dc transmission. Technical Report CAS2004-25/NLP2004-37, IEICE, September 13 2004.